THE
PHYSICAL REVIEW
A Journal of Experimental and Theoretical Physics Established by E. L. Nichols in 1893

VOL. 59, NO. 8 APRIL 15, 1941 SECOND SERIES

The Diffuse Scattering of X-Rays by Rocksalt

R. Q. GREGG AND N. S. GINGRICH
University of Missouri, Columbia, Missouri

(Received January 20, 1941)

A "monochromatic Laue pattern" of rocksalt has been obtained with crystal reflected Mo $K\alpha$ radiation, and shows forty diffuse spots. The positions of these spots, their intensities and their half-widths at half-maximum are compared with values for these quantities predicted by Zachariasen. In general, the agreement is good.

THE diffuse scattering of x-rays has recently attracted the attention of a number of investigators, particularly with regard to the interpretation of diffuse spots or streaks in Laue patterns. To illustrate this diffuse scattering, many Laue patterns taken with polychromatic radiation have been shown,[1] but as far as we are aware, only one pattern taken with monochromatic radiation has been published.[2] Preston took this pattern with Ag $K\alpha$ radiation parallel to the 001 direction in aluminum at a temperature of 500°C. Under this condition the usual Laue spots are missing and a much more satisfactory study of diffuse scattering can be made. In the present work, a pattern of rocksalt has been taken in the usual Laue method with the exception that monochromatic x-rays were used in place of polychromatic radiation, in order to illustrate the diffuse scattering of x-rays.

A Laue camera of the usual design was used to obtain these patterns. Two circular holes 1.6 mm in diameter separated by 7.7 cm served to limit the size and divergence of the beam of x-rays. The crystal of rocksalt from which the pattern was made was 0.6 mm thick and placed with its cleavage surface perpendicular to the incident beam with the crystal-to-film distance 4.90 cm. The exposures were made with the crystal at room temperature and with no intensifying screen. X-rays from a Mo target tube were monochromatized by reflection from a large rocksalt crystal set to reflect the Mo $K\alpha$ radiation. The divergence of the beam passing through the camera and crystal slip was determined by a series of exposures taken at various points along the path of the beam. In a vertical plane, the beam completely filled the collimating holes along the vertical diameter and the vertical divergence was about 1.7°. In the horizontal plane, the beam was not wide enough to fill the collimating holes and the horizontal divergence of the beam was about 9.5 minutes.

The pattern shown in Fig. 1 was taken with monochromatic Mo $K\alpha$ radiation and the spots are due to diffuse scattering of x-rays. It is evident that the distribution of intensity of diffusely scattered x-rays is markedly different from the slowly varying distribution predicted by the early theory of Debye.[3] In a theoretical

[1] E.g., C. V. Raman and P. Nilakantan, Proc. Ind. Acad. **12**, 141 (1940).
[2] G. D. Preston, Proc. Roy. Soc. **172**, 116 (1939).
[3] P. Debye, Ann. d. Physik **43**, 49 (1914).

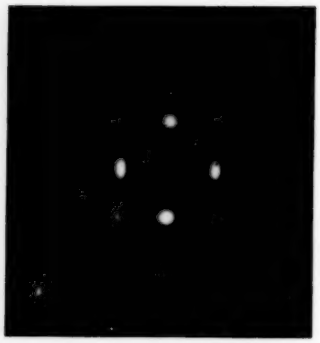

FIG. 1. The pattern of diffuse spots obtained by passing Mo $K\alpha$ radiation through a thin slip of rocksalt parallel to the 100 direction. Forty spots were located on the original film.

study of the diffuse scattering of x-rays by crystals, Zachariasen[4] predicted the existence of diffuse maxima and he derived expressions for the positions of these maxima, for their half-widths, and for their intensities. The experimental results of Siegel and Zachariasen,[5] of Preston,[2] of Lonsdale, Knaggs and Smith,[6] and of Raman and Nilakantan[1] have been offered in support[7] of Zachariasen's theory. In addition, Raman and Nilakantan have sought to use their experimental results in support of an explanation which they present for the origin of these diffuse spots. The pattern which is presented here, was obtained primarily to illustrate in a better way the diffuse spots which have been observed in Laue patterns, but in view of the interest in having this pattern studied more carefully, we have measured the positions of these spots on the original film, their half-widths at half-maximum and their relative intensities. The

TABLE I. *Distances of spots from center of pattern, planes which produce the spots, and calculated and observed angles.*

OBSERVED DISTANCES	*hkl*	$2\theta_m$ OBS.	$2\theta_m$ CALC.*	$2\theta_B$
1.23	200	14° 5′±8′	14° 9′	14° 29′
1.81	220	20° 14′±15′	19° 37′	20° 32′
2.18	311	23° 59′±1°	24° 31′	24° 8′
2.81	(400) (402)	29° 51′±45′	(26° 46′) (33° 59′)	(29° 12′) (32° 44′)
3.00	331	31° 27′±25′	31° 28′	31° 54′
3.39	(420) (422)	34° 40′±40′	(29° 25′) (37° 1′)	(32° 44′) (35° 58′)
4.63	442	43° 22′±30′	43° 38′	44° 26′
4.94	602	45° 13′±1°	45° 19′	47° 0′

* We are indebted to Dr. Zachariasen for these values.

[4] W. H. Zachariasen, Phys. Rev. **57**, 597 (1940).
[5] S. Siegel and W. H. Zachariasen, Phys. Rev. **57**, 795 (1940).
[6] K. Lonsdale, I. E. Knaggs and H. Smith, Nature **146**, 332 (1940).
[7] W. H. Zachariasen, Phys. Rev. **59**, 207 (1941).

TABLE II. *Comparison of observed and calculated intensities and half-widths at half-maximum.*

hkl	INTENSITY OBS.	INTENSITY CALC.*	$x_{1/2}$ OBS.	$x_{1/2}$ CALC.*
200	100	106	1° 23′±15′	1° 46′
220	37	28	2° 11′±27′	3° 46′
311	4.6	3	1° 24′± 1°	2° 17′
(400) (402)	17	(7) (11)	2° 50′±26′	(6° 34′) (5° 42′)
331	8.4	11	1° 13′±25′	1° 24′
(420) (422)	20	(5) (21)	2° 58′±48′	(8° 3′) (3° 41′)
442	42	55	1° 48′±19′	1° 44′
602	6.4	13	2° 50′±40′	3° 15′

* We are indebted to Dr. Zachariasen for these values.

microphotometering was done along radial lines and the values for similar spots were averaged. Table I gives the distance of each type of spot from the center of the pattern, the crystallographic planes responsible for these spots, the observed angle $2\theta_m$, the angle $2\theta_m$ calculated from Zachariasen's expression, and the Bragg angle $2\theta_B$. By considering only errors in the crystal-to-film distance and in the observed distances from the center of the pattern to the spots, limits of error are indicated as estimated for each measurement. Table II compares the observed and calculated intensities and half-widths at half-maximum. In order to obtain the observed intensities, a slowly varying background was arbitrarily subtracted from the actual microphotometer trace. The form and amount subtracted was substantially the same along all radial lines

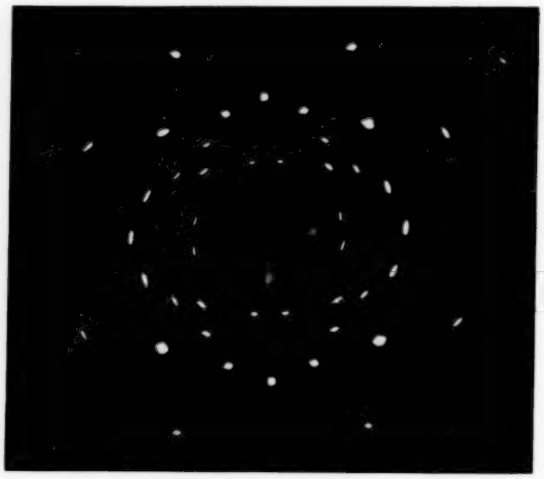

FIG. 2. Laue pattern taken with polychromatic radiation for comparison with Fig. 1.

which were microphotometered. It is reasonable to ascribe this background to air scattering, to incoherent radiation from the crystal and possibly also to Debye diffuse scattering as pointed out by Jauncey and Harvey.[8] Limits of error are estimated for the half-width values, and, as above, it is believed that any value outside these limits would be inconsistent with the facts.

In the cases where spots are due to two planes, comparison between theory and experiment is somewhat ambiguous, but in other cases, comparisons can be made. Spots due to 200, 331, 442 and 602 do not occur at $2\theta_B$, but are reasonably close to $2\theta_m$; the spot due to 220 lies between $2\theta_B$ and $2\theta_m$; the spot due to 311 was too weak to make discriminating measurements. The observed and calculated intensities are in good accord considering the difficulties of measurement of some of the weaker spots. The half-widths at half-maximum are observed as generally less than predicted, but it appears that there is a tendency for qualitative agreement.

For convenience of comparison, a Laue pattern taken with polychromatic radiation is shown in Fig. 2. The diffuse spots are smeared out into diffuse streaks due to the fact that each wave-length in the incident beam produces its own diffuse pattern with angles of scattering smaller for the shorter wave-lengths. The most intense streaks seem to show the effects of the short wave-length cut-off and the silver absorption edge.

A third type of pattern was also taken, with the rocksalt crystal slip tilted about a 010 axis at an angle of 11° from its previous position, and with monochromatic radiation. This picture is not reproduced because it is fairly weak, but certain interesting observations made by others have been verified. The pattern is approximately the same as Fig. 1 except that some of the spots are weakened while others are strengthened. Thus, to a first approximation the pattern is altered only in the relative intensities of the spots and not in the positions of the spots.

We are indebted to Dr. W. H. Zachariasen for his generous assistance in the interpretation of certain features of the above diffuse pattern. It is a pleasure to acknowledge that this work was aided by a grant made to one of us (N. S. G.) by the Elizabeth Thompson Science Fund.

[8] G. E. M. Jauncey and G. G. Harvey, Phys. Rev. **58**, 179 (1940).

APRIL 15, 1941 PHYSICAL REVIEW VOLUME 59

Burst Production by Mesotrons of Spin One-Half and Zero Magnetic Moment

S. B. BATDORF, *Department of Physics, University of Nevada, Reno, Nevada*
AND
ROY THOMAS, *Department of Physics, University of California, Berkeley, California*

(Received February 21, 1941)

The cross section for the initiation of energetic cascades or bursts by bremsstrahlung is calculated for a mesotron of spin one-half and zero magnetic moment. Our results are very similar to those obtained by Christy and Kusaka for a Proca particle; our cross section is about 0.7 of theirs.

BECAUSE of the few experimental facts known about the mesotron one is unable at the present time to assign a definite spin and magnetic moment which excludes all other possibilities. Corben and Schwinger[1] have investigated the probability of a mesotron transferring an appreciable fraction of its energy to an electron. They have obtained closely similar results for mesotrons of spin one-half, magnetic moment zero and also of spin one unit magnetic moment. Christy and Kusaka[2] found the cross section for bremsstrahlung by a mesotron of spin one and magnetic moment one. To complete this investigation we thought it would be useful to investigate the burst cross section by bremsstrahlung for a mesotron of spin one-half and zero magnetic moment.

[1] H. C. Corben and J. Schwinger, Phys. Rev. **58**, 953 (1940).
[2] R. F. Christy and S. Kusaka, Phys. Rev. **59**, 414 (1941). We are indebted to these authors for discussions on their papers on burst production.

The penetrating or hard component of cosmic rays is assumed to consist of mesotrons. On passing through the Coulomb field of a heavy nucleus the mesotron will emit a gamma-quantum and lose an appreciable fraction of its energy. This gamma-ray will, in passing through matter, give up its energy to a large number of particles by means of the cascade process. If the cascade is energetic enough we have a burst.

In order to compare our results for spin one-half and zero magnetic moment with those of spin one and unit magnetic moment (Proca particle), obtained by Christy and Kusaka, we proceed in the following manner. First we find the cross section for Compton scattering by this particle of spin one-half. Now by resolving the Coulomb field external to the nucleus by the virtual quanta method, one finds the bremsstrahlung cross section. By multiplying this cross section by a suitable mesotron distribution function, we integrate over the mesotron energy, keeping the energy of the burst constant. This is the burst production cross section. For a given burst energy the calculated values for spin one-half and zero magnetic moment are about seven-tenths as large as those for spin one and unit magnetic moment.

Calculations

For a Pauli particle of arbitrary magnetic moment, the wave equation of the system is

$$[\gamma^\mu(p_\mu+e\phi_\mu)-iMc+n\gamma^\nu\gamma^\mu F_{\nu\mu}]_{\nu>\mu}\psi=0,$$

where the p_μ are the relativistic four vector components of momentum, $F_{\mu\nu}$ is the antisymmetrical field tensor. Here also ψ is the four-component Dirac wave function. By transforming the wave equation to the ordinary energy H, momentum $\mathbf{P}$, and the Dirac α's we find

$$H=c\boldsymbol{\alpha}\cdot(\mathbf{p}-(e/c)\mathbf{A})+\beta Mc^2+e\phi-n\beta[\boldsymbol{\sigma}\cdot\mathbf{H}-i\boldsymbol{\alpha}\cdot\mathbf{E}].$$

Taking the nonrelativistic approximation it is seen that for $n=-eh/2Mc$ the magnetic moment of our particle is zero. Here e is the mesotron charge while M is its mass. The coupling energy with the radiation field is then

$$H'=-e(\boldsymbol{\alpha}\cdot\mathbf{A})+e\phi+(eh/2Mc)\beta[\boldsymbol{\sigma}\cdot\mathbf{H}-i\boldsymbol{\alpha}\cdot\mathbf{E}].$$

$\mathbf{A}$ and ϕ are the ordinary vector and scalar potentials while $\mathbf{E}$ and $\mathbf{H}$ are the field strengths.

Using the above coupling energy we now calculate the Compton scattering of a light quantum by this mesotron of spin one-half and zero magnetic moment. The transition probability for this scattering process is

$$w=\frac{2\pi}{h}\left[\frac{H_{A1}H_{1F}}{E_A-E_1}+\frac{H_{A11}H_{11F}}{E_A-E_{11}}\right]^2\rho_F,$$

where ρ_F denotes the number of final states per unit energy interval dE_F of the mesotron. E_A is the rest energy of the mesotron and incident light quantum, E_1 is the first intermediate state in which no light quanta are present while the intermediate state E_{11} contains initial and scattered light quanta.

If k_0 is the energy of the incident light quantum, k the scattered quantum, the matrix elements for the transition probability are

$$H_{A1}=-e\left(\frac{2\pi h^2c^2}{k_0}\right)^{\frac{1}{2}}u_0^*\left[1+\frac{k_0}{2Mc^2}\beta(1+\alpha k_0)\right]\alpha_0 u',$$

$$H_{1F}=-e\left(\frac{2\pi h^2c^2}{k}\right)^{\frac{1}{2}}u'^*\left[1-\frac{k}{2Mc^2}\beta(1+\alpha_k)\right]\alpha u,$$

$$H_{A11}=-e\left(\frac{2\pi h^2c^2}{k}\right)^{\frac{1}{2}}u_0^*\left[1-\frac{k}{2Mc^2}\beta(1+\alpha_k)\right]\alpha u'',$$

$$H_{11F}=-e\left(\frac{2\pi h^2c^2}{k_0}\right)^{\frac{1}{2}}u''^*\left[1+\frac{k_0}{2Mc^2}\beta(1+\alpha k_0)\right]\alpha_0 u.$$

Here u_0, u, u' and u'' are the Dirac amplitudes of the mesotron in the initial, final, first and second intermediate states. Also α_0 and α_{k_0} are the components of $\boldsymbol{\alpha}$ in the direction of polarization and propagation of the incident light quantum k_0. α and α_k represent similar quantities with respect to the scattered quanta k. The actual calculation of the Compton scattering for this process follows identically the method used by Heitler in the derivation of the Klein-Nishina formula, the only difference being that we have the additional terms in **E** and **H** in the coupling energy.

The differential scattering cross section then becomes

$$d\phi=\frac{1}{2}\left(\frac{e^2}{Mc^2}\right)^2\frac{k^2}{k_0^2}\left[\frac{k_0}{k}+\frac{k}{k_0}-\sin^2\theta\right]d\Omega-\frac{1}{8}\left(\frac{e^2}{Mc^2}\right)^2\left(\frac{k}{Mc^2}\right)^2\frac{k}{k_0}[1-\cos\theta][1-3\cos\theta]d\Omega$$

$$+\frac{1}{4}\left(\frac{e^2}{Mc^2}\right)^2\left(\frac{k}{Mc^2}\right)^2\frac{k}{k_0}d\Omega,$$

where θ is the angle of scattering and $d\Omega$ is the differential solid angle of the scattered quantum. The first term in the expression is the ordinary Klein-Nishina formula, the last term is the part of the pure magnetic moment interaction which gives the main contribution for θ small. The second term gives the interference effects.

In order to find the bremsstrahlung cross section we consider a coordinate system in which the mesotron is initially at rest while the nucleus is moving past with a high velocity. We now neglect impacts within the nuclear radius $\sim\hbar Z^{\frac{1}{3}}/Mc$, and analyze the contracted Coulomb field by means of virtual quanta.

The total energy of frequency k_0/h to $(k_0+dk_0)/h$ to pass the particle is

$$C(k_0)=\frac{2}{\pi}\left(\frac{e^2}{\hbar c}\right)Z^2dk_0\int_{\hbar Z^{1/3}/Mc}^{E\hbar/Mck_0}\frac{dr}{r}=\frac{2}{\pi}\alpha Z^2dk_0\log\frac{E}{k_0Z^{\frac{1}{3}}},$$

where E is the mesotron energy and Z the nuclear charge. The energy of this frequency incident is $c(k_0)d\phi$ and the number of incident quanta of energy k_0 is $c(k_0)d\phi/k_0$. If k is the energy of the scattered quanta we obtain for the scattered energy $c(k_0)d\phi(k/k_0)$.

The scattering quantum k in the laboratory system is $k'=k\zeta(1-\cos\theta)$ and the scattered energy in this system becomes $[c(k_0)d\phi/k_0]k\zeta(1-\cos\theta)$ and therefore the probability of emission of quantum of energy k' is

$$[c(k_0)d\phi/k_0k']k\zeta(1-\cos\theta). \tag{1}$$

If we let ϵ be the fraction of mesotron energy taken up by the gamma-quantum, then $k'=\epsilon E$ where E is the mesotron energy. From the energy conservation law

$k=\dfrac{Mc^2k_0}{Mc^2+k_0(1-\cos\theta)}$, and the relative transformation $k'=k\zeta(1-\cos\theta)$, we obtain

$$(1-\cos\theta)=\frac{Mc^2}{k_0}\frac{\epsilon}{1-\epsilon},\quad\text{and}\quad\frac{k}{k_0}=1-\epsilon.$$

The element of solid angle becomes

$$d\Omega=2\pi\frac{Mc^2}{k_0}\frac{d\epsilon}{(1-\epsilon)^2}.$$

The scattering formula may now be expressed as

$$d\phi(\epsilon,k_0)=\frac{\pi}{2}\left(\frac{e^2}{Mc^2}\right)^2\frac{k_0}{Mc^2}d\epsilon\left[(1-\epsilon)+\epsilon\frac{Mc^2}{k_0}+\frac{8-8\epsilon+\epsilon^2}{2(1-\epsilon)}\left(\frac{Mc^2}{k_0}\right)^2-\frac{4\epsilon}{1-\epsilon}\left(\frac{Mc^2}{k_0}\right)^3+2\frac{\epsilon^2}{(1-\epsilon)^2}\left(\frac{Mc^2}{k_0}\right)^4\right].$$

Inserting these expressions in (1) we get for the cross section for bremsstrahlung

$$\sigma_1(\epsilon, E)d\epsilon=\alpha\left(\frac{e^2}{Mc^2}\right)^2 Z^2 d\epsilon\int_{\epsilon/2(1-\epsilon)}^{E/Mc^2Z^{\frac{1}{3}}} dk_0\int_{Z^{\frac{1}{3}}}^{E/Mc^2k_0}\frac{dr}{r}\left[(1-\epsilon)+\epsilon\frac{1}{k_0}+\frac{8-8\epsilon+\epsilon^2}{2(1-\epsilon)}\frac{1}{k_0^2}-\frac{4\epsilon}{1-\epsilon}\frac{1}{k_0^3}+\frac{2\epsilon^2}{(1-\epsilon)^2}\frac{1}{k_0^4}\right].$$

The lower limit of k_0 is not zero, to produce $k'=\epsilon E/Mc^2$, k must be at least $\epsilon/2$, in which case k_0 will be $\epsilon/2(1-\epsilon)$. The upper limit of k_0 is so defined that nuclear collisions, $r<\hbar Z^{\frac{1}{3}}/Mc$ are not included in the process. After performing the double integration we obtain

$$\sigma_1(\epsilon, E)d\epsilon=\alpha\left(\frac{e^2}{Mc^2}\right)^2 Z^2 d\epsilon\left[(1-\epsilon)\frac{E}{Mc^2Z^{\frac{1}{3}}}+\frac{\epsilon}{2}\left[\log\frac{2E(1-\epsilon)}{Mc^2Z^{\frac{1}{3}}\epsilon}\right]^2+\left[\frac{\epsilon}{2}+\frac{16}{3}\frac{(1-\epsilon)}{\epsilon}\right]\log\frac{2E(1-\epsilon)}{Mc^2Z^{\frac{1}{3}}\epsilon}\right].$$

Mc^2 is the rest energy of the mesotron and Ze the charge on the nucleus. The above differential cross section is very similar to one, considering the mesotron having a spin unity and unit magnetic moment, which is[2]

$$\sigma_2(\epsilon, E)d\epsilon=\alpha\left(\frac{e^2}{Mc^2}\right)^2 Z^2 d\epsilon\left[\frac{2-2\epsilon+7\epsilon^2}{12}\frac{E}{Mc^2Z^{\frac{1}{3}}}+\frac{\epsilon(34-34\epsilon+7\epsilon^2)}{24(1-\epsilon)}\left[\log\frac{2E(1-\epsilon)}{Mc^2Z^{\frac{1}{3}}\epsilon}\right]^2\right.$$
$$\left.+\left[\frac{\epsilon(26-26\epsilon-5\epsilon^2)}{24(1-\epsilon)}+\frac{16}{3}\frac{(1-\epsilon)}{\epsilon}\right]\log\frac{2E(1-\epsilon)}{Mc^2Z^{\frac{1}{3}}\epsilon}\right].$$

Experimentally it is known that the mesotron distribution is represented fairly accurately by an inverse cube law in energy. We therefore let $N(E)dE=\text{const}\ (Mc^2/E)^3dE$ be the mesotron distribution in the energy range between E and $E+dE$. If E_1 is the burst energy, $E_1=\epsilon E$.

The cross section for bursts of energy between E_1 and E_1+dE_1 is then

$$B(E_1)dE_1=\int N(E)\sigma(\epsilon, E)d\epsilon dE=\int N\left(\frac{E_1}{\epsilon}\right)\sigma\left(\epsilon, \frac{E_1}{\epsilon}\right)d\epsilon\frac{dE_1}{\epsilon}.$$

Inserting $\sigma_1(\epsilon, E_1/\epsilon)$ and integrating over ϵ from zero to $\epsilon_{\max}=1-Mc^2/E_1$ one has

$$B_1(E_1)dE_1=\text{const}\left(\frac{Mc^2}{E_1}\right)^3\left(\frac{e^2}{Mc^2}\right)^2\alpha Z^2\left[\frac{1}{12}\frac{2E_1}{Mc^2Z^{\frac{1}{3}}}+\frac{1}{8}\left[\log\frac{2E_1}{Mc^2Z^{\frac{1}{3}}}\right]^2+\frac{89}{144}\log\frac{2E_1}{Mc^2Z^{\frac{1}{3}}}\right]dE_1.$$

For high energy bursts the term linear in the bracket dominates the expression, while for moderate bursts all terms give a contribution of about equal magnitude.

For mesotrons of spin one and unit magnetic moment we obtain

$$B_2(E_1)dE_1=\text{const}\left(\frac{Mc^2}{E_1}\right)^3\left(\frac{e^2}{Mc^2}\right)^2\alpha Z^2\left[\frac{25}{288}\frac{2E_1}{Mc^2Z^{\frac{1}{3}}}+\frac{7}{72}\left[\log\frac{E_1}{Mc^2}\right]^3-\frac{7}{24}\left[\log\frac{E_1}{Mc^2}\right]^2\log\frac{2E_1}{Mc^2Z^{\frac{1}{3}}}\right.$$
$$+\frac{7}{24}\log\frac{E_1}{Mc^2}\left[\log\frac{2E_1}{Mc^2Z^{\frac{1}{3}}}\right]^2+\frac{5}{48}\left[\log\frac{E_1}{Mc^2}\right]^2-\frac{5}{24}\log\frac{E_1}{Mc^2}\log\frac{2E_1}{Mc^2Z^{\frac{1}{3}}}$$
$$\left.-\frac{449}{1440}\left[\log\frac{2E_1}{Mc^2Z^{\frac{1}{3}}}\right]^2+\frac{66}{24}\log\frac{2E_1}{Mc^2Z^{\frac{1}{3}}}\right]dE_1.$$

For values of E_1/Mc^2 between 100 and 2000, B_1/B_2 varies from $\frac{2}{3}$ to about $\frac{4}{5}$.

The authors are pleased to acknowledge the helpful suggestions of Professor J. R. Oppenheimer and Dr. J. Schwinger.

A Note on Ionization by Meteors

J. A. PIERCE
Cruft Laboratory, Harvard University, Cambridge, Massachusetts
(Received March 3, 1941)

Experimental evidence of atmospheric ionization by meteoric bombardment is presented. This kind of measurement may be useful in studying diffusion and recombination in the upper atmosphere and in counting meteors in the daytime or in cloudy weather.

AT the time of the Leonid meteor shower in 1940 data were gathered in an effort to augment the evidence[1–5] of atmospheric ionization by meteoric bombardment. These observations were made in Queenstown, South Africa, (lat. 31° 54′ S., long. 27° 55′ E.) where the author was engaged in gathering control data for a study of the behavior of the ionosphere during the solar eclipse of October 1.

The visual observation of meteors was hampered by persistent cloudiness, but a number of coincidences were obtained between observed meteors and the appearance of ionized regions in the upper atmosphere. The radio technique employed was the automatic recording against time of the apparent height of reflection of pulses of short duration transmitted at a suitably chosen radiofrequency. In Fig. 1*A* the transmitted pulses form the base line at the bottom of the record, while first- and second-order reflections from the *F* layer give the broader lines in the middle and at the top of the figure. This record was made between $3^h\ 10^m$ and $3^h\ 27^m$, local mean time, on the morning of November 14, 1940, at a frequency of 3000 kilocycles, and the apparent height of the first *F* layer reflection is 340 kilometers. At the times indicated by the two arrows (about 0313 and 0318) meteors were visually observed, the identifying marks at the tails of the arrows being the author's estimate of their stellar magnitudes. The passage of the second magnitude meteor was followed, after about 16 seconds, by a burst of radio reflections from a distance of 150 kilometers, the reflections lasting nearly a minute. The reflection pattern corresponding to the brighter meteor appeared at 105 km after 24 seconds and lasted at least 7.3 minutes.

Record *B* in the same figure was obtained at 6425 kc, and is similar to the other except that the vertical and horizontal scales are respectively 1.5 times greater and 15 times smaller. At this frequency *F* layer reflection does not begin until after sunrise. The record runs from 2^h to 6^h L.M.T. on the same date and shows similar meteoric effects. In addition to the meteors "2" and "−1," there were two others seen at about $2^h\ 2^m$ and $3^h\ 5^m$. A trace corresponding to the first appears on the record, but there is none for the second, perhaps because the meteor appeared at a lower elevation (30° above the horizon) than any of the others and was presumably farther away. The equipment used in making record *A* was not in operation at this time.

Before four o'clock the sky became too bright for visual observations. Record *B*, however, indicates that the number of meteors increased after that time. Between 4^h and 6^h at least 14 traces can be identified at distances varying between 100 and 210 kilometers.

The record for the corresponding 4-hour period of November 8, several days before the Leonid shower, is shown at *C*. Only one or two possible meteor traces appear, and they are probably too faint to show in reproduction.

When a meteor passes through the atmosphere, its energy of impact is sufficient[6] to ionize any particle with which it comes in contact. Thus a "line" of ionized atoms or molecules is established, along which the density of free electrons is very great. The charged particles immediately begin to diffuse radially. Reflection of an electromagnetic wave can occur when a cylinder of

[1] A. M. Skellett, Phys. Rev. **37**, 1668 (1931).
[2] A. M. Skellett, Proc. I. R. E. **20**. 1933 (1932).
[3] S. K. Mitra, P. Syam and B. N. Ghose, Nature **133** 533 (1934).
[4] A. M. Skellett, Proc. I. R. E. **23**. 132 (1935).
[5] J. N. Bhar, Nature **139**, 470 (1937).
[6] H. B. Maris, Terr. Mag. **34**, 309 (1929).

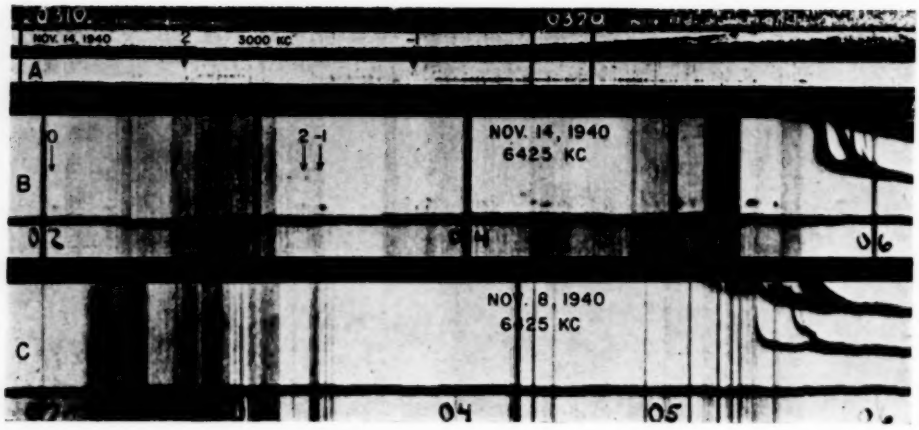

FIG. 1. Height-time radio sounding records showing evidence of meteoric bombardment. The arrows indicate the times at which meteors were seen.

ionization a few wave-lengths in diameter develops, provided that the density of ionization throughout this volume is greater than the critical value which is required to reflect a wave of the frequency in question. The density of ionization decreases because of diffusion and recombination. In the case of a large meteor the density might, after a time, become nearly uniform over an area many wave-lengths in diameter. In this event the rate of change of the maximum density of ionization would not be greatly affected by diffusion so that it might be used as a measure of the recombination coefficient.

At the time of disappearance of the meteor trace at a known radiofrequency, the maximum density of ionization (over a region a few wave-lengths in diameter) is

$$N = 1.24\ 10^{-8} f^2 \text{ free electrons/cm}^3,$$

where f is the frequency in cycles per second. If we neglect diffusion, the equivalent recombination coefficient is

$$\alpha' = (N_1 - N_2)/N_1 N_2 t \text{ cm}^3/\text{free electron} \cdot \text{second},$$

where N_1 and N_2 are the free electron densities measured at two instants separated by t seconds.

In the case of our trail "2," the trace disappears about 0.5 minute later at 3.0 Mc than at 6.4 Mc. The equivalent recombination coefficient is, therefore,

$$\alpha' = \frac{(5.1-1.1)10^5 \text{ electrons/cm}^3}{5.1 \cdot 1.1 \cdot 10^{10} \text{ electrons}^2/\text{cm}^6 \cdot 30 \text{ sec.}}$$

$$= 2 \cdot 10^{-7} \text{ cm}^3/\text{electron sec.}$$

This value is an order of magnitude larger than that believed to obtain at this height in the atmosphere, so we may infer that, in the case of a meteor which left only a short record at 6.4 Mc, diffusion is an important factor.

For meteor "−1," where the traces last about 1.5 minutes at 6.4 Mc and 7.3 minutes at 3.0 Mc, the equivalent recombination coefficient is $2 \cdot 10^{-8}$ cm³/electron·second, which is near the value estimated by other methods.

It is hoped that by simultaneous observation from two or three locations and by recording reflections at several frequencies, a useful study of recombination and diffusion can be made. Pending these results it is interesting to note that this method may be made sufficiently sensitive to compare with photographic registration of meteors, and that meteor counts can be made automatically without regard to time of day or weather conditions. It is unfortunate that the orientation of the meteor trail[7] presumably has an effect upon the intensity of the radio echo, so that further investigation of the method will be necessary before we can determine the magnitudes of meteors in this way.

[7] J. A. Pierce, Proc. I. R. E. **26**, 892 (1938).

Statistics of Excited Energy States of Nuclei

H. MARGENAU
Sloane Physics Laboratory, Yale University, New Haven, Connecticut
(Received February 8, 1941)

The spacing of nuclear energy levels at excitation energies of about 8 Mev is calculated by numerical summation over the individual particle states, thus avoiding the use of the asymptotic Sommerfeld formulas whose validity in nuclear considerations is far from exact. The model used as basis is that of free particles moving in a spherical well. The results indicate that deviations from Bethe's formula for the level density, which represents correctly the mean trend with both excitation energy and atomic number, can be very great indeed. The group structure introduced by the free particle model has a strong effect on the spacing. The fluctuations thus shown to exist permit an explanation of the fact that heavy nuclei, which according to current theory should be strong absorbers of slow neutrons, do not as a rule possess this property.

THEORETICAL treatments[1–6] of the density of nuclear energy states aim chiefly to explain two facts: the rapid convergence of the levels of any given nucleus with growing excitation energy, and the increase in density, at constant excitation energy, as the atomic number increases. The methods used to achieve these results are those of statistical mechanics. Each particle in the nucleus is considered to occupy one of a well-defined set of individual-particle levels, ϵ_i, the same for all particles; the sum of the individual-particle energies is the total energy of the nucleus; and the number of ways in which a given energy E of the total system can be realized, divided by the unit of energy, is taken to be the energy density of the levels about E. This quantity is called ρ.

The exact dependence of ρ on the number of particles and on E is conditioned by the detailed arrangement of the ϵ_i. In previous treatments it is assumed that there exists a continuous density of states ϵ_i, which implies, of course, that these states are very numerous in the region of energies normally occupied by particles. This assumption then permits integrations instead of summations over the various states. When the excitation energy is not too high, it allows, indeed, the application of Sommerfeld's formulas, familiar from the theory of metals, to the nuclear problem. Bethe[1] and Bardeen,[2] in their discussion of the problem, assume the ϵ_i to be the levels of a free particle in a box the shape of which is a parallelepiped.[3] Van Lier and Uhlenbeck[4] consider more general distributions and point out that ρ depends essentially on the density of single-particle levels near the top of the Fermi distribution, and not appreciably upon the distribution of ϵ's in other regions.

The physical meaning of the ϵ's is rather vague because the individual-particle picture is not a very good model of the nucleus. Bardeen and Feenberg,[5] and also Motz and Feenberg,[6] have refined the statistical picture by applying symmetry considerations and have shown that the uniform trend with atomic number of the asymptotic formula of Bethe and Bardeen may be interrupted by local variations, at least for the lighter nuclei. The detailed effect of a change in the discrete structure of the ϵ arrangement has not been investigated.

The reason why one might expect this arrangement to have a considerable effect on ρ is seen in the fact that the ϵ's are not very numerous, so that any irregularity in their spacing, especially near the top of the Fermi distribution, might cause a large variation in ρ. The number of occupied levels can at most, i.e., when all degeneracies are removed, be equal to the number of particles composing the nucleus. For any simple potential field, such as the spherical well or the oscillator model, degeneracy is great and

[1] H. A. Bethe, Phys. Rev. **50**, 332 (1936).
[2] J. Bardeen, Phys. Rev. **51**, 799 (1937).
[3] For a container of nuclear size it matters considerably whether the free particles move within a parallelepiped or a sphere.
[4] C. van Lier and G. E. Uhlenbeck, Physica **4**, 531 (1937).
[5] J. Bardeen and E. Feenberg, Phys. Rev. **54**, 809 (1938).
[6] L. Motz and E. Feenberg, Phys. Rev. **54**, 1055 (1938).

there are only about 10 energy levels occupied in a nucleus of intermediate weight. In this case, then, the assignment of densities to represent individual-particle levels is not very significant, and what usually passes as the statistical theory based on the free particle model has indeed very little relation to this model, though it may approach reality in some respects quite closely.

The very fact that the distribution of ϵ's is so sparse, however, makes possible a computation of ρ which avoids the use of integrals instead of summations, and of the asymptotic Sommerfeld formulas which are valid only for extreme degeneration of the Fermi gas composing the nucleus. For excitation energies of the order of 10 Mev, the summations encountered in the statistical problem converge so fast that—with the model here chosen—hardly more than 12 terms are appreciable. The sums are therefore easily computed numerically. Since we are interested in the effect of irregularities of spacing, possible group structure and the like, the model of free particles moving in a potential well is most suitable for our use, for it produces a non-uniform and somewhat erratic system of energy levels (Fig. 1). It should be noted in particular that there occurs an anomalously large jump beyond the first G level. This level is just filled when the nucleus contains 58 particles of one kind. Irregularities may therefore be expected if the calculations are carried out for n around 58, n being the number of neutrons (or of protons). If sufficiently large deviations from the asymptotic formula can occur, they may explain (1) why the spacing of the levels found in actual nuclei do not show a unique trend with atomic number; (2) why many heavy nuclei do not absorb slow neutrons as abundantly as they should if their level density obeyed the asymptotic formula. Attention has first been called to this latter difficulty by Goudsmit;[7] it has again been emphasized by van Lier and Uhlenbeck.[4]

		Energy of level	No. of particles in level	Total No. of particles
ϵ_{10}				
ϵ_9	H			
ϵ_8	D	8.38	10	68
ϵ_7	G	6.78	18	58
ϵ_6	P	6.04	6	40
ϵ_5	F	4.94	14	34
ϵ_4	S	4.00	2	20
ϵ_3	D	3.37	10	18
ϵ_2	P	2.04	6	8
ϵ_1	S	1.00	2	2

FIG. 1. Arrangement of first ten individual particle energies in accordance with the model of a spherical potential well. Energies are given as multiples of ϵ_1, the energy of the lowest level above the bottom of the well.

TEMPERATURE AND LEVEL DENSITY FOR AN ASSEMBLY CONTAINING ONE TYPE OF PARTICLE

The points to be discussed are easily seen in connection with a simplified assembly, containing n particles, all of the same kind. The ϵ_i are given in Fig. 1. The unit of energy is taken to be ϵ_1, the separation of the lowest level from the bottom of the well. This unit depends on the radius of the well R and on the height of its wall. For an infinitely deep potential well

$$\epsilon_1=\frac{h^2}{8MR^2}=\frac{2.06}{r^2}\times 10^{-24}\text{ Mev if } r \text{ is in cm},$$

where M is the mass of a single particle. If the wall is of finite height, the relative positions of the levels are not appreciably altered,[8] but the unit ϵ_1 becomes somewhat smaller. Thus both cases can be treated at once if ϵ_1 is not regarded as fixed.

The statistical problem is best solved by the method of Darwin and Fowler, as was done by van Lier and Uhlenbeck.[4] Suppose one is dealing with n particles and a total energy $E=E_0+U$, where E_0 is the smallest energy which n particles

[7] S. Goudsmit, Phys. Rev. **51**, 64 (1937).
[8] H. Margenau, Phys. Rev. **46**, 613 (1934).

may possess in accordance with the scheme of Fig. 1, and U the excitation energy. It is then necessary to find two numbers, a and b, such that

$$\sum_i \frac{g_i}{1+ab^{\epsilon_i}}=n, \quad \sum_i \frac{g_i\epsilon_i}{1+ab^{\epsilon_i}}=E. \tag{1}$$

In these formulas g_i represents the number of particles which the ith level is capable of containing. With these two constants we then compute four other quantities:

$$\begin{aligned} R&=\textstyle\sum_i g_i \log (1+a^{-1}b^{-\epsilon_i});\\ A&=\textstyle\sum_i g_i ab^{\epsilon_i}(1+ab^{\epsilon_i})^{-2};\\ B&=\textstyle\sum_i g_i ab^{\epsilon_i}\epsilon_i(1+ab^{\epsilon_i})^{-2};\\ C&=\textstyle\sum_i g_i ab^{\epsilon_i}\epsilon_i^2(1+ab^{\epsilon_i})^{-2}. \end{aligned} \tag{2}$$

In terms of these,

$$\rho=e^R a^n b^E/2\pi(AC-B^2)^{\frac{1}{2}}. \tag{3}$$

The connection between b and the temperature T is simply

$$\log b=1/kT. \tag{4}$$

A, B, and C appear in the integration across the saddle point;[4] the greater their values, the steeper is the descent from the saddle point. In fact, formula (3) is valid only if A, B, $C\gg 1$. In the nuclear problem this is not always true for the quantity A. The present calculations, for instance, yield values of A around 2. This means that the denominator of (3) is no longer to be trusted in detail, i.e., that the additive term in the entropy $S=\log\rho$—which is of little interest in ordinary thermodynamics—is not given accurately by the present method, or any of the methods proposed thus far.

When the quantities (2) are evaluated in the usual way by integration, a being assumed very large, Eq. (3) goes over into Bethe's:[1]

$$\rho=48^{-\frac{1}{2}}U^{-1}\exp(2U/kT'), \tag{5}$$

provided kT' is defined as in the theory of metals,

$$kT'=(2/\pi)(\xi_0 U/n)^{\frac{1}{2}}. \tag{6}$$

The characteristic energy, ξ_0, is defined, for instance, in Bethe's paper; it is a function of ϵ_1 and n.

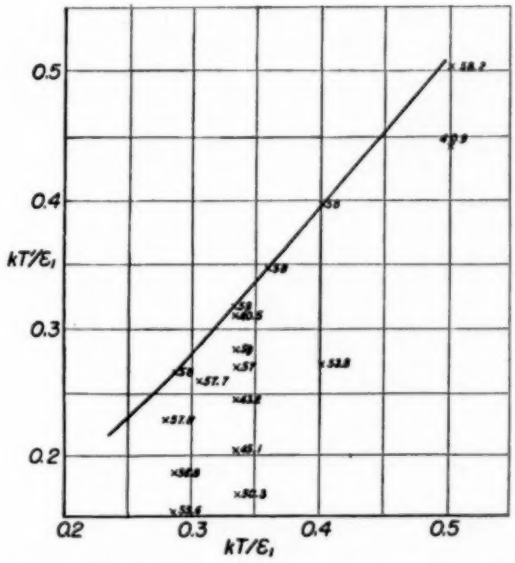

FIG. 2. Comparison of temperatures T', as computed by means of the asymptotic formula, with temperatures T computed by evaluating the summations. Curve connects points for which $n=58$. Numbers appearing near points give values of n.

Perhaps it is of interest first to compare the true temperature, as given by (4) after numerical computation of a, with the asymptotic values given by (6), for some choices of n and E. This is done in Fig. 2. It will be seen that T' and T are most nearly equal for the closed shell value $n=58$ and that they depart from equality very considerably for smaller n. The closed shell, value $n=40$ causes them to approach equality again. The values of U are not specified on this graph. In the computations from which this and the following figures have been constructed, care was taken to deal rather thoroughly with the case $n=58$ and the parameters a and b were adjusted, by repeated trials, to yield this value of n. In the other choices we have been satisfied with nonintegral n which, though they have no physical meaning, indicate the trends equally well.

In Fig. 3 the dependence of excitation energy on the true temperature for various values of n is shown. Again, the deviations from the asymptotic formula (6), which is also plotted as kT' *vs.* U, are quite appreciable, although the curve for any given value of n is roughly parallel to that corresponding to (6).

The main results are given in Fig. 4, where the natural logarithm of the numerator of Eq. (3)

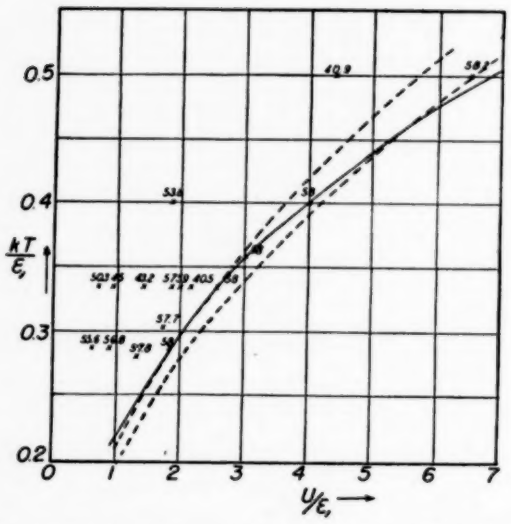

FIG. 3. Nuclear temperature T as function of excitation energy U. Numbers appearing near points give values of n. Solid line connects points for which $n=58$. Dotted lines represent limits within which the points should fall in accordance with the asymptotic formula; the upper dotted line corresponds to $n=40$, the lower to $n=60$.

is plotted against U. The denominator of ρ is fairly regular and differs insignificantly from the corresponding factor in (5), that is by no more than a factor of 2. Since it is not accurate anyway, we shall not discuss it further. If the asymptotic formula were correct, all points computed should lie within the shaded region of Fig. 4, the upper boundary of which represents $2U/kT'$ in accordance with (5) and (6) and computed from $n=60$, the lower for $n=40$. The points are scattered very widely. The solid line represents the locus of S *vs.* U for $n=58$. In the region here considered it lies below the Bethe curve by more than 5 units, which means that the density as given by (5) is about $e^5 \cong 150$ times too high. As we depart from the closed-shell value, $n=58$, in either direction, the points move upward; they cross the shaded region and reach a maximum boundary approximately 5 units above the Bethe curve when n is somewhere near the middle of the closed shell; after that they move down again until the closed shell value $n=40$ finds them once more below the shaded region, though not as low as for $n=58$.

In this discussion the effect of the scale factor ϵ_1 must not be forgotten. Since R decreases with decreasing n, ϵ_1 increases so that the points for smaller n in Fig. 4 belong to larger excitation energies. This fact does not, however, account even approximately for the rise of the points as we proceed from $n=58$ downward. Assuming, for instance, that $R \propto n^{\frac{1}{2}}$ we see that in passing from $n=58$ to 57, the scale factor ϵ_1 changes by less than 2 percent; from the slope of the solid curve near $U/\epsilon_1=2$ this would cause an increase in S of about 0.1 unit, whereas the actual increase is about 1.

Two Types of Particle

In generalizing the formula for the level density to apply to an assembly containing two types of noncombining particles we may assume, without great detriment to our conclusions, that the total number of particles is $2n$; the number of neutrons is taken to be equal to the number of protons. Physically, the only change which must then be made in the former situation is this: To the temperature discussed above there now corresponds an excitation energy U which is twice as great as before, one-half belonging to the neutrons, one-half to the protons. This explains qualitatively the changes which occur

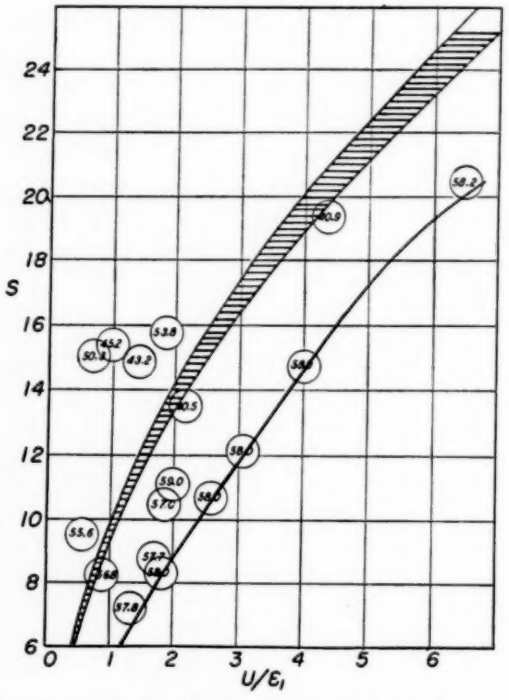

FIG. 4. Logarithm of the density of levels (S) *vs.* excitation energy U. Solid line connects points for which $n=58$. Centers of circles represent points having n equal to the numbers appearing in circles. According to asymptotic formulas, all points should fall within shaded region.

in formula (3), except for the new multiplying factor:[4]

$$\rho = e^{2R} a^{2n} b^E / 4\pi^{\frac{1}{2}} A^{\frac{1}{4}} (AC - B^2)^{\frac{1}{4}}. \quad (7)$$

When the usual approximations are made, this reduces to Bethe's formula,[9] the exponential part of which reads:

$$\rho \propto \exp\left[\pi (2nU/\xi_0)^{\frac{1}{2}}\right]. \quad (8)$$

Formula (7) represents the total level density, regardless of angular momentum. For comparison with experiment, it is more interesting to know the density of all levels with a given angular momentum. An approximate formula for this has also been worked out by Bethe.[1] We note here that the latter density is proportional to the former. The following remarks concerning the deviations from (7) and (8) refer, therefore, to the densities for fixed angular momentum also.

In studying these formulas we again confine our attention to the exponential parts. Then no calculations beyond those of the former section are required. For if we take U to be $2U_1$ and interpret U_1 as the excitation energy of, say, the neutrons, the exponent in (8) is simply twice that in (5) (with U replaced by U_1). Similarly, if E in (7) is taken to be twice E_1, the total energy of the neutrons, then the numerator in (7) is the square of the one in (3) (with E replaced by E_1).

When it is desired, for instance, to find the density on the free particle model of a nucleus composed of 58 neutrons and 58 protons at an excitation energy of 8 Mev, we look up ρ in Fig. 4 for $n=58$ and an excitation energy of 4 Mev, then square this value. If we assume, following Bethe,[10] that $R=2(2n)^{\frac{1}{3}}\times 10^{-13}$ cm, the value of R in this case is $\approx 10^{-12}$ cm, so that $\epsilon_1 = 2$ Mev. An excitation energy of 4 Mev therefore corresponds to $U_1/\epsilon_1 = 2$. In this region we find a discrepancy by a factor $e^{5.4}$ between the computed points and the asymptotic formula, the latter giving too high a density. For the nucleus in question the density given by the asymptotic formula would therefore be in error by a factor $e^{10.8}$ or nearly 50,000. At $n=54$, and for the same excitation energy, the error would be by a factor 50 in the other direction.

The reason for such discrepancies as these is easily seen when the formulas used in the derivation of (8) are examined. To exhibit only one example: The relation $E=\frac{3}{2}kTR$, which is used in passing from (7) to (8), is valid if no other assumption is made than that the summations in E and R may be converted into integrations. Nevertheless the use of this simple relation leads to errors of $50\epsilon_1$ in $E \approx 280\epsilon_1$.

It is not believed that the calculations here presented have any exact numerical significance because the model of free particles within a potential well, here chosen, is as poor an approximation to reality as any other simple model. We regard it as certain, in fact, that the density given by Bethe's formula represents a fairly accurate mean over large ranges of atomic numbers, as the present analysis indicates. The reason for this is to be seen in the fact that the "simple particle" levels of an actual nucleus are more numerous (because the degeneracies of the ϵ_i have been removed) than the ones here assumed, and in the circumstance that the first ϵ_i which can be filled on excitation is just as likely to be abnormally low as abnormally high. Even the fluctuations about the asymptotic formula calculated here are probably too large for similar reasons.

But even if they are reduced by a very considerable amount, they are significant in these respects. They indicate that group structure, if it exists, has a large influence on the spacing of nuclear levels; that exact agreement of experimental data with formulas like (8) should not be expected. They also explain the relative rarity of slow neutron absorbers among heavy elements all of which should have an extremely high density of levels and therefore be capable of strong absorption if (8) were valid. Thus (8) predicts a decrease in level spacing by a factor 1000 as one passes from atomic weight ≈ 100 to 200 for excitation energies corresponding to capture of slow neutrons.[10] But it is known from the work of Goldsmith and Rasetti[11] that the

[9] This may still be written in the form $\exp[2U/kT']$, like (5), but the temperature is now given by $kT' = (2/\pi) \times (U/2n)^{1/2}$.

[10] H. Bethe, Rev. Mod. Phys. **9**, 85 (1937).

[11] H. H. Goldsmith and F. Rasetti, Phys. Rev. **50**, 328 (1936). W. J. Horvath and E. O. Salant, Phys. Rev. **59**, 154 (1941), have recently found a spacing of about 30 volts for Co^{59} by determining the absorption of resonance neu-

level spacing for nuclei with $A \approx 100$ is a few volts, hence it should be a few millivolts for heavy nuclei. It is difficult to see why these should not capture slow neutrons very abundantly. The present considerations indicate how this difficulty may be removed. If the nuclear radius, or some equivalent parameter, were so adjusted that only the elements whose points lie high above the asymptotic curve in Fig. 4 possess a sufficiently large ρ to be strong neutron absorbers, there would be many elements of insufficient ρ interspersed between the absorbers.

trons. It is interesting to note that experiments of W. L. Davidson, Jr., (unpublished), who determined the levels of Co^{60} and several other neighboring elements by deuteron bombardment, found spacings around 1.25 Mev in the neighborhood of $U \approx 3$ Mev. Theory would predict a ratio of about 400 for the spacings in cobalt at $U = 3$ Mev and 8 Mev, whereas the data cited yield about 40,000. Whether this discordance can be removed by supposing that the bombardment experiments yield only a small fraction of the total number of levels (cf. in this connection E. Pollard, Phys. Rev. **59**, 466 A (1941)) remains to be seen.

APRIL 15, 1941 PHYSICAL REVIEW VOLUME 59

Intensity Measurements in the Molecular Spectrum of Hydrogen

N. GINSBURG AND G. H. DIEKE
Johns Hopkins University, Baltimore, Maryland

(Received September 13, 1940)

Quantitative intensity measurements were made in the visible and infra-red of the H_2 spectrum for different conditions in the discharge tube. The present paper reports on the Fulcher bands. It appears that at the lower pressures no equilibrium exists and that therefore the concept of temperature has no meaning. By varying the pressure and current in the discharge tube the effective rotational temperature can be varied from 240°K to 1500°K. Whereas higher rotational states are favored with an increase in pressure, the higher vibrational states are suppressed, and this effect is largely independent of the current. From the behavior of the relative intensities with pressure and current density conclusions can be drawn regarding the elementary processes in the discharge. The results show that extreme care must be used when intensity measurements in band spectra are used for temperature measurements. Apart from the fact that the conditions in the discharge tube may be far from equilibrium, our results on the *P*- and *R*-branches show that the transition probabilities may be quite different, even in simple bands, from the values predicted by the elementary theory.

1. INTRODUCTION

THE present paper gives some measurements of the changes in intensity of the lines of the Fulcher bands in hydrogen as the conditions in the discharge tube are varied, as the first part of a general survey of the intensities in the H_2 spectrum. The main purpose of the investigation was to relate these changes of intensity to the classification of the lines in the hope that the extension of such measurements to other lines would be helpful for the further analysis of the spectrum. We chose the Fulcher bands because of their relatively simple structure and the likelihood that by selecting particularly simple cases first we could get at least a qualitative picture of what happens in more complex cases. In carrying out these measurements we have adopted a reasonable compromise between high precision and extensiveness of the survey. We have taken all reasonable precautions to secure accuracy, but have made no effort to maintain the ultimate precision.

The first and only extensive quantitative intensity measurements were made by Ornstein, Kapuscinski and Eymers[1] and Kapuscinski and Eymers[2] on the stronger lines below 6441A.

As most of the stronger unclassified lines lie in the infra-red, it is very desirable to extend the measurements into the infra-red as far as possible, particularly since no quantitative intensity measurments of any kind exist beyond 6441A, and intensity estimates give no indication of the strength of the infra-red lines as compared to that of the visible lines.

However, the *changes* in the relative intensities

[1] L. S. Ornstein, W. Kapuscinski and J. G. Eymers, Proc. Roy. Soc. **A119**, 83 (1928).
[2] W. Kapuscinski and J. G. Eymers, Proc. Roy. Soc. **A122**, 58 (1929).

of the lines when the conditions in the discharge tube are altered are of more significance for the classification of the lines than the intensities themselves. Previous measurements of such changes[3,4] were all of a qualitative nature[5] and did not include the infra-red. Because the classification of the spectrum was then only imperfectly known, the nature of the observed changes could not be well ascertained. But even these qualitative observations have proved to be of great help in the classification of the H_2 spectrum.[4]

The study of the intensity distribution in a band system as a function of the conditions in the discharge tube proves a very effective and promising way for the analysis of the elementary processes in an electrical discharge. Some of our results are only tentative and should be checked by experiments especially designed for the particular purpose. The H_2 spectrum is particularly suited for such experiments, as several well-developed band systems occur with all bands perfectly resolved in a spectrograph of medium or even small size.

2. Experimental Arrangement.

Spectrograph

For our measurements we chose a 15-foot concave grating spectrograph with a dispersion of 3.6A per mm. With this instrument the lines are satisfactorily resolved even when a wide slit (convenient for intensity measurements) is used. The astigmatism of the grating when corrected in the middle of the plate by a cylindrical lens between slit and grating, was small enough to be harmless over the portion of the plate actually used.

Discharge

The discharge tube, which was of the type used in this laboratory for wave-length measurements[6] was entirely of fused quartz and was water-cooled. The horizontal part was 42 cm long with an internal diameter of 5.5 mm and was viewed end on. Guided by the experience of others and by preliminary experiments, we carried out the measurements under the following five conditions:

Symbol	p	Current	Voltage Source
L	0.06 mm	0.014 amp.	30,000-v spark coil
N	0.2	0.4	5,200-v transformer
H	20	0.4	13,500-v transformer
H′	20	0.04	13,500-v transformer
He	0.2 mm of H_2 in 150 mm of He		13,500-v transformer

The symbols L to He will be used throughout this paper to designate these types of discharge.

The pressures were measured when the tube was not in operation and are, therefore, directly proportional to the density of the gas. To reduce the dead volume, the tube, during operation, was shut off from the McLeod gauge and pump. Nevertheless that volume was not negligible and the densities during operation are slightly less than those corresponding to the given pressures.

Calibration of the plates

Intensity marks were applied to the plates in much the same way as by Ornstein, Kapuscinski and Eymers. The light from a tungsten filament fell on a step slit with six openings of from 0.169 to 4.08 mm width, and produced continuous spectra, the intensity of which was proportional to the width of the respective slits. These spectra were, of course, on the same plate as the H_2 spectrum and had the same exposure time. The intensity of the standard lamp was cut down when necessary by means of a rotating sector with two openings, the speed being adjusted to interrupt the light about 120 times per second, which is also the frequency of the light in the hydrogen discharge. These continuous spectra were photometered[7] about every 20 mm on each plate to obtain the calibration curves.

The standard tungsten lamp used for most of the work originated in the laboratory of the N. V. Philips Gloeilampenfabriek in Eindhoven, Holland, and was calibrated by Dr. W. de Groot in 1929, so that the intensity distribution as function of the wave-length was known. This enabled us to correct for the variations of the

[3] T. R. Merton and S. Barratt, Phil. Trans. Roy. Soc. **A222**, 369 (1922); J. C. McLennan, H. Grayson-Smith and W. T. Collins, Proc. Roy. Soc. **A116**, 277 (1927).

[4] For others, see O. W. Richardson, *Molecular Hydrogen and its Spectrum* (New Haven, 1934).

[5] Some measurements by F. Goos[3] on the change of the intensities in a limited part of the spectrum form a notable exception. They will be discussed later on in this paper.

[6] G. H. Dieke and R. W. Blue, Phys. Rev. **47**, 261 (1935).

[7] The construction of the microphotometer used in this work was aided by a grant from the Rumford Committee of the American Academy of Arts and Sciences, which we acknowledge gratefully. The photometer employs a photronic cell, and it was constructed in such a way that a continuous record of a 15-inch-long plate can be taken.

TABLE I. *Fulcher bands $2p^3\Pi \rightarrow 2s^3\Sigma$. Intensities of Q branches.*

K	L	N	H	K	L	N	H	K	H′	He	L	N	H
							0→0					0→1	
1					323	202	60	173.0	110.6	35.6	21.4	10.1	
2					61.5	47.3	25.4	47.0	38.2	174.	4.6	3.0	
3					81.1	81.1	81.1	81.1	81.5	81.1	5.9	5.5	
4					8.7	10.7	24.0	18.5	17.5	19.0	2.4	5.3	
5					8.6	13.2	57.6	21.3	22.9	55.2		1.6	
6							13.5			15.0			
7					1.8	4.9	24.2		6.5	28.8			
8							5.5			8.3			
9						3.2	13.0			19.4			
			1→0				1→1					1→2	
1		14.7	6.1	43.6	391	166	46.9	152.0	86.8	5.9	28.2	24.1	6.2
2		3.5	2.9	10.9	75.4	43.8	23.5	51.0	35.4	4.8	15.8	6.4	3.7
3		15.9	7.0	16.0	77	74.5	96.2	78.7	77.4	15.0	23.2*c*	26.9*c*	21.3*c*
4		1.1	3.3		21.6	8.9	11.9	17.9	16.8	4.7			3.5
5			5.5		1.6	10.7	47.0	19.6	20.4	10.2		1.9	6.9
6			2.4			2.3	12.0			3.6			
7			3.1			3.9	21.0		6.5	7.1		1.7	3.4
8						1.3	4.9			2.9			
9						3.6	9.1			5.0			
			2→1				2→2					2→3	
1		23.2	6.7	60.9	382	154	32.9	137.0	66.0	2.9	199	31.6	7.5
2		8.5	5.0	38.8	68.5	37.5	15.8	44.5	23.6	6.1	31.5	9.4	3.4
3		10.0	9.5	30.0	84.2	59.7	48.1	68.0	48.2	3.9	29.0	15.0	10.5
4		1.7	3.6	4.0	10.1	7.5	14.5	15.8	11.3		4.9	2.6	3.5
5		1.9	6.6	3.8	7.7	10.9	33.3	16.4	14.9	4.5		2.8	7.1
6			2.6			1.4	7.4					.59	2.2
7		1.2	4.0		1.7	2.8	14.6		7.7			.91	3.6
8						.91	3.3						
			3→2				3→3					3→4	
1	57.5*c*	24.1*c*	6.9*c*	73.5*c*	216	101	17.0	91.0	34.7		165	27.4	6.4
2	14.8	6.1	3.2	20.0	39.7	22.4	8.0	32.1	13.4		24.0	8.3	3.4
3	15.5	8.3	6.5	26.3	40.0	31.3	20.2	44.2	21.4		28.9	11.7	7.8
4	6.1*c*	3.8*c*	4.2*c*	17.3*c*	3.1	2.5	5.8				5.7	1.2	
5	2.9	1.3	3.5	2.5	3.1	4.7	17.5	9.6	10.8			1.4	4.4
6													
7						1.1	4.8					.61	2.2
8						.49	1.7					.43	
			4→3				4→4					4→5	
1	22.7	11.0	3.5	26.5	48.5	26.8	6.2	29.6			108	17.1	12.0
2	5.6	3.6	3.5	7.7	9.9	5.0	3.0	12.8			8.5	3.2	2.0
3	6.3*c*	4.6	5.0	13.0	10.6	8.0	9.5	18.0			17.7*c*	7.8	6.4
4	2.7*c*	3.0*c*	*c*	7.1*c*	1.6	1.3	2.8					1.2	2.3
5	1.7*c*	1.1*c*	3.5*c*		1.3	1.2	5.3					1.0	3.2
6						.51	1.9					1.2	2.9
7					1.9*c*	.85	2.4						
			5→4				5→5					5→6	
1	15.4*c*	6.2	3.0		19.2		3.3				29.7	10.0	3.0
2	2.7*c*	1.9			4.7	2.6	1.9				5.9	2.5	2.2
3	3.7	2.9	3.2		5.6	3.9	4.1				7.1	3.8	3.9
4		1.8										.91	2.1
5											*c*	*c*	*c*
			6→5									6→7	
1	7.6	3.9	2.1								14.9	5.7	2.3
2	1.9	1.2										1.8	
3	1.8	1.6	2.7									2.9*c*	

sensitivity of the photographic plates with wavelength. When doubts arose as to the correctness of the calibration, we obtained, through the courtesy of Dr. W. E. Forsythe, another calibrated tungsten lamp which had been calibrated in the G. E. Laboratories by Dr. B. T. Barnes. We compared this lamp with the Eindhoven lamp and found that the results obtained with the two lamps agreed within the limits of experimental errors.

TABLE II. *Intensities of P and R branches.*

K''	L	N	H	K	L	N	H	K	H′	He	L	N	H
							0→0					0→1	
							P branch					*P branch*	
2					39.3	21.6	13.4	24.4	20.3	5.8	9.4	4.2	
3					131.0	90	36.5	67.0	56.3	23.3	7.3	3.7	2.2
4					28.8	24.9	15.8	29.5	20.8	11.4	4.8		
5					31.6	36.0	41.9	36.0	35.9	29.5		1.9	2.2
6					8.5	7.4	18.8	12.9	17.2	10.3			
7					6.7	7.8	26.1	11.7	14.6	23.8		0.74	1.8
8						1.6	6.3			7.2			
9					1.9	3.2	13.0						
							R branch					*R branch*	
0					68.6	37.0	12.1	40.0	25.6	8.4	18.4	4.9	
1					179	130	63	120.0	85.1	28.6	14.3	8.6	
2					30.3*c*	29.3*c*	31.7*c*	34.7*c*	34.2	29.5*c*	5.5*c*	3.5*c*	
3					29.1	29.9	35.1	38.0	29.5	25.5		3.7	
4					6.7	5.2	9.4	10.1	10.3	9.0			
5					3.5	6.2	17.9	10.8	10.2	17.3			
6							5.6			7.6			
7							8.1			10.5			
			1→0				1→1					1→2	
			P branch				*P branch*					*P branch*	
2		2.0		4.9	51.6	22.5	8.0	27.4	14.4	8.1	142*c*	25.8*c*	6.4*c*
3		5.7	3.3	14.1	159	85.6	30.6	69.0	51.1	15.5	45.5	12.3	4.7
4					22.2	14.5	12.2	20.6	17.4	2.3	*c*	*c*	*c*
			R branch				*R branch*					*R branch*	
0		5.0*c*	2.9	13.7*c*	95.2	40	10.3	44.1	23.7	2.8	14.8	5.1	
1		8.3	4.4	27.0	2.1	113	39.4		70.9	6.5	19.8*c*	13.0*c*	
2		1.9	2.2	5.3	31.5	23.4	27.9	32.2	33.6	4.0	5.2	1.6	
3				4.5			12.0			19.3			
			2→1				2→2					2→3	
			P branch				*P branch*					*P branch*	
2		3.4		9.9	49.8	20.4	5.1	26.3	11.9		14.7	8.1*c*	
3		10.5	5.0	32.7	121	65.0	20.6	64.3	33.0		38.5	9.5	3.3
4	4.3	2.6	2.9	7.3	23.1	18.1	25.7	25.2	17.0		11.6	4.1	2.6
5	*c*	*c*	4.1*c*	*c*	27.4	23.0	22.2	32.5	20.5		6.5	3.3	3.7
6		1.6*c*	3.8	2.5*c*								0.84	
					8.7	6.2	14.6	16.2					
			R branch				*R branch*					*R branch*	
0		5.5	2.6	15.7	78.4	33.9	7.5	37.5	17.5		44.0	10.5	3.8
1		11.9	5.9	43.0*c*	87.9	69.1	22.7	69.3	36.4		27.8*c*	23.7	10.1
2			2.5	6.7	23.6	11.6	7.4	21.7	9.5		9.4	4.2	2.6
3		3.3	4.5	9.0	26.1	16.1	17.7	28.0	16.6	2.7	10.1	6.5	6.4
4					5.2	3.5	10.4	11.3	7.2	3.4		1.6	
5									6.4			1.8	
			3→2				3→3					3→4	
			P branch				*P branch*					*P branch*	
2	10.2	3.1		8.6	26.3	6.8	2.5	15.8	6.8		8.9	2.1	
3	28.6	11.3	4.0	30.0	90.5	44.6	11.0	48.5			29.0	8.1	2.8
4	5.1	2.8		7.8	16.9	9.4	5.0	16.1			11.6*c*	49*c*	4.2*c*
			R branch				*R branch*					*R branch*	
0	19.0	5.3	2.6	25.1	39.9	17.1	4.0	21.4	9.5		55.8	8.4	7.6*c*
1	27.8	10.5	4.2	32.7	86.6	41.3	12.3	46.3	17.5		101	23.3	5.7
2	13.0	5.8	3.8	24.9	14.3	7.8	4.3	15.0	7.4		142*c*	25.8*c*	6.4*c*
3						0.56	2.8						

The photographic plates used were the Eastman spectroscopic plates best suited for the various regions. In the infra-red it was necessary to hypersensitize the plates with ammonia. This causes a greater chance for irregularities in that region, which could not be avoided, as without the hypersensitization the plates were too slow. However, the hypersensitization was never pushed to the limit, so that the plates were free from fog. Comparison of different plates in the same region showed that big irregularities did not occur.

The relative intensities derived from the plates were on an arbitrary scale which was different for

TABLE III. *Values of σ and T′ for the main Fulcher bands.*

	p IN MM	CURRENT IN MA	0→0		1→1		2→2		3→3		4→4	
			σ	T'	σ	T'	σ	T'	σ	T'	σ	T'
L	0.06	14	0.178	237	0.205	200	0.183	207	0.207	173	0.174	193
N	0.2	400	0.145	290	0.148	271	0.147	258	0.170	210	0.151	222
K	0.17	33	0.119	353	0.119	337	0.120	316	0.127	281		
H′	20	40	0.101	417	0.0972	413	0.0956	397	0.0882	405		
H	20	400	0.0474	888	0.0616	652	0.0467	812	0.0520	687	0.0505	664
He*	0.2 in	400	0.0326	1290	0.0321	1250	0.0307	1240				
He*	150 mm He	400	0.0276	1524								

* The He values are obtained from two different plates taken under slightly different conditions. The lower one is the better plate but contains only the 0→0 band.

each plate. In order to simplify comparison of different plates and also to compare our results with those of Kapuscinski and Eymers, all the results were adjusted to a common scale which was, as much as possible, identical with that of Kapuscinski and Eymers. For this purpose the line $Q(3)$ of the 0→0 Fulcher band ($3p^3\Pi \rightarrow 2s^3\Sigma$) at 6031.900A was taken as the standard line and as its intensity, taken arbitrarily, the value 81.1 of Kapuscinski and Eymers. All intensity values on the different plates were multiplied by a constant factor so that they would agree with this scale. The choice of this intensity standard for plates taken under different conditions is nothing but a convenience and has the result that the average intensity of all the lines is roughly the same.

As the infra-red beyond 7500A could not be compared directly with the standard because one plate covers, at most, a region of 1500A, it was necessary to establish some intermediate standards in the region around 7000A. For this purpose the lines $Q(3)$ of the 0→1 and 1→2 Fulcher bands at 7105.846A and 7179.376A were taken, as their intensity compared to that of the $Q(3)$ lines in the 0→0 and 1→1 bands should be independent of the discharge conditions. These lines were carefully compared with the Fulcher lines around 6000A.

In view of the different adjustments necessary it is obvious that, in general, the relative intensities in a narrow spectral region taken on one plate are more reliable than those over a wide region. As the strong lines were overexposed on a plate which showed the weak lines to best advantage, and vice versa, it was necessary to take in general a weak, a medium, and a strong exposure for each region. In general the figures given do not represent averages of several plates but the actual value of the best plate in the particular region in question, as we found that, especially for the low pressures, the unsteadiness of the discharge is the greatest source of errors. To average two plates taken at slightly different discharge conditions would give less consistent results than to take only one plate, although the mean error is slightly larger. Again, this makes the situation less favorable for the intensities of lines lying in widely different parts of the spectrum than for closely adjacent lines.

3. RESULTS

Our measurements were carried out in the wave-length interval from 5500–8900A. The interval from 5500 to 6400A which is covered both by us and Kapuscinski and Eymers gives ample opportunity to compare the two sets of measurements.

For most of the spectrum, measurements are available only for the three discharges L, N and H mentioned in §2, except for the measurements of Kapuscinski and Eymers for the visible. For the diagonal Fulcher bands we have also the measurements at high pressure and low current density (H′), and those in a mixture of hydrogen and helium (He). Furthermore, there exist for these bands the measurements of Goos[8] for varying pressures and temperatures.

Tables I and II give the intensities measured in the types of discharges mentioned in §2. Furthermore, they include the intensity values of Kapuscinski and Eymers (K) where they are available. A c attached to an intensity value means that the line is known to be superimposed

[8] F. Goos, Zeits. f. Physik **31**, 229 (1924).

TABLE IV. *Comparison between observed and calculated intensities Q branch of 0→0 band*

	L		N		H		H′		K		He	
K	CALC.	OBS.	CALC.	OBS.	CALC.	OBS.	CALC.	OBS.	CALC.	OBS.	CALC.	OBS.
1	219	323	171.9	202	56.8	60.0	104.7	110.6	200.0	173.0	37.8	38.7
2	59.7	61.5	53.4	47.3	26.1	25.4	38.8	38.2	63.2	47.0	18.8	20.4
3	86.2	81.1	93.8	81.1	82.5	81.1	88.8	81.5	113.8	81.1	66.8	81.1
4	8.9	8.7	12.6	10.7	24.2	24.0	20.0	17.5	15.8	18.5	22.9	22.4
5	8.2,	8.6	10.8	13.2	55.2	57.6	22.6	22.9	14.1	21.3	63.8	58.5
6			0.73		12.3		2.7		1.0		18.1	18.0
7							2.2	6.5			42.4	40.0
8											10.3	11.1

by, or confused with, another line and that therefore these values are less reliable. There may be, of course, many unrecognized blends with as yet unclassified lines. Whereas the wavelength measurements of such blends are only slightly affected, the intensities may be completely wrong. A strongly abnormal intensity will in general be an indication that such a blend exists. (See, e.g., the discussion of Table XI). Except for unfavorable lines we can reproduce the measurements to within five percent.

A direct comparison of the measurements of Kapuscinski and Eymers with ours is difficult because they were taken under different conditions. However, by comparing pairs of lines in the red and green which have the same initial state, the relative intensities of which should not be affected by the discharge conditions, we find that the green compared to the red is from two to three times stronger in the K and E measurements than in ours. We assured ourselves that neither our tungsten comparison lamp nor the small remnant astigmatism of our spectrograph could be the cause of the discrepancy. We are at a loss to account for it.

4. THE *Q* BRANCHES

DETERMINATION OF ROTATIONAL TEMPERATURES

If there is thermal equilibrium, the number of molecules in a given rotational state characterized by the rotational quantum number K is proportional to $e^{-E_K/kT}$. These numbers multiplied by a so-called intensity factor involving the *a priori* probability of the state and the transition probability will give the relative intensities in a given band.

For the determination of the temperature from band spectrum intensities, it is assumed that the intensity factors are known and that there is actually thermal equilibrium. We shall see that neither of these conditions is even approximately satisfied in some cases.

The intensity factors are well-known simple functions of K for the standard types of coupling. However, they are affected when interaction with other electronic states occurs, and in many cases more so than the frequencies. Therefore it is advantageous to begin by investigating lines where this interaction is a minimum and this is the case for the Q-branches of the Fulcher bands.[9]

For a Q-branch of a $\Pi\rightarrow\Sigma$ transition the intensities are proportional to $(2K+1)e^{-E_K/kT}$ where, with sufficient approximation,[10] the energy of the initial state is

$$E_K=\text{const.}+\frac{h^2}{8\pi^2\mu r^2}K(K+1)$$
$$=\text{const.}+B_VK(K+1).$$

If we let

$$\sigma=B_V/kT,$$

then the intensities can be written

$$I(K)=A(2K+1)e^{-\sigma K(K+1)},$$

where A is a constant factor independent of K. We must take into account the intensity alternations which, in the H_2 spectrum, cause successive lines in any band to alternate in the ratio 3 : 1. In the following considerations the in-

[9] G. H. Dieke, Phys. Rev. **48**, 610 (1935).

[10] If there is any need for greater accuracy the actual empirical values for the energy may be used. This would make the computations slightly more bothersome, but not greatly so. However, the increase in accuracy obtained in this way is insignificant compared to the uncertainties due to other causes.

TABLE V. *Effective rotational temperatures computed from Goos' data.*

T	Pressure in mm Actual p	$p_{295°}$	Current in ma	0→0 σ	0→0 T'	1→1 σ	1→1 T'	2→2 σ	2→2 T'	3→3 σ	3→3 T'
87°	0.06	0.20	4.6	0.231	182	0.227	167	0.286	125		
	0.15	0.51	3.8	0.223	207	0.213	178	0.272	131	0.291	115
	0.69	2.36	3.9	0.188	224	0.159	239	0.241	148	0.281	119
	1.47	4.97	4.0	0.165	255	0.136	279	0.219	163		
295°	0.163	0.163	4.7	0.170	248	0.173	219	0.197	181	0.229	146
	0.326	0.326	3.9	0.162	260	0.163	233	0.198	180	0.213	157
	0.655	0.655	3.6	0.150	280	0.150	253	0.190	188	0.197	170
	1.36	1.36	3.4	0.132	319	0.128	296	0 178	201	0 199	168
495°	0.189	0.114	5.2	0.116	362	0.123	308	0.132	271	0.151	222
	0.41	0.24	3.8	0.102	412	0.109	348	0.129	277	0.141	238
	1.01	0.60	3.8	0.087	485	0.092	412	0.123	290	0.133	252
	2.41	1.47	3.8	0.079	532	0.084	452	0.112	319	0.120	279

tensities of all the weak lines (lines of para-hydrogen) are multiplied by 3 to make them directly comparable with the other lines. However, whenever possible, the ortho and para lines have not been mixed in any calculation, although doing so at the high temperatures employed here should not cause any appreciable error.

The temperature may be calculated in the following way:

$$\sigma K(K+1)=\ln A-\ln \frac{I}{2K+1}.$$

By subtracting this for two different values of K the unknown constant A is eliminated. In this way by using the first 5 lines of the various Q branches, the values of σ given in Table III were obtained.

The temperatures T' given in the table are obtained from the relation

$$T'=B/\sigma$$

where $B=h^2/8\pi^2\mu r^2$ is the value for the initial state of the emission. Then with this value of T' or σ the intensities of the lines were calculated, and Table IV shows the agreement between observed and calculated intensities of the 0→0 bands. This is quite satisfactory for the high pressure discharges (H, H′ and He) but far from satisfactory for the normal pressure (N and K). For the low pressure the agreement would be satisfactory if the first line were excluded. The significance of the agreement or the lack of it will be further discussed later.

The calculated temperature is not equal to the room temperature, and the increase above room temperature, which most values show, could easily be explained by saying that the discharge heats the gas and that therefore the temperature inside the discharge tube must be higher. This reasoning, however, does not explain the fact that T' for the low pressure discharge comes out to be 237° in the 0→0 band, more than 50° lower than room temperature. There can be little doubt that this is a real effect, as all the bands show it.

The explanation for the apparent discrepancy lies in the fact that the assumption of thermal equilibrium, necessary to carry out the calculations, is entirely inadequate for these cases. The question of whether or not there is thermal equilibrium in a gas discharge has been considered by many previous investigators, and several instances have been recorded where deviations from the equilibrium distribution were found. The problem has been discussed in detail by Oldenberg.[11] However, practically all these cases are concerned with rather abnormal conditions in the discharge tube, and we have here, perhaps, the first clear case of a decidedly non-equilibrium distribution of a simple diatomic gas in an ordinary discharge. Questions very similar to those treated here were investigated for OH by E. R. Lyman[12] with results partly similar to ours and partly reaching the opposite conclusions. A comparison of these results with ours is not directly possible because of the more complicated mechanism of excitation for the OH

[11] O. Oldenberg, Phys. Rev. **46**, 210 (1934), where the literature concerning the known cases is given.
[12] E. R. Lyman, Phys. Rev. **53**, 379 (1938).

bands. This is even more true for the results of Rieke[13] on HgH, although there are many points of similarity. Van Wijk[14] investigated this problem for the H_2 discharge with the help of intensity measurements in two violet bands with complicated structure, and came to the conclusion—undoubtedly justified in his case—that there are no serious deviations from the Boltzmann distribution.

As a knowledge of the rotational distribution is quite essential for an understanding of the intensity distribution in all band systems of the H_2 spectrum, we must discuss it somewhat in detail. We see the situation clearly by taking an extreme case where the pressure is so low that the molecule, after it has been excited, has no chance to make a collision before it radiates. The unexcited gas is at equilibrium and the molecules are distributed over the different rotational states as they should be for thermal equilibrium at room temperature. If a discharge is started in this gas the exciting electrons will bring the molecule into an excited state without, however, in first approximation, being able to change the angular momentum of the nuclei. The rotational distribution for the excited molecules is, therefore, still that which corresponds to room temperature equilibrium for the *unexcited* molecule. This is not the room temperature equilibrium for the excited state, which has a much larger moment of inertia. The rotational distribution is determined only by the quantity $\sigma = B/T$. If B changes by a factor $\frac{1}{2}$, the rotational distribution which has remained unchanged looks now like the rotational distribution for the excited molecule at half the room temperature. However, there is no longer equilibrium between rotation and translational motion. The translational temperature $T = 290$ is still room temperature whereas the rotational temperature is $T'_r = 145$. The concept of temperature in the usual sense is, of course, without any meaning.

In the H_2 molecule the B value of the excited $3p^3\Pi$ state is very nearly half that of the normal state, and if there were no collisions we would expect to obtain as the rotational temperature, which is the temperature measured from the rotational distribution in band spectra, just half the value of room temperature.

Actually there are collisions.[15] If nothing but an exchange of rotational and translational energy were concerned, the rotational temperature would be increased and the translational temperature decreased by the collisions until both are equal, or if the collisions with the walls of the vessel are more effective, until the rotational temperature is back to room temperature.

However, in the process of excitation the molecule also has acquired electronic and vibrational energy and the latter especially is capable of being transformed into rotational and translational energy (temperature motion) during a collision.[16] Therefore the temperature of the gas will be increased above room temperature and the increase will be the greater the more collisions take place, i.e., the higher the gas pressure. Of course, there is no justification for speaking of a temperature as long as statistical equilibrium is not fully established. Unless that is the case the distribution over the different rotational states will not be according to Boltzmann's law. The temperatures computed above are only effective rotational temperatures and have the meaning that the actual rotational distribution is closest to the equilibrium (Boltzmann) distribution of that temperature. In the actual discharge tube

TABLE VI. *The intensities of the Fulcher bands. The sum of the intensities of all measured bands is 1510.*

V'	$V''=$ 0	1	2	3	4	5	6	7
0	355	21						
1	27	326	48					
2		46	261	61				
3			37	137	46			
4				19	35	25		
5					13	17	17	
6						7.8		11

[13] F. F. Rieke, J. Chem. Phys. **4**, 513 (1936); **5**, 831 (1937). See also W. Kapuscinski and J. G. Eymers, Zeits. f. Physik **54**, 246 (1929).

[14] W. R. van Wijk, Zeits. f. Physik **75**, 584 (1932).

[15] It is not possible to calculate the number of collisions which the excited molecules make, as the collision cross sections are unknown. It must be assumed that they are much larger than the gas kinetic cross section for the normal molecule.

[16] There are, in a discharge, other elementary processes than those discussed in this paper. In a complete analysis of the discharge the relative importance of all these processes would have to be ascertained. It is not our purpose to do this in the present paper. It is evident that a transfer of vibrational energy cannot be the only process causing an increase in temperature, as monatomic gases are also heated by an electrical discharge. It also must be kept in mind that the situation may be entirely different in other molecules, even in different band systems of H_2.

TABLE VII. *Relative intensities of the vibrational transition derived from the Q (1) lines. The intensity of the 0→0 band is taken as 100 in every case.*

	L	K	N	H′	H	He	$T=87°$				$T=295°$				$T=495°$			
$p_{mm}°$	0.06	0.2	0.2	20	20	150	0.20	0.51	2.36	5.0	0.16	0.33	0.66	1.36	0.11	0.24	0.60	1.47
0→0	100	100	100	100	100	100	100	100	100	100	100	100	100	100	100	100	100	100
1→1	121	88	82	79	78	17	128	111	109	104	108	106	102	100	113	108	103	100
2→2	118	79	76	60	55	8	125	118	114	104	101	100	98	94	105	104	98	92
3→3	67	53	50	31	28		88	77	85	76	71	58	56	57	72	66	60	57
4→4	15	17	13				24	22	32	36	23	23	25	31	23	23	25	26

we have, in addition, the fact that in a pulsating discharge the temperature will change with time and also that the temperature in the middle of the tube will be different from that at the walls, so that the calculated effective temperatures are time and space averages.

Notwithstanding these limitations the effective temperatures are quite useful for a rough description of the state of the gas. Table III shows that the behavior of the actual gas is just what must be expected. At an infinitely low pressure the observed effective temperature should be about 145°K. Collisions have increased this value to 237°K for the lowest observed pressure, and the fact that this value is below room temperature shows that we must be far from equilibrium. The higher the pressure the more excitation energy will be transferred into rotational energy and the higher the temperature. It is noted that Kapuscinski and Eymers had a considerably higher temperature (353°K *vs.* 290°K) at slightly lower pressure and much lower current density than we had. That is easily explained by the fact that their discharge tube was quite different from ours. It had a much narrower capillary and was not water-cooled, so that the temperature would be expected to be higher.

The two high pressure sets H and H′ serve to show the influence of current density. They were taken at identical pressures (20 mm) but H with a current of 0.4A and H′ with a current of 0.04A. This tenfold increase in current density, while nothing else is changed, means approximately a tenfold increase in the number of excited molecules. There is, therefore, a larger transfer of excitation energy into rotational and translational energy with a corresponding increase in temperature.

A comparison of the second and last rows in Table III shows that it makes very little difference whether the collisions of the excited molecules are with other H_2 molecules or with inert atoms like He atoms. The partial pressure of H_2 and the current density are unchanged. The presence of 150 mm of He causes the effective temperature to rise from 290° to 1520°K. This is exactly the opposite of the result obtained by E. R. Lyman[12] for OH. There it was found that the collisions with rare gas atoms were ineffective.

The observations of Goos are entirely in agreement with this. They have been discussed by one of us before[17] and used as proof for the correctness of the classification of the Fulcher bands. However, at that time the knowledge of the structure of molecular spectra was not far enough advanced for quantitative considerations. In Goos' measurements, pressure and temperature are varied independently, which has not been done in any one else's measurements. The pressures given here are the values for the gas at room temperature and are therefore proportional to the density.

Table V, which gives the values of σ and T' calculated from Goos' measurements, shows indeed the variations which we should expect from the preceding arguments. Goos' variations in pressure (from 0.11 to 5 mm) are not as extreme as ours (from 0.06 to 150 mm) and he works with much lower current densities (about 4 ma as compared with 400 ma in most of our experiments). But the changes in the effective temperature are of the same type: For a constant temperature of the tube the effective rotational temperature of the gas increases with increasing gas pressure. Many of the values of T' are below the temperature at which the tube is operated. For a constant density, of course, the effective rotational temperature goes up with the tube

[17] G. H. Dieke, Zeits. f. Physik **32**, 180 (1925).

temperature. A quantitative comparison with our values is not possible, as the construction of the tubes and the manner in which they were operated is quite different in the two cases.

The much weaker off-diagonal bands in the green and infra-red can be treated in the same way as the diagonal bands, with essentially the same results, but because the bands are so much weaker the results are correspondingly less accurate and are not given in detail.

Table VI gives the intensities of all the measured bands in the Fulcher system. The numbers are approximately the total intensity of all the lines in the bands for discharge type N on the same scale as Table I. The relative intensities of bands in different horizontal rows depends, of course, on the excitation conditions. The values given are obtained from averages with the elimination of the obviously unsuitable lines. The values would be slightly different if the other types of discharges had been used, which must be attributed to the fact that the calibration of the plates for large wave-length intervals is not perfect.

5. The Vibrational Changes

The preceding analysis has established the fact that the chief effect of an increase in pressure in the discharge tube is a marked increase in the effective rotational temperature. At high enough pressures this will be closely equal to the actual gas temperature, as equilibrium will then be nearly reached. A possible mechanism by which the energy necessary for the rise in temperature can be obtained from the discharge becomes apparent by a study of the changes in the vibrational distribution. We leave out of consideration possible effects of the wall of the tube and the complication which arises from the fact that there are several excited electronic states with approximately the same energy, which may be converted into each other by collisions.

Table VII shows the relative intensities of the various $Q(1)$ lines of the main Fulcher sequence. In order to facilitate a comparison, the $Q(1)$ line of the $0\rightarrow 0$ band is arbitrarily taken as 100.

Although the figures show considerable individual variations, their trend is clear. Again the measurements of Goos cannot be directly compared with the others, as Goos' plates were not calibrated for the variation of the sensitivity with wave-length. Only the changes are significant.

The main fact which is revealed by the measurements is that the higher vibrational states become less frequent compared with the zero vibrational state when the pressure is increased. This is one of the effects discussed by Oldenberg.[11]

For infinitely low pressures, when collisions cannot affect the state of affairs, the distribution over the various excited vibrational states is determined by something very similar to the Franck-Condon principle, as the excitation is produced chiefly by electrons which are so light that they cannot affect directly the motion of the nuclei.

In a collision with another molecule (or He atom) the vibrational energy, or part of it, can be transferred into translational or rotational energy of the whole molecule. The excited atom will find itself, after the collision, in a lower vibrational state, possibly also in a different rotational state.

Table VIII shows what percentage of the vibrational states have disappeared compared to the vibrationless state. A number 68, e.g., means that in that particular discharge (N) and vibrational state ($V=1$), 68 percent of the molecules are left at the time radiation occurs, compared to the number which would be left at low pressure and compared to the molecules left in the $V=0$ state. Of course, the actual number of the molecules which disappeared out of that state will be larger, as some will have gone even at the low pressure. The table is derived from the $Q(1)$ lines and in it enter the full experimental errors for these lines. Similar tables can be made for the other Q lines, and these have been taken into account in drawing the conclusions, although the tables themselves have been omitted for brevity's sake.

Table VIII. *Loss of higher vibrational states due to collisions. Percentage of molecules left in the various vibrational states compared to the $V=0$ state and compared to the situation at low pressure.*

V	L	K	N	H′	H	He
0	100	100	100	100	100	100
1	100	73	68	65	65	14
2	100	67	65	51	46	7
3	100	79	75	47	42	
4	100	114	88		69	

TABLE IX. *The intensity ratios $P(K+1)/Q(K)$ and $R(K-1)/Q(K)$.*

	$P(K+1)/Q(K)$							$R(K-1)/Q(K)$						
K	THEOR.	L	N	K	H′	H	He	THEOR.	L	N	K	H′	H	He
				0→0							0→0			
1	0.33	0.37	0.32	0.42	0.55	0.67	0.49	0.67	0.64*c*	0.55*c*	0.69*c*	0.69*c*	0.61*c*	0.71*c*
2	0.40	1.72	0.63	0.48	0.59	0.48	0.45	0.60	0.97*c*	0.92*c*	0.85*c*	0.74*c*	0.83*c*	0.55*c*
3	0.43	1.07	0.92	1.09	0.77	0.58	0.42	0.57	1.21	1.08	1.28	1.26	1.17	1.09
4	0.44	1.21	1.22	0.65	0.68	0.58	0.52	0.56	1.11	0.91	0.68	0.56	0.49	0.45
5	0.45	2.96*c*	1.68*c*	1.81*c*	2.25*c*	0.98*c*	0.56*c*	0.55	2.34	1.18	1.42	1.35	0.49	0.49
6						0.64	0.53						0.44	0.38
7						0.78	0.75						0.69	0.79
				1→1							1→1			
1	0.33	0.40	0.41	0.54	0.50	0.51	4.1	0.67	0.73	0.72	0.87	0.82	0.66	1.42
2	0.40	0.70	0.65	0.45	0.48	0.43	1.08	0.60	0.98	0.86		0.67	0.56	0.45
3	0.43	0.87	0.58	0.79	0.67	0.38	0.46	0.57	1.23*c*	0.94*c*	1.23*c*	1.30*c*	0.87*c*	0.80*c*
				2→2							2→2			
1	0.33	0.39	0.40	0.82	0.54	0.47		0.67	0.62	0.66	0.82	0.80	0.68	
2	0.40	0.59	0.58	0.48	0.47	0.46		0.60	0.43	0.61	0.52	0.51	0.48	
3	0.43	0.82	0.91	1.11	1.06	1.60		0.57	0.84	0.58	0.96	0.59	0.46	
4	0.44	0.90	1.02	0.69	0.60	0.51		0.56	0.86	0.72	0.59	0.49	0.41	
5								0.55	2.03	0.96	2.07	1.45	0.94	
6						0.66		0.54						
				3→3							3→3			
1	0.33	0.37	0.20	0.52	0.59	0.44		0.67	0.55	0.51	0.71	0.82	0.71	
2	0.40	0.75	0.66	0.50		0.46		0.60	0.73	0.61	0.48	0.44	0.51	
3	0.43	1.27	0.90	1.09		0.74		0.57	1.07	0.75	1.02	1.04	0.64	

It is quite evident that the higher the pressure, i.e., the larger the number of collisions, the more pronounced is the disappearance of the higher vibrational states. Again the discharge in He with a trace of H_2 forms an extreme case with about 90 percent of the vibrational states removed. The data are not quite clear as to whether the higher vibrational states are more strongly affected than the $V=1$ or $V=2$ states. From the He plates it would appear that the molecules remaining in the $V=2$ state are only about half the number of those in the $V=1$ state, but the discharges with the other conditions do not prove this tendency conclusively. The 4→4 band falls rather out of line, but as this is a very much weaker band than the other bands, it should, perhaps, not count too much.

The comparison of the H and H′ data shows that the vibrational loss is practically independent of the current density. There seems to be a slight but distinctly greater loss for H, which can easily be accounted for by the slightly larger number of collisions due to the higher temperature. This behavior is quite different from the rotational effect, as the temperature increase was considerably larger for the high current density (H). It is, however, just what must be expected. The percentage of molecules disappearing from a given vibrational state is only given by the number of collisions, which are determined essentially by the pressure. For a higher current there will be more excited molecules and more will be taken out by collisions, but the relative number should remain the same. It is different for the rotations. If there are more excited atoms, more vibrational energy can be transferred into temperature motion. As this is distributed over all molecules, excited and unexcited alike, and the total number remains constant, the temperature increase must be larger for a larger current.

In this connection the fact that according to Tables III and VI the higher vibrational states seem to have the lower effective temperatures is of interest. The reality of this effect is by no means certain, but if it is, it would mean that the molecules left in the higher vibrational states have had, in the average, a smaller number of collisions, for there is a definite chance in each collision that the molecule will be removed from that vibrational state. The fewer collisions, the less chance there is for an increase in temperature motion.

The conclusion that in the hydrogen discharge with an excess of helium the higher vibrational

states are partly suppressed has already been drawn by Richardson.[4] This matter has been further investigated by Smith,[18] who used pressures of helium as high as 400 mm. He also observed the increase in the intensity of the higher rotational lines and gave an explanation for this substantially the same as that adopted here, namely that vibrational energy is transferred into rotational energy. This was first suggested by Oldenberg[11] in connection with abnormal rotations observed in certain other band spectra.[19]

However, our observations seem to show that in the case of H_2 in an excess of helium, we are not dealing with abnormal rotation, as the effect in helium is only an extreme case of the same effect with moderate or high pressures of pure H_2. Our observations do not agree with Smith's finding that in the 2→2 and 3→3 bands the higher rotational lines are weakened instead of enhanced as in the 0→0 and 1→1 bands. The 3→3 band is too weak for measurement, but on our plates the 2→2 band, although much weaker than the 0→0 and 1→1 bands, shows exactly the same behavior. This is apparent from Tables I and III.

Smith reported that at a pressure of 400 mm of helium the high rotations decrease again. However, Smith's observation at 400 mm was made with a different tube and a current of only 5 ma, whereas all the other observations were made with a current of 35 ma. We have seen that the rotational effect depends decidedly on the current density and should also depend on the type of tube used, so that the observation at 400 mm should not be compared directly with the others.

[18] N. D. Smith, Phys. Rev. **52**, 728 (1937).

[19] There is, however, one fundamental difference between the point of view taken by us and that by Oldenberg and Smith. Oldenberg thinks that the excited H_2 molecule which collides with a helium atom is the one which acquires the high rotational energy while all the others are unaffected, and there is good evidence that this is the case in other band spectra. We believe that before radiation takes place, the vibrational energy is dissipated throughout the whole gas so that a genuine increase in temperature results. To this contribute not only the excited electronic states but also the higher vibrational states of the ground state of the molecule. For most excited molecules after they have emitted one or more quanta of radiation will find themselves back in the ground state of the molecule, but with several quanta of vibrational energy. These will have to be dissipated as temperature motion and, as there will be more molecules of this kind than excited molecules in any of the individual excited states capable of emitting visible radiation, this may be a more important process. In the real gas it is, of course, only a question which picture gives a better approximation, as the true state of affairs is vastly more complex. We believe that the dependence of the rotational effect on the current density and the independence from it of the vibrational effect is good evidence in favor of our point of view. We want, however, to defer a further discussion of this question until the data for other electronic states become available.

6. The P and R Branches

It would not be very useful to treat the intensities of the P and R branches in the same way as those of the Q branches were treated in §4. In the first place, the $3p^3\Pi^+$ state which is the initial state of the P and R branches interacts[9] with the $3p^3\Sigma$ state and this interaction gives rise to considerable perturbations in the energy. We must expect that the intensities will also be affected by this interaction so that it is no longer safe to apply the theoretical formulae for the intensity factors.

The observed intensities of the P and R branches seem to be decidedly more irregular than those of the Q branches. These irregularities can be only partly explained by actual irregularities in the transition probabilities. The P and R branches are roughly only half as strong as the Q branches, so that accidental overlappings would affect them more strongly. Further experiments will have to decide the nature of some of these irregularities.

Table IX gives the intensity ratio of the $P(K+1)$ and $R(K-1)$ lines to $Q(K)$. The initial state of all three lines has the same quantum number K and so nearly the same energy that the statistical probability is practically the same. Unless other considerations of a different nature enter, the ratios given in the tables should be simply the ratios of the transition probabilities.

The table shows the surprising fact that contrary to expectations, these ratios are not at all independent of the discharge conditions and that, besides, the values are in most cases entirely different from the theoretical values. Again, indi-

Table X. $P(K+1)/Q(K)$.

$K=$	1	2	3	4	5
0→0	0.37	1.72	1.07	1.21	2.96 *c*
1→1	0.40	0.70	0.87		
2→2	0.39	0.59	0.82	0.90	
3→3	0.37	0.75	1.27		
Theor.	0.33	0.40	0.43	0.44	0.45

TABLE XI. *The intensity ratios $R(K-1)/P(K+1)$.*

K	L	K	N	N′	H	He	Av.	Theor.
				0→0				
1c	1.79	1.64	1.30	1.26	0.63	1.4		2.00
2c	1.37	1.79	1.44	1.51	1.73	1.23		1.50
3	1.05	1.18	1.18	1.64	2.01	2.59		1.33
4	0.92	1.06	0.83	0.82	0.84	0.86	0.85	1.25
5c	0.78	0.78	0.70	0.64	0.50	0.87		1.20
6	0.52	0.92.	0.79	0.70	0.69	0.73	0.74	1.17
				1→1				
1	1.84	1.61	1.78	1.64	1.29			2.00
2	1.39		1.32	1.38	1.29	0.42	1.35	1.50
3c	1.42	1.56	1.61	1.93	2.29	1.77		1.33
				2→2				
1	1.57	1.43	1.66	1.47	1.50		1.55	2.00
2	0.73	1.08	1.06	1.10	1.10		1.08	1.50
3	1.02	0.86	0.64	0.56	0.29			1.33
4	0.95	0.86	0.70	0.81	0.80		0.82	1.25
				3→3				
1	1.52	1.35	2.51	1.40	1.60		1.51	2.00
2	0.96	0.95	0.93		1.12		1.00	1.50
3	0.85	0.93	0.83		0.86		0.84	1.33

vidual lines may show widely discordant results due to overlappings, but the general trend stands out quite clearly. Take, for instance, the ratio $P(K+1)/Q(K)$ as function of K for low pressures. These ratios are given in Table X.

For $K=1$ the observed values are very close to the theoretical value and depart from it more and more for increasing K so that at the higher values of K the observed ratios are several times the theoretically expected ones. As this happens at the lowest pressures where the effect of collisions is reduced to a minimum, this increase in the numbers of the Π^+ states with respect to the Π^- states for higher values of K must be due chiefly to the excitation. This is connected with the fact that for the excitation of a $p\Pi^+$ state the assumption made in §4 that the rotational quantum number remains unchanged is not a good approximation. The exact mechanism of the excitation, however, is not yet quite clear, and we leave this point now until the data for other electronic states become available.

If the pressure is increased, the experimental evidence shows that collisions remove the Π^+ states for higher values of K much more effectively than the corresponding Π^- states. This may be due to the fact that the state can interact with other neighboring electronic states, which is not possible for the Π^- state.

Finally the question may be raised whether the transition probabilities themselves do have the values which the simple theory predicts. As the preceding considerations show that we cannot assume that the Boltzmann formula will give us the relative numbers in the various rotational states, we have no way of finding directly the empirical intensity factors which contain the transition probabilities. However, as the lines $R(K-1)$ and $P(K+1)$ issue from the same initial state, the ratio of their intensities should be the ratio of the respective transition probabilities.

Table XI shows that these ratios are indeed independent of the excitation conditions for a number of lines. In the ratios where one of the lines is known to be a blend, the values change considerably and systematically from left to right, either decreasing, as, e.g., $K=1$ in the 0→0 band, or increasing as for $K=3$ of the 1→1 band. There are a few other lines which show the same kind of behavior (e.g., $K=3$ of 0→0 and 2→2 and $K=1$ of 1→1). We must assume that one of the lines involved in these ratios is also a blend. The other ratios show irregular fluctuations of a much smaller magnitude and presumably the lines involved there are free from serious overlappings. The average values are given in these cases (K and He excluded from average). The individual values of these ratios are usually within considerably better than 10 percent of the average, which gives an idea of the accuracy of the measurements.

The important thing is that even in those cases where we have reason to believe that the lines are entirely free from blends, the empirical ratios are quite different from the theoretically expected ones (given in the last column of Table X). Such a discrepancy by as much as 50 percent is likely to be due to the interaction of the $3p^3\Pi$ state with the $3p^3\Sigma$ state, although the magnitude of the discrepancy is surprising for this type of interaction. We shall leave the details of this interaction until we discuss the bands coming from the latter state.

However, the results show how necessary it is to be careful when intensity measurements in band spectra are used to calculate the temperature of the gas or other constants. For in such cases the relative transition probabilities have always been assumed to be the values derived from the elementary theory.

New Absorption Spectra of the Alkaline Earth Fluorides

CHARLES A. FOWLER, JR.
Department of Physics, University of California, Berkeley, California
(Received February 24, 1941)

Investigation of the absorption spectra of the alkaline earth fluorides under high dispersion reveals several new band systems in the ultraviolet region as far as λ1950. Vibrational analyses of these systems give the vibration frequencies and electronic terms of one new state of MgF, three of CaF, four of SrF, and four of BaF. Some changes in the previous analyses of the $A \leftrightarrows X$ system of MgF and the $C \rightleftarrows X$ system of CaF are made. An increased binding in all of these higher energy states as indicated by the values of the constants is discussed with regard to the probable electron configurations.

THE electronic spectra of the diatomic alkaline earth fluorides, first photographed by Datta,[1] constitute one of the best examples of spectra of a series of homologous molecules. They have usually been observed in emission from the flame of a cored carbon arc, although, with the exception of BeF, the absorption spectra have also been observed for a limited range of wavelengths.

In the search for new band spectra, absorption spectra have several advantages over arc spectra. Among these are the fact that the band heads are usually more pronounced, because of the lower temperature, and the fact that extraneous bands and lines due to impurities are much less troublesome. Moreover, the speed with which absorption spectra can be obtained is important. Although it is true that in absorption one observes only those bands whose lower electronic state is the normal state, such observations give additional information about the character of the excited states, since they must be among the types which can combine, according to the selection rules, with the normal state. No transitions between two excited states have so far been observed in the emission spectra of this group of molecules.

The present work was undertaken with a view to extending the observations on the absorption spectra of these fluorides from the resonance system to the limit of transmission of air in the ultraviolet.

At furnace temperatures below 1500°C only the known band systems were developed, but at higher temperatures twelve new higher energy states were revealed. Figure 1 shows the spectra under low dispersion. Table I summarizes the number of previously known and of newly discovered band systems of these molecules.

[1] S. Datta, Proc. Roy. Soc. **A99**, 436 (1921).

EXPERIMENTAL

The electric furnace, a carbon tube vacuum type, which has been previously described,[2] has a well-controlled temperature range between 900° and 2200°C. The fluoride vapors were produced by heating a small amount (~10 g) of the salt at the center of the resistor tube in an atmosphere of nitrogen. A hydrogen lamp of the conventional design was used as the source, with which suitably exposed plates of the ultraviolet region as far as the O_2 bands at λ1950 were

TABLE I. *Band systems of the alkaline earth fluorides.*

MOLECULE	NUMBER OF SYSTEMS PREVIOUSLY KNOWN AND WAVE-LENGTH RANGE	NUMBER OF NEWLY DISCOVERED SYSTEMS AND WAVE-LENGTH RANGE
BeF	1, λλ2816–3393	0, ——
MgF	2, 3468–3686 2649–2742	1, λλ2249–2387
CaF	3, 6024–6301 5145–5421 3371–3525	3, 3081–3245 2754–3035 2554–2700
SrF	3, 6283–6870 5621–5852 3646–3795	4, 3345–3592 3052–3218 2916–3069 2775–2915
BaF	4, 7862–8738 6716–7734 4842–5139 4136–3650	4, 3475–3608 3278–3451 3069–3210 (2)

[2] F. A. Jenkins and G. D. Rochester, Phys. Rev. **52**, 1135 (1937).

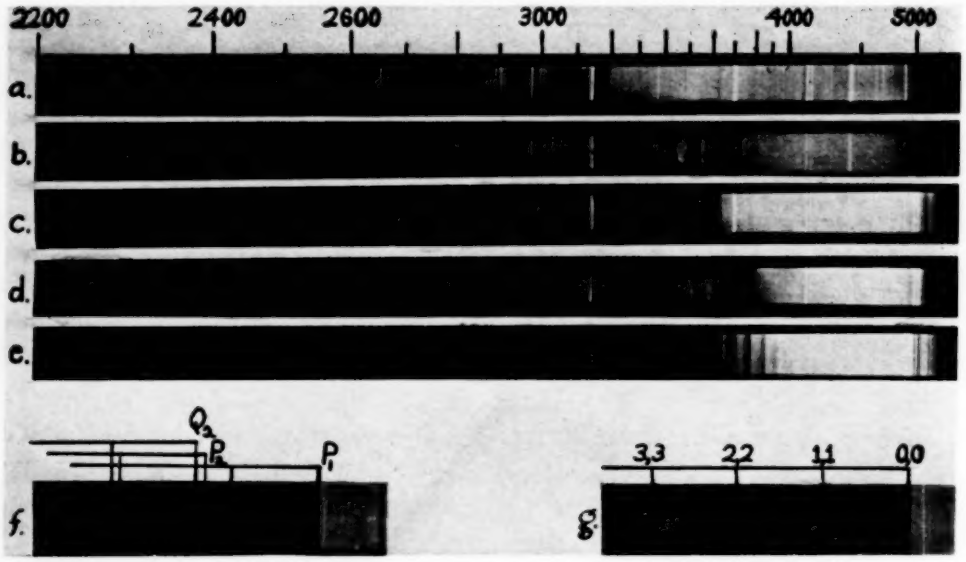

FIG. 1. Low dispersion spectra of (a) BeF, (b) MgF, (c) CaF, (d) SrF, (e) BaF. High dispersion spectra of (f) the $E^2\Pi$, $X^2\Sigma$ and (g) the $D^2\Sigma$, $X^2\Sigma$ systems of SrF.

obtained in 20 to 30 minutes. Exploratory work was done with a Hilger E-37 quartz spectrograph in the ultraviolet and with a Bausch and Lomb constant deviation spectroscope in the visible, furnace temperatures being increased by 100° increments beginning below the melting point. High dispersion spectrograms were obtained by means of the 30,000-lines-per-inch, 21-foot concave aluminum grating, with average dispersion of 1.3A/mm in the first order. This grating has the property of concentrating about 60 percent of the ultraviolet light (λ2536) in the first order. Ilford Q-2 plates were used below λ2400. Measurements of certain very weak or diffuse heads were made from microphotometer traces containing some standard iron lines.

OBSERVATIONAL DATA

1. BeF

A series of low dispersion spectrograms taken at gradually increasing temperatures showed that the $^2\Pi$, $^2\Sigma$ system, known from emission observations,[3–5] begins to be apparent at 1500°C and becomes rapidly stronger as the temperature rises. At the same time a continuous band, not observed below 1500° and whose maximum lies somewhere beyond the short wave-length limit of observation, extends to longer wave-lengths until at a temperature of 2000° it begins to overlap the 1,0 $^2\Pi$, $^2\Sigma$ band at λ2909. The presence and behavior of this continuum is typical of all the molecules here investigated and indicates the existence of one or more repulsive electronic states well above the normal state. The plates showed no system of BeF except the $^2\Pi \leftarrow ^2\Sigma$ down to the limit of observation (λ1950). If such a system exists above λ1950 it must be considerably weaker than the $A^2\Pi$, $X^2\Sigma$ system, and although it might appear at the highest temperatures, it would then be covered by the overlying continuum. A consideration of the trend of $B^2\Sigma$ states of the other alkaline earth fluorides indicates that for BeF the $B^2\Sigma \leftarrow X^2\Sigma$ system probably lies in the vacuum region.

The high dispersion spectrograms show the sequences $v'-v''=-1, 0, +1, +2$ of the $^2\Pi$, $^2\Sigma$ system with R_2, R_1 and Q_1 branches. In addition the 0,0 and 1,0 bands each possess a very weak branch forming heads at λ3001.86 and λ2903.21 respectively. An application of combination differences with the data of Jenkins[5] proves that these are the R_{21} branches, to be expected if the $^2\Pi$ state is not strictly a state with case (b) coupling. No trace of an isotope head due to Be^9F was found.

[3] S. Datta, Proc. Roy. Soc. **A101**, 187 (1922).
[4] W. Jevons, Proc. Roy. Soc. **A122**, 211 (1929).
[5] F. A. Jenkins, Phys. Rev. **35**, 315 (1930).

TABLE II. *Wave number residuals (O−C) and estimated intensities of the band heads of the new systems. A dash indicates a band observed but too weak for measurement. (P) indicates a perturbation.*

v′, v″	O−C	I
MgF, $C \leftarrow X$		
0,1	−1.0	2
1,2	−0.1	1
2,3	—	0
0,0	0.0	10
1,1	−0.6	5
2,2	—	0
1,0	−0.3	5
2,1	+0.5	4
3,2	−0.5	3
4,3	−0.2	1
5,4	—	0
2,0	−0.4	1
3,1	+0.7	2
4,2	−0.1	3
5,3	−0.2	2
6,4	—	0
CaF, $C \leftarrow X$		
0,2	−0.1	2
1,3	+0.2	3
2,4	−0.1	3
3,5	−0.2	2
4,6	+0.0	1
5,7	—	0
0,1	−0.2	7
1,2	+0.1	6
2,3	−0.5	5
3,4	+0.1	3
4,5	−0.1	1
0,0	0.0	10
1,1	+0.6	2
2,2	—	0
1,0	−0.2	5
2,1	−0.1	5
3,2	−0.7	3
4,3	−0.1	1
2,0	—	0
3,1	+0.1	1
4,2	−0.1	1
5,3	—	0
CaF, $D \leftarrow X$		
0,0	0.0	10
1,1	−0.2	8
2,2	+0.2	6
3,3	+0.7	2
1,0	+0.2	6
2,1	+0.2	8
3,2	0.0	9
4,3	0.0	8
5,4	0.0	7
6,5	−0.2	5
7,6	−0.1	2
8,7	+0.1	1
2,0	0.0	1
3,1	+0.1	5
4,2	0.0	7
5,3	−0.1	7
6,4	0.0	7
7,5	0.0	6
8,6	0.0	5
9,7	+0.1	4
10,8	−0.3	3
11,9	−0.1	2
12,10	−0.1	1
CaF, $E \leftarrow X$		
0,1	+0.2	4
1,2	+0.7	3
2,3	−0.3	1
0,0	0.0	10
1,1	+0.4	4
1,0	−0.5	8
2,1	+0.3	7
3,2	−1.0	4
4,3	−0.7	1
5,4	—	0
2,0	+0.8	4
3,1	−0.7	6
4,2	−0.8	7
5,3	−0.4	6
6,4	+0.1	3
7,5	—	0
4,1	−1.0	1
5,2	−0.6	2
6,3	−0.1	3
7,4	+0.1	3
8,5	+0.2	2
9,6	0.0	1
CaF, $F \leftarrow X$		
0,1	−0.5	6
1,2	+1.1	5
2,3	+0.6	3
0,0	0.0	10
1,1	−0.1	5
2,2	+0.1	1
1,0	+0.4	6
2,1	−0.6	5
3,2	−0.3	3
4,3	—	0
2,0	+0.4	1
3,1	0.0	2
4,2	+0.1	1
5,3	—	0
SrF, $D \leftarrow X$		
0,1	0.0	2
0,0	0.0	9
1,1	−0.1	10
2,2	−0.1	8
3,3	+0.3	6
4,4	−0.3	3
1,0	+0.1	4
2,1	−0.1	7
3,2	−0.3	7
4,3	+0.2	6
5,4	+0.1	5
6,5	−0.1	3
7,6	−0.3	2
8,7	−0.1	1
3,1	−0.7	2
4,2	0.0	3
5,3	0.0	4
6,4	0.0	4
7,5	−0.1	4
8,6	+0.3	3
9,7	+0.2	3
10,8	+0.2	2
11,9	0.0	2
12,10	−0.1	1
13,11	−0.4	1
SrF, $E \leftarrow X$		
0,1	−0.9	5
1,2	+0.1	2
0,0	0.0	10
1,1	−0.4	3
2,2	+0.1	1
1,0	−0.5	7
2,1	−0.6	6
3,2	+0.1	3
4,3	0.0	1
2,0	—	0
SrF, $F \leftarrow X$		
0,1	−0.1	6
1,2	−0.6	4
2,3	−0.3	2
3,4	—	0
0,0	0.0	8
1,1	−0.6	1
1,0	−0.3	10
2,1	+0.8	7
3,2	+0.7	3
4,3	+0.2	1
2,0	+0.2	5
3,1	+0.7	7
4,2	+0.3	6
5,3	+0.2	2
6,4	—	0
SrF, $G \leftarrow X$		
0,1	+0.4	4
0,0	0.0	10
1,0	−0.4	8
2,1	0.0	5
2,0	+0.4	6
3,1	−0.5	5
BaF, $E \leftarrow X$		
0,1	−0.3	3
0,0	0.0	10
1,1	−0.1	3
1,0	−0.3	5
2,1	−0.1	2
BaF, $F \leftarrow X$		
0,1	−0.3	4
1,2	−0.1	2
2,3	—	0
0,0	0.0	10
1,1	−3.9(P)	8
2,2	—	0
1,0	+0.2	7
2,1	+0.6	8
3,2	+0.5	6
4,3	+0.5	4
2,0	+0.1	2
3,1	−0.1	1
4,2	—	0
BaF, $H \leftarrow X$		
0,0	0.0	10
1,1	−0.5	6
2,2	−0.7	2
1,0	0.0	6
2,1	−0.2	7
3,2	+0.2	6
4,3	+0.2	4
5,4	+0.1	1
2,0	−0.9	2
3,1	−0.1	4
4,2	+0.1	5
5,3	0.0	3
6,4	+0.1	1

2. MgF

The known bands of the molecule MgF constitute a $^2\Pi$, $^2\Sigma$ system at λλ3470–3690 and a $^2\Sigma$, $^2\Sigma$ system at λλ2650–2740.[4,6,7] Both systems were developed with increasing intensities above 1350°C, and at 1800° a new system appeared extending from about λ2250 to λ2400. Good high dispersion plates were obtained with a furnace temperature of 1900°C, showing the new system as four sequences of single-headed bands degraded to shorter wave-lengths. In the 0,0 band the rotational structure is well enough resolved to show the presence of a P and an R branch only. Since the ground state is $^2\Sigma$, this proves that the new excited state is $^2\Sigma$ also. The twelve measured heads of this $C^2\Sigma \leftarrow X^2\Sigma$ system are given by the formula

$$\nu = 42{,}528.0 + 821.9u' - 4.82u'^2 - 717.1u'' + 3.67u''^2,$$

where $u = v + \frac{1}{2}$. The residuals (obs.−calc.) from the formula and the estimated intensities are given in Table II, which includes similar data for the new systems of the heavier molecules.

The system just described is not the one at λ2275 that Jenkins and Grinfeld mention as possibly due to MgF.[7] That single, closely spaced sequence of bands has appeared with more or less intensity not only on my MgF plates but also on the plates of BeF, BaF, SrF, and AlF. That it is actually due to the AlF molecule is readily seen by comparing its microphotometer trace given by Jenkins and Grinfeld with the reproduction of the $v' - v'' = 0$ sequence of AlF included in a recent paper by Rochester.[8]

The value of 717.1 cm^{-1} for ω_e'' of the $C \leftarrow X$ system does not agree with the accepted value for the normal state, namely, 690.75 cm^{-1}. Investigation revealed that the previous vibrational analysis[6] of the $A^2\Pi$, $X^2\Sigma$ system was in error. A reassignment of vibrational quantum numbers, using Datta's measurements, gives for the Q_2 heads of that system,

$$\nu = 27{,}847.4 + 746.0u' - 3.97u'^2 - 718.2u'' + 4.02u''^2.$$

The three heads of each band are the Q_2, P_2 and

[6] R. C. Johnson, Proc. Roy. Soc. **A122**, 189 (1929).
[7] F. A. Jenkins and R. Grinfeld, Phys. Rev. **45**, 229 (1934).
[8] G. D. Rochester, Phys. Rev. **56**, 305 (1939).

P_1 heads as pointed out by Jenkins and Grinfeld, who concluded that the $A^2\Pi$ state has a doublet separation of -34.3 cm^{-1}.

At the high temperatures employed, other sequences of the $B^2\Sigma \leftarrow X^2\Sigma$ system appear, namely $v'-v''=+2, -2, -3$. In the $+1$ and $+2$ sequences the isotope effect is clearly brought out in the appearance of well-developed heads due to $Mg^{25}F$ and $Mg^{26}F$. At about 1800°C a continuum appears at the short wave limit of observation and extends as far as λ2275 when the temperature is 2000°C.

3. CaF

Three band systems of this molecule are known in emission and absorption, involving the four states $X^2\Sigma$, $A^2\Pi$, $B^2\Sigma$, $C^2\Pi$, and lying in the red, green, and near ultraviolet respectively.[9,10] They begin to appear at a furnace temperature of 1350°C along with a region of continuous absorption covering roughly 100A with its center at λ2180, which spreads until it reaches λ2500 at 2000°. At about 1700° other bands begin to appear in the ultraviolet, and at 2000° they cover the entire region λλ2500–3500.

High dispersion plates were taken of this region at temperatures of 1735°, 1835°, and 2000°C to bring out the weak and strong parts of the spectrum with intensities suitable for measurement. Nearly all the bands were readily grouped into four electronic systems. No evidence of an isotope effect was found in any of them. These systems, with the equations for the heads, are

$$C^2\Pi \leftarrow X^2\Sigma(Q_1) \quad \nu = 30{,}255.9 + 481.7u' - 2.02u'^2 - 588.2u'' + 2.75u''^2,$$
$$D^2\Sigma \leftarrow X^2\Sigma \quad \nu = 30{,}772.3 + 650.7u' - 2.89u'^2 - 587.5u'' + 2.85u''^2,$$
$$E^2\Sigma \leftarrow X^2\Sigma \quad \nu = 34{,}135.2 + 646.3u' - 3.24u'^2 - 587.8u'' + 2.90u''^2,$$
$$F^2\Pi \leftarrow X^2\Sigma(P_1) \quad \nu = 37{,}547.9 + 681.7u' - 3.55u'^2 - 586.9u'' + 2.82u''^2.$$

The system $C^2\Pi \leftarrow X^2\Sigma$ is not new, but was observed in emission and measured by Datta.[1] Other investigators have failed to reproduce it because of its intrinsic weakness. Johnson[9] using Datta's measurements, and guided by the ground state constants already known from the other systems has attempted a vibrational analysis. The reason for the unsatisfactory nature of the results appears immediately from my high dispersion spectrograms. Datta's pictures did not reveal the two strongest and most important sequences, namely the 0 and $+1$ sequences with leading members at λ3305 and λ3254. With these added bands there is no ambiguity in making the v' and v'' assignments. The four observed heads are interpreted as R_{21}, R_2, R_1 and Q_1, and the formula has been calculated from the Q_1 heads. Table III lists the wave number separations of the other heads from the head given by the equation, as well as similar data for all of the other systems having multiple heads.

The system $D \leftarrow X$ and the considerably weaker $E \leftarrow X$ are quite certainly $^2\Sigma$, $^2\Sigma$ transitions. The bands are clearly of a single-headed type, and the rotational structure, where not confused by the structure of other bands of the sequence, apparently contains two branches only. Bands of both systems are degraded to shorter wavelengths. Superposed on part of the $E \leftarrow X$ system was another set of bands with well-resolved

TABLE III. *Wave number separation of heads in the multiple-headed bands.*

v', v''	R_1-Q_1	R_2-Q_1	$R_{21}-Q_1$
CaF, $C^2\Pi \leftarrow X^2\Sigma$			
0,2	—	29.7	—
1,3	12.0	28.9	—
2,4	12.2	30.3	—
0,1	10.8	29.5	45.5
1,2	10.3	29.2	—
2,3	10.7	29.8	—
3,4	10.8	30.2	—
0,0	10.2	29.3	43.0
1,1	9.7	28.6	—
1,0	8.0	28.7	41.3
2,1	7.3	28.4	40.7
3,2	8.5	28.1	—

v', v''	P_2-P_1	Q_2-P_1
CaF, $F^2\Pi \leftarrow X^2\Sigma$		
0,1	2.1	11.8
0,0	2.0	11.2
1,0	2.1	12.4

v', v''	P_2-P_1	Q_2-P_1
SrF, $E^2\Pi \leftarrow X^2\Sigma$		
0,1	80.7	86.1
1,2	78.0	—
0,0	80.4	86.1
1,1	79.4	85.2
2,2	—	—
1,0	79.8	85.8
2,1	79.7	—
3,2	—	—
2,0	80.0	—

BaF, $F^2\Sigma \leftarrow X^2\Sigma$	
0,1	7.3
1,2	—
0,0	8.6
1,1	6.8*
1,0	9.8
2,1	9.2
3,2	9.4
4,3	8.7
2,0	11.0

* Perturbation.

[9] R. C. Johnson, Proc. Roy. Soc. **A122**, 161 (1929).
[10] A. Harvey, Proc. Roy. Soc. **A133**, 336 (1931).

rotational structure, and with first differences for the lower and upper states of 837 cm^{-1} and 1002 cm^{-1} respectively. This is obviously not due to CaF. It may possibly be ascribed to CaO or CaN. Recent spectrograms of the absorption of CaO taken by Mr. R. E. Harrington fail to show it.

The $F \leftarrow X$ system consists of four sequences of bands of which at least the leading (and strongest) members possess three very closely grouped heads, the bands being again shaded toward the further ultraviolet. These are probably the P_1, P_2, and Q_2 heads of a $^2\Pi$, $^2\Sigma$ transition, similar to the BeF bands. The vibrational constants have been calculated from the leading (P_1) heads since in the weaker bands they alone were measurable. As to the doublet separation in the $^2\Pi$ state, one can only say that $2.0 < A < 11.7$ cm^{-1}, where the two limits are the P_1, P_2 and the P_1, Q_2 separations in the 0,0 band.

TABLE IV. *Wave numbers and intensities of band heads of the $G \leftarrow X$ system of* SrF. *(v', v'') assumed for calculation of vibrational constants.*

$v'-v''$	ν		I	$v'-v''$	ν		I
−1	34,298.2	(0,1)	4	+1	35,346.6		2
	34,302.0		1		35,359.4		5
	34,309.4		3		35,366.3	(1,0)	8
	34,320.0		3		35,373.8		6
	34,367.7		3		35,399.1		5
					35,408.5		2
0	34,767.1		3		35,421.2		5
	34,787.0		4		35,437.9	(2,1)	5
	34,795.4	(0,0)	10				
	34,810.1		3	+2	35,919.3		1
	34,818.4		3		35,935.9	(2,0)	6
					35,977.6		2
					35,991.1		3
					36,000.4		1
					36,003.7	(3,1)	5

4. SrF

The known states of the SrF molecule are completely analogous to the first four of CaF, namely, a $^2\Sigma$ normal state, with $A^2\Pi$, $B^2\Sigma$, and $C^2\Pi$ excited states.[9,10] Their energies, too, are comparable though somewhat depressed, as is expected in going to a heavier molecule of a homologous group. The visible systems, involving states A and B, were apparent at temperatures of 1200°C and up. The system $C \leftarrow X$ was developed at about 1480°, and from 1600° to 2000° four new band systems in the ultraviolet were observed, all shaded to shorter wave-lengths. Also present was a continuum extending from beyond the shortest wave-lengths to λ2500 at a furnace temperature of 2000°C. The band heads of the new systems can be represented by the equations

$$D^2\Sigma \leftarrow X^2\Sigma \qquad \nu = 28{,}296.6 + 552.1u' - 2.15u'^2 - 501.3u'' + 2.19u''^2,$$
$$E^2\Pi \leftarrow X^2\Sigma(P_1) \qquad \nu = 31{,}528.7 + 564.4u' - 3.20u'^2 - 500.5u'' + 2.10u''^2,$$
$$F^2\Sigma \leftarrow X^2\Sigma \qquad \nu = 32{,}820.3 + 598.5u' - 3.42u'^2 - 502.0u'' + 2.45u''^2,$$
$$G^2\Pi \leftarrow X^2\Sigma \qquad \nu = 34{,}759.2 + 573.9u' - 1.28u'^2 - 501.9u'' + 2.13u''^2.$$

The presence of sharp, single-headed bands, and the appearance of a P and an R branch only in certain of the stronger bands where resolution is sufficiently complete indicate that the systems $D \leftarrow X$ and $F \leftarrow X$ are $^2\Sigma$, $^2\Sigma$ transitions. These bands are similar to those of the $D \leftarrow X$ and $E \leftarrow X$ systems, respectively, of CaF in the number and length of the sequences, intensity distribution among the bands, and general appearance.

That the $E \leftarrow X$ system is a transition to a $^2\Pi$ state is shown by the fact that the strongest of the bands have three heads, two very close together and a third of considerably lower frequency. They are the Q_2, P_2, and P_1 heads, an interpretation indicated by the small, but nevertheless real, change in the $Q_2 - P_2$ separation wherever both heads were measurable. The direction of the change is that for $B' > B''$, which is the case here since the bands are degraded to the ultraviolet. The separation of the two components of the $^2\Pi$ state is probably rather near the difference of the heads Q_2 and P_1, or 86.1 cm^{-1}. The vibrational constants have been derived from the P_1 heads, since these are the most completely observed.

Inasmuch as the heads of the $G \leftarrow X$ system are definitely multiple, and because $\Delta\Lambda = 2$ is forbidden, the state G must be $^2\Pi$, but attempts to reconcile the number of and spacing between the observed heads with a $^2\Pi$, $^2\Sigma$ transition have been unsuccessful. The bands have three, four, or five apparently associated heads, whose positions and intensities are not explainable in the usual way. Furthermore, the separations are much too large

to be due to isotopes. The most plausible explanation of the irregular arrangement of the heads is that the levels of this state suffer strong perturbations from a neighboring state. A v', v'' assignment was finally made by choosing certain of the thirty observed heads which yielded the proper ground state constants and a $\Delta G'(v+\frac{1}{2})$ that decreased regularly with increasing v'. The constants obtained in this way are probably good approximations to the actual values. Table IV lists the wave numbers and estimated intensities of all of the band heads of this system and indicates which were used in the calculation of the vibrational constants.

5. BaF

For this molecule, as for CaF and SrF, the known systems in the visible and near ultraviolet[11] were developed at the lower furnace temperatures, increased in strength as the temperature became greater, and at temperatures above 1800°C three groups of bands containing four new electronic systems were evident. The equations for the band heads are

$$E^2\Sigma \leftarrow X^2\Sigma \quad \nu = 28{,}134.1 + 538.4u' - 1.90u'^2 - 468.9u'' + 1.79u''^2,$$
$$F^2\Sigma \leftarrow X^2\Sigma \quad \nu = 29{,}411.3 + 529.9u' - 2.00u'^2 - 469.5u'' + 1.90u''^2,$$
$$G^2\Sigma \leftarrow X^2\Sigma \quad \nu = 31{,}451.9 + 510.4u' - 0.83u'^2 - 469.9u'' + 2.08u''^2,$$
$$H^2\Sigma \leftarrow X^2\Sigma \quad \text{only three heads observed.}$$

Since it is similar but even weaker than the $E \leftarrow X$ system of CaF, the system $E \leftarrow X$ of BaF is probably a $^2\Sigma$, $^2\Sigma$ transition also. There is no evidence of multiple heads, but the branches in the bands cannot be distinguished because of the over-all low intensity.

The most noticeable feature of the $F \leftarrow X$ system is that its bands have double heads of about the same intensity. In general appearance it strongly resembles the red $B^2\Sigma \leftarrow X^2\Sigma$ system of BaF where the double heads are attributed to spin doubling.[11] A similar doubling of the heads is also found in both the CaF and SrF $B^2\Sigma \leftarrow X^2\Sigma$ systems.[10] Apparently closely associated with the main sequences 0 and +1 are two very faint sequences of bands, which were at first assumed to be the lower energy component of a $^2\Pi$, $^2\Sigma$ transition. A consideration of the intensity of the bands in the two sets, however, shows that this cannot be the case. Not only are the intensities of a different order of magnitude, but the relative intensity distributions among the bands of the two sets are unlike. Therefore, in view of the similarity of the strong bands to the red system, the upper state has been interpreted as a $^2\Sigma$ state, and its constants have been calculated from the higher frequency heads. First differences of the weak heads suggest that they are also due to BaF, if certain leading heads of the sequences are assumed to be too weak to be observed, indicating another electronic level, $\nu \approx 29{,}235$ cm^{-1}, with a vibration frequency nearly the same as that of the neighboring $F^2\Sigma$ state.

The bands in the region λλ3069–3210 apparently belong to a single electronic system, but a careful consideration of the position and intensities of the band heads indicates that they probably constitute two overlapping systems. The more extensive contains three sequences, the 0, +1, and +2, with no sign of a −1 sequence. The other system shows only the 0,1, 0,0, and 1,0 heads, the last two being of intensities equal to the corresponding bands in the more extensive system. If this were a $^2\Pi$, $^2\Sigma$ system, the appearance or nonappearance of certain of the heads in the different sequences might be explained by assuming certain relations between B' and B'', as is the case in the $A \leftarrow X$ system of SrF,[10] but the appearance of strong 0,0, 1,0 and 0,1 bands and the complete absence of other members of these sequences cannot be explained in this way. It seems more likely that two systems are present here, the upper states, probably $^2\Sigma$, lying only some 130 cm^{-1} apart. The heads of the less extensive system are at 31,136.8, 31,602.2 and 32,107.2 cm^{-1} which indicates that the ω_e values of the two new states are very nearly equal.

In addition to the systems described, a short wave-length continuum was present extending up to λ2450 with a furnace temperature of 2000°C. The spectrograms also contain the bands λλ3650–

[11] F. A. Jenkins and A. Harvey, Phys. Rev. **39**, 922 (1931).

TABLE V. *Electronic terms and vibration frequencies for the alkaline earth fluorides.*

MOLECULE	STATE	T_e	ω_e
	$A^2\Pi$	33,241.8 33,225.4	1172.6
BeF	$X^2\Sigma$	0	1265.6
	$C^2\Sigma$	42,528.0	821.9
	$B^2\Sigma$	37,151.7	757.8
	$A^2\Pi$	27,847.4 27,813.1	746.0
MgF	$X^2\Sigma$	0	718.2
	$F^2\Pi$	37,547.9	681.7
	$E^2\Sigma$	34,135.2	646.3
	$D^2\Sigma$	30,772.3	650.7
	$C^2\Pi$	30,285.2 30,255.9	481.7
	$B^2\Sigma$	18,895.9 18,889.3.	541.5
	$A^2\Pi$	16,557.2 16,482.1	593.4 591.9
CaF	$X^2\Sigma$	0	586.7
	$G^2\Pi$	34,759.2	573.9
	$F^2\Sigma$	32,820.3	598.5
	$E^2\Pi$	31,614.8 31,528.7	564.4
	$D^2\Sigma$	28,296.6	552.1
	$C^2\Pi$	27,041.3 26,977.8	452.5
	$B^2\Sigma$	17,301.9	488.9
	$A^2\Pi$	15,348.9 15,068.9	505.9 506.1
SrF	$X^2\Sigma$	0	500.1
	$H^2\Sigma$	31,582	509
	$G^2\Sigma$	31,451.9	510.4
	$F^2\Sigma$	29,411.3	529.9
	$E^2\Sigma$	28,134.1	538.4
	$D'^2\Sigma$	26,222.3	504.9
	$D^2\Sigma$	24,152.3	508.4
	$C^2\Pi$	20,197.2 19,998.2	456.0
	$B^2\Sigma$	14,064.4 14,070.6	424.4
	$A^2\Pi$	12,281.1 11,647.3	436.7 435.5
BaF	$X^2\Sigma$	0	468.9

4136 observed by Jenkins and Harvey, who concluded that they compose a single system whose upper state is a wide doublet of separation 2070 cm^{-1}. Despite the near equality of the vibration constants, it now seems more reasonable to interpret them as two distinct states, probably $^2\Sigma$. The wide separation, the differences in intensity and intensity distribution, and certain analogs such as the $D^2\Sigma$ and $E^2\Sigma$ states of CaF, all make this the more natural conclusion.

DISCUSSION

Table V gives the electronic energies and vibration frequencies of all the states now known for this group of molecules. Excluding BeF, where only one excited state is known, certain analogous states can readily be traced from molecule to molecule, particularly the first four excited states of CaF, SrF, and BaF. The analogy of the $D^2\Sigma$ and $E^2\Sigma$ states of CaF with the $D^2\Sigma$ and $D'^2\Sigma$ states of BaF is clear. The vibration frequencies of the first pair are nearly equal (651 and 646 cm^{-1}) and the same is true for the last pair (508 and 505 cm^{-1}). Other possible analogies, as well as some obvious discrepancies, may be detected. In general the expected decrease of excited state energies as one goes from lighter to heavier molecules of the group is observed, together with a diminution of the vibration frequencies.

Rather striking is the fact that all of the band systems involving states above $C^2\Pi$, thirteen in all for CaF, SrF and BaF, are without exception shaded toward shorter wave-lengths. This is also true of the two highest states of MgF. These excited states are, therefore, more tightly bound than the ground state. The outer electron configuration of the normal states of these molecules, like that of BeF, is in Mulliken's notation $z\sigma^2 y\sigma^2 w\pi^4 x\sigma$. Mulliken suggests that the first two excited states, $A^2\Pi$ and $B^2\Sigma$, arise from the excitation of a $w\pi$ and $y\sigma$ electron, respectively, into the $x\sigma$ orbit. The $C^2\Pi$ state is very likely due to the transition of the $x\sigma$ into the $v\pi$ orbit. It is reasonable to assume that the electronic states of higher energies are obtained from the normal state configuration by exciting the $x\sigma$ electron to σ and π orbits derived from atomic orbits of still higher total quantum number, leaving the closed shell configuration $z\sigma^2 y\sigma^2 w\pi^4$ undisturbed. The more highly excited the $x\sigma$ electron, the more nearly should the resulting state resemble the normal state of the ionized molecule (which it becomes in the limit). The spectra of the ionized molecules of this group are unknown, but the approximate magni-

tude of the binding can be determined by a consideration of the oxides, which are isoelectronic with the ions. For example, the vibration frequency of the normal state of CaO is 843 cm^{-1}.[12] A correction for the difference of reduced mass gives 790 cm^{-1} as an approximate estimate of the vibration frequency of CaF^+, indicating considerably stronger binding than in the CaF normal state ($\omega_e'' = 587$ cm^{-1}). SrF and BaF give similar results. It seems reasonable, then, on the hypothesis that the excitation of the $x\sigma$ electron alone determines the higher energy states of this group of molecules, that those states should be more firmly bound than the normal state configuration.

[12] P. H. Broderson, Zeits. f. Physik **104**, 135 (1936).

The continua that appear at the ultraviolet limit of the spectrum in the case of every molecule investigated can be reasonably attributed each to its specific molecule. Some repulsive excited states of relatively high energy are theoretically predicted for most molecules, and only in absorption at high temperature can transitions involving such states be observed in many cases. Although the possibility exists that all the continua are due to some persistent impurity, the appearance of the λ2180 continuum of CaF is certainly characteristic, and probably the others are also.

In conclusion the writer wishes to thank Professor F. A. Jenkins, whose direction and criticism were of considerable assistance in this investigation.

APRIL 15, 1941 PHYSICAL REVIEW VOLUME 59

On the Joint Action of Diffusion and Recombination of Ions

GEORGE JAFFÉ
Louisiana State University, University, Louisiana
(Received February 3, 1941)

The differential equation which describes the joint action of diffusion and recombination of ions is solved, for the one-dimensional case, by a method previously developed by the author. In Section I, the decay of a given initial distribution of ions is treated. The observable coefficient of recombination, as modified by diffusion, depends strongly in the initial stage on the given distribution. For later times it depends in a simple way on the density of ionization and the distance between the collecting plates. In Section II, the establishment of the steady state, with constant production of ions, is calculated. Diffusion introduces a linear term which may, for sufficiently small values of the ionic density and the electrode distance, mask the usual quadratic term. In Section III, it is shown that anomalies observed by Gardner in the recombination coefficient of oxygen and by Power in the establishment of the steady state in air are explained, without further assumptions, by diffusion to the walls.

INTRODUCTION

IN all measurements on recombination of ions diffusion plays a noticeable and often an important part. This holds whether the ionized volume extends to the collecting electrodes or not. For, in the former case, ions are lost to the electrodes and, in the latter case, the ionized volume increases by diffusion, thus affecting the apparent coefficient of recombination.

Langevin[1] was the first to recognize the importance of diffusion in measurements on recombination. As early as 1905 he solved the problem of the steady state created by a constant production of ions between parallel plates under the joint action of recombination and diffusion. His results do not seem to have found the attention which they deserve. In quite a number of cases where their application would have been of value they were replaced by less accurate computations. In more recent measurements on recombination, all observers had to correct their results for diffusion and did it somehow or other,[2] but none of the formulae used are adequate.

[1] P. Langevin, J. de phys. (4) **4**, 322 (1905).

[2] A. D. Power, J. Frank. Inst. **196**, 327 (1923); L. C. Marshall, Phys. Rev. **34**, 618 (1929); O. Luhr, Phys. Rev. **35**, 1394 (1930); **36**, 24 (1930); P. Kraus, Ann. d. Physik **29**, 449 (1937); M. E. Gardner, Phys. Rev. **53**, 75 (1938); J. Sayers, Proc. Roy. Soc. **A169**, 83 (1938).

Under these circumstances it seemed desirable to the author to develop formulae for the non-steady state, because Langevin's results are of no avail in cases where the change of ionization with time is observed. The following calculations refer to the case where the problem depends only on one local coordinate, x.

I. Decay of a Given Initial Distribution

We shall disregard the difference in mobility of positive and negative ions. Let n signify, under these conditions, their common density, D their coefficient of diffusion and α the coefficient of recombination. Then the problem to be solved will be given by

$$\partial n/\partial t = D\partial^2 n/\partial x^2 - \alpha n^2 \tag{1.01}$$

with suitable boundary and initial conditions. We shall assume that the volume under consideration extends from $x=0$ to $x=l$. Then it will be required that

$$n=0 \quad \text{for} \quad x=0 \quad \text{and} \quad x=l, \tag{1.02}$$

and that n reduces to a given initial distribution

$$n=n_0(x) \quad \text{for} \quad t=0. \tag{1.03}$$

The nonlinear partial differential equation (1.01) can be solved by a rigorous method developed by Lichtenstein,[3] but the results are involved and hold only for sufficiently small values of t. The author, therefore, has preferred to use an approximate method which was introduced by him into the theory of columnar ionization and which has been used since in various cases.[4] Its usefulness lies in the fact that it is applicable to all values of t and all values of the involved parameters.

The method is as follows. Let $n'(x, t)$ be the exact solution of (1.01) in the case where recombination is disregarded ($\alpha=0$). Then it is assumed that the solution of the complete Eq. (1.01) is of the form

$$n(x, t) = N(t)n'(x, t). \tag{1.04}$$

The function $N(t)$ is determined by introducing (1.04) into (1.01), integrating with regard to x from $x=0$ to $x=l$ and thus transforming (1.01) into an ordinary differential equation for $N(t)$, namely

$$dN/dt = -\alpha f(t) N^2, \tag{1.05}$$

where

$$f(t) = \int_0^l n'^2 dx \Big/ \int_0^l n' dx. \tag{1.06}$$

We shall normalize n' by the condition

$$\int_0^l n'(x, 0)dx = 1. \tag{1.07}$$

Then N will represent the total ionization per cm² section and N_0 the respective initial value.

The solution $n'(x, t)$ is easily found by known methods. If the initial distribution is supposed to be given in the form of a Fourier series

$$n'(x, 0) = \sum_{m=1}^{\infty} A_m \sin(m\pi x/l) \tag{1.08}$$

(where the A_m's have to be subjected to the condition resulting from (1.07)) we shall have

$$n'(x, t) = \sum_{m=1}^{\infty} A_m e^{-m^2\tau} \sin(m\pi x/l), \tag{1.09}$$

where

$$\tau = D\pi^2 t/l^2. \tag{1.10}$$

Making use of (1.09) we can evaluate (1.06) and then solve (1.05) by separation of the variables. For our purposes, however, it is preferable to introduce first the "mean ionic density" defined by

$$\bar{n}(t) = (N(t)/l)\int_0^l n'(x, t)dx. \tag{1.11}$$

Differentiating Eq. (1.04) with regard to t we find after some transformations

$$d\bar{n}/dt = -\bar{\alpha}\bar{n}^2 - \bar{D}\bar{n}, \tag{1.12}$$

where

$$\bar{\alpha} = \alpha l\left[\int_0^l n'^2 dx \Big/ \left(\int_0^l n' dx\right)^2\right] \tag{1.13}$$

and

$$\bar{D} = D\left[\left(\left(\frac{\partial n'}{\partial x}\right)_0 - \left(\frac{\partial n'}{\partial x}\right)_l\right) \Big/ \int_0^l n' d\ \right]. \tag{1.14}$$

[3] L. Lichtenstein, J. f. d. reine u. angew. Math. **158**, 80 (1927).

[4] G. Jaffé, Ann. d. Physik **42**, 303 (1913); **1**, 977 (1929); D. E. Lea, Proc. Camb. Phil. Soc. **30**, 80 (1934); L. B. Loeb, *Fundamental Processes of Electrical Discharge in Gases* (John Wiley and Sons, New York, 1939), p. 134 and following.

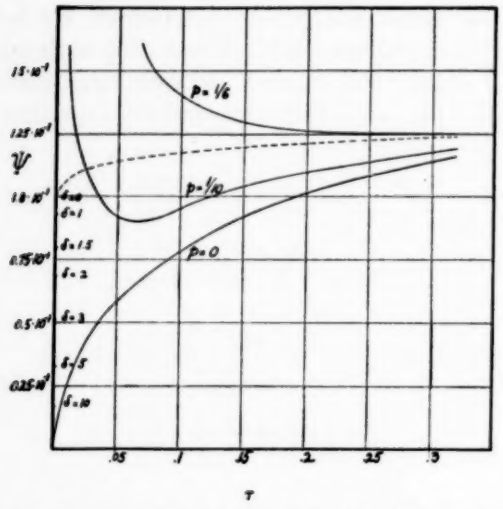

FIG. 1. Representation of Ψ as a function of τ. The three full curves correspond to constant initial ionization of different breadth, the parameter $p=a/l$ being given by 0, 1/10, 1/6 respectively. The broken line corresponds to the parabolic initial distribution which results from diffusion alone (see (1.26)).

Equation (1.09) then yields

$$\bar{\alpha}=\alpha\pi^2 S_1/8S_3^2, \tag{1.15}$$

$$\bar{D}=D\pi^2 S_2/l^2 S_3, \tag{1.16}$$

where S_1, S_2, S_3 represent the sums

$$S_1=\sum_{m=1}^{\infty} A_m^2 \exp(-2m^2\tau), \tag{1.17}$$

$$S_2=\sum_{\mu=0}^{\infty}(2\mu+1)A_{2\mu+1}\exp(-(2\mu+1)^2\tau), \tag{1.18}$$

$$S_3=\sum_{\mu=0}^{\infty}(2\mu+1)^{-1}A_{2\mu+1}\exp(-(2\mu+1)^2\tau). \tag{1.19}$$

Thus the mean ionic density decreases according to a law involving a quadratic and a linear term, and the respective coefficients, $\bar{\alpha}$ and $\bar{D}$, are average values depending on the initial distribution (the A_m's) and the time (τ).

For comparison with experimental data (1.12) can be written in the form

$$d\bar{n}/dt=-\alpha^*\bar{n}^2, \tag{1.20}$$

where

$$\alpha^*=\bar{\alpha}(1+\bar{D}/\bar{\alpha}\bar{n}). \tag{1.21}$$

This α^* can be interpreted as the "instantaneous coefficient of recombination" which varies with time owing to diffusion.

The quotient

$$\bar{\alpha}\bar{n}^2/\bar{D}\bar{n}=(\alpha/D)\bar{n}l^2\psi, \tag{1.22}$$

where

$$\psi=S_1/8S_2S_3 \tag{1.23}$$

represents the ratio of the loss by recombination to that by diffusion.

Let us now evaluate $\bar{\alpha}$ and ψ in two special cases.

(a) First case

The initial distribution is given by the following:

$$n_0(x)=0 \quad \text{for} \quad 0<x<a,$$
$$n_0(x)=\text{const.} \quad \text{for} \quad a<x<(1-a),$$
$$n_0(x)=0 \quad \text{for} \quad (1-a)<x<1.$$

The constant is determined by the normalizing equation (1.07). We obtain

$$A_{2\mu+1}=[4/(\pi(l-2\alpha)(2\mu+1))]$$
$$\times\cos((2\mu+1)\pi a/l), \quad \mu=0, 1, 2\cdots \tag{1.24}$$

and this solution includes the limiting case $a=0$ where the initial ionization extends to the collecting plates. Upon introducing (1.24) into (1.15) and (1.23) it is seen that $\bar{\alpha}$ and ψ depend only on τ and the parameter

$$p=a/l. \tag{1.25}$$

They are represented in Figs. 1 and 2 for the three values $p=0$, $\frac{1}{10}$, $\frac{1}{6}$ as functions of τ.

(b) Second case

The initial distribution is assumed to be

$$n_0(x)=qx(l-x)/2D, \tag{1.26}$$

where q is a constant. This assumption leads to

$$N_0=ql^3/12D \tag{1.27}$$

and

$$A_{2\mu+1}=48/(l\pi^3(2\mu+1)^3), \quad \mu=0, 1, 2\cdots. \tag{1.28}$$

The corresponding curves for $\bar{\alpha}$ and ψ are drawn by broken lines in the Figs. 1 and 2.

The significance of (1.26) is that it represents the steady state distribution if there is a constant production of q pairs of ions per sec. and cm^3 and if conditions are such that recombination can be disregarded.

In the more general case where diffusion and recombination must be considered the steady

state distribution depends, according to Langevin,[1] on a "reduced distance" for which we choose[5]

$$\delta = l(q\alpha/36D^2)^{\frac{1}{4}}. \qquad (1.29)$$

The steady state distribution is then given by an elliptic function and the coefficients A_m can be evaluted, even in this case, by harmonic analysis. However, this necessity will rarely occur. The above calculations give $\bar{\alpha}$ and ψ in the limiting case $\delta \ll 1$. In the other limiting case, $\delta \gg 1$, the distribution will approach $n_0 = \text{const.}$, i.e., case (a) with $p=0$. Thus the curves for variable δ will lie between those limiting cases. Furthermore, the points from which they start at $\tau=0$, can be determined from calculations which the author has made in another connection.[6] Some such points are indicated in Fig. 1 and it will be seen that a fair estimate of ψ can be made for all values of δ and τ by graphical interpolation. The changes of $\bar{\alpha}$ are unimportant.

Our Fig. 1 shows that, for small values of τ, there are significant changes of ψ with τ, depending on the initial distribution. For values $\tau > 0.2$ all curves approach the asymptotic value $\psi = 0.125$ which holds for all distributions (see (1.23)).

The initial stage of rapid changes does not extend much beyond the period of initial recombination which our theory does not include. Therefore, for small values of τ, our calculations are not applicable and for larger values it will, in most cases, be sufficient to give ψ its asymptotic value. The relative influence of diffusion can then easily be deduced from (1.22). This formula brings out the influence of l and the ionic density. For sufficiently large values of the time diffusion will always be predominant owing to the decrease of $\bar{n}$.

The changes in $\bar{\alpha}$ are far less important, as is seen from Fig. 2. The larger the parameter p, the more marked is the initial decrease of the apparent coefficient of recombination. This increase is due to the broadening of the ionized volume. It must be stressed that our calculations (according to (1.11)) refer $\bar{\alpha}$ to the total volume extending from $x=0$ to $x=l$. If the volume is referred to the part initially ionized, as is generally done by experimenters, our values of $\bar{\alpha}$ have to be multiplied by $(l-2a)/l$ which makes them start with the normal value $\bar{\alpha}=\alpha$ and then decrease. The asymptotic value of $\bar{\alpha}$ is given by $\bar{\alpha} = \alpha\pi^2/8$ for all initial distributions.

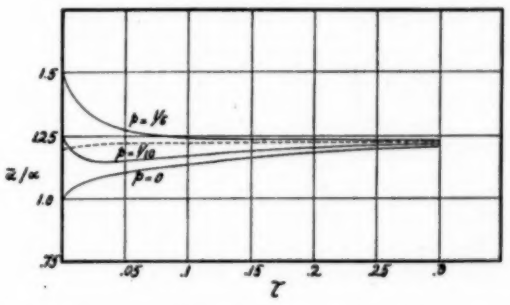

FIG. 2. Representation of $\bar{\alpha}/\alpha$ as a function of τ. The three full curves correspond to constant initial ionization of different breadth, the parameter $p=a/l$ being given by 0, 1/10, 1/6 respectively. The broken line corresponds to the parabolic initial distribution which results from diffusion alone (see (1.26)).

II. ESTABLISHMENT OF THE STEADY STATE

We will assume that there is no ionization up to $t=0$ and that, from $t=0$ on, there is a constant production, of q pairs of ions per sec. and cm³, in the whole volume. The differential equation then becomes

$$\partial n/\partial t = q + D\partial^2 n/\partial x^2 - \alpha n^2, \qquad (2.01)$$

with the same boundary conditions as in Section I.

Let us assume

$$n_\infty(x) = \sum_{m=1}^{\infty} B_m \sin(m\pi x/l) \qquad (2.02)$$

as the solution for the steady state. Then we attempt to solve (2.01) by putting

$$n(x,t) = n_\infty(x) - N_1(t)n'_1(x,t). \qquad (2.03)$$

Here $N_1(t)$, a function of time only, is normalized by

$$N_1(0) = 1 \qquad (2.04)$$

and

$$n_1'(x,t) = \sum_{m=1}^{\infty} B_m e^{-m^2\tau} \sin(m\pi x/l) \qquad (2.05)$$

[5] G. Jaffé, Ann. d. Physik **43**, 249 (1914).

[6] Reference 5, p. 267 and following. Table I on p. 270 may be used but it must be mentioned that the indications of this table are not sufficiently accurate for the present purpose for values of $\delta < 0{,}4$. Also the expansions (52) and (56) must be carried further.

is that solution of

$$\partial n_1'/\partial t = D\partial^2 n'_1/\partial x^2, \tag{2.06}$$

which reduces, for $t=0$, to $n_.(x)$.

It is evident that (2.03) satisfies the initial and boundary conditions. To determine $N_1(t)$ we use the same procedure as in Section I and find the ordinary differential equation

$$dN_1/dt = -2\alpha f_1(t) N_1 + \alpha f_2(t) N_1^2, \tag{2.07}$$

where

$$f_1(t) = \int_0^l n_\infty n_1' dx \Big/ \int^l n_1' dx \tag{2.08}$$

and

$$f_2(t) = \int_0^l n_1'^2 dx \Big/ \int_0^l n_1' dx. \tag{2.09}$$

Introducing again the "mean ionic density"

$$\bar{n}_1 = (N_1(t)/l) \int_0^l n_1' dx \tag{2.10}$$

we find

$$d\bar{n}_1/dt = -(2\bar{\alpha}_1 \bar{n}_\infty + \bar{D})\bar{n}_1 + \bar{\alpha}\bar{n}_1^2. \tag{2.11}$$

Here $\bar{\alpha}$ and $\bar{D}$ are defined as in (1.13), (1.14) (n_1' replacing n') and $\bar{\alpha}_1$ is given by

$$\bar{\alpha}_1 = \alpha l \left[\int_0^l n_\infty n_1' dx \Big/ \left(\int_0^l n_\infty dx \cdot \int_0^l n_1' dx \right) \right]. \tag{2.12}$$

To compare conditions with those prevailing in the absence of diffusion we solve the differential equation

$$dn/dt = q - \alpha n^2 \tag{2.13}$$

by

$$n = n_\infty - n_t. \tag{2.14}$$

Here n_∞ represents the solution for the steady state

$$n_\infty = (q/\alpha)^{\frac{1}{2}}, \tag{2.15}$$

and n_t is subject to the condition:

$$n_t = n_\infty \quad \text{for} \quad t=0.$$

Substituting (2.14) into (2.13) we find

$$dn_t/dt = -2\alpha n_\infty n_t + \alpha n_t^2, \tag{2.16}$$

and this equation has to be compared with (2.11).

From (2.16) we see that, even in the absence of diffusion, the rate of change dn_t/dt ($= -dn/dt$) can be represented by the sum of a linear and a quadratic term. If, now, diffusion is taken into account comparison with (2.11) shows that the linear term is increased by a term involving $\bar{D}$. Thus the establishment of the steady state will tend to deviate from the quadratic law towards a linear law. The larger $\bar{D}$ is in comparison with $2\bar{\alpha}_1\bar{n}_\infty$ the more the linear term will prevail. The conditions of experiment will then determine whether we obtain a better representation by a quadratic law

$$d\bar{n}_1/dt = -\alpha^* \bar{n}_1^2 \tag{2.17}$$

using the time-dependent coefficient of recombination

$$\alpha^* = (2\bar{\alpha}_1\bar{n}_\infty + \bar{D})/\bar{n}_1 - \bar{\alpha}, \tag{2.18}$$

or by a linear law

$$d\bar{n}_1/dt = -\beta^* \bar{n}_1, \tag{2.19}$$

where

$$\beta^* = 2\bar{\alpha}_1\bar{n}_\infty - \bar{\alpha}\bar{n}_1 + \bar{D}. \tag{2.20}$$

For large values of δ, only thin layers near the plates are affected by diffusion. For δ larger than 2 or 3, n_∞ in (2.02) can be replaced by its limiting value (2.15). Under these conditions we have, from (2.12)

$$\bar{\alpha}_1 = \alpha. \tag{2.21}$$

III. Comparison with Experiment

The preceding formulae were developed to yield adequate corrections for measurements on recombination. Their application clarifies anomalies in previous measurements.

(a) Experiments on decay

The most accurate measurements of α concerning a well-defined pure gas are presumably those of Gardner[7] on oxygen. These measurements show the striking fact that the observed values of α depend strongly on the time of exposure, t', and on the ionic density. After the first large drop (due to initial recombination) the observed values become practically constant, but the apparently constant value decreases as t' increases. Furthermore, the values belonging to different t''s move apart if the pressure, or the distance between the plates, is decreased. Loeb[8] has shown that these phenomena cannot be explained by his theory of initial recombination

[7] M. E. Gardner, reference 2.
[8] L. B. Loeb, reference 4, p. 136 and following.

TABLE I. *The values of α observed by Gardner are compared with values calculated from formula (1.21).*

	t'	n_0	$\alpha^*\times10^6$ CALC. $t=0.1$ SEC.	$\alpha^*\times10^6$ CALC. $t=0.3$ SEC.	$\alpha\times10^6$ OBS. $t=0.1$ SEC.
$V=190$ cm³					
$l=3$ cm	0.5	1.00×10^6	2.00	2.03	1.99
$a=0.3$ cm	0.25	6.45×10^5	2.03	2.06	2.12
$P=76$ cm Hg	0.0625	1.79×10^5	2.20	2.22	2.25
$\alpha=1.98\times10^{-6}$					
$D=4.7\times10^{-2}$	0.0313	0.90×10^5	2.42	2.45	——
$V=190$ cm³					
$l=3$ cm	0.5	6.07×10^5	1.61	1.65	1.58
$a=0.3$ cm	0.25	3.45×10^5	1.72	1.75	1.64
$P=38$ cm Hg	0.0625	8.93×10^4	2.41	2.44	2.07
$\alpha=1.48\times10^{-6}$					
$D=9.4\times10^{-2}$	0.0313	4.46×10^4	3.32	3.37	——
$V=700$ cm³					
$l=7$ cm	0.5	1.84×10^5	1.05	1.06	1.04
$a=1$ cm	0.25	9.42×10^4	1.32	1.33	1.56
$P=10$ cm Hg	0.125	4.72×10^4	1.87	1.88	2.55
$\alpha=0.85\times10^{-6}$					
$D=3.57\times10^{-1}$	0.0625	2.37×10^4	2.96	2.98	4.86

unless improbable values for the coefficient of diffusion are assumed.

Our formulae show that the observed phenomena are due, at least to a considerable part, to diffusion to the walls. In order to apply our exact formula (1.21) we should know accurately the initial distribution of the ions. Now, this initial distribution depends strongly on the time of exposure t'. It would be possible to calculate the distribution of the ions as a function of t' by the method of Section II. Such a calculation, however, would hardly be worth while because the initial distribution affects mainly the changes in $\bar{\alpha}$ for those intervals of time where initial recombination is prevalent and masks the changes foreseen by our theory. We have, therefore, applied the approximate asymptotic formulae.

Some of the results of our calculations are compared, in Table I, with the observed values as taken from Gardner's diagrams. As the exact values of the ionic densities were not known, they were calculated under the assumption that $n_0=1\times10^6$ for atmospheric pressure and that q is proportional to the pressure. For this purpose the observed *apparent* values of α were substituted into the simple law (2.13).[9]

[9] The author is very much indebted to Professor Loeb and Professor Gardner for furnishing him information concerning the measurements.

The values of D used and the true values of α, as corrected for diffusion, are also indicated in the table. From the calculated values it will be seen that diffusion, under the conditions of Gardner's experiments, has a very marked influence on the coefficient of recombination. It will be noticed that the values of α^* may appear to be constant over a considerable interval of time though they are different from the true value α. Furthermore, the apparent values move apart with decreasing t' and n_0, as observed.

The numerical agreement is about as good as might be expected from the approximate nature of the calculations. The theoretical deviations are too large for the pressure $P=38$ cm Hg and too small for $P=10$ cm Hg. The former deviation is probably due to the fact that the assumed values of n_0 are too small, the latter deviation to the fact that initial recombination (at $P=10$ cm Hg) is not yet quite over at $t=0.1$ sec.

It must be emphasized that the only numerical values assumed arbitrarily in the preceding calculations are the true values of α which are to be determined. The apparent increase in the observed values is due to the fact that, at the time when the initial recombination is over, diffusion to the walls has become important. Because of the decrease of $\bar{n}$, the observable α^* ought to increase slowly afterwards (see (1.21)) and should pass through a very flat minimum. This mini-

TABLE II. *The values of α and β observed by Power are compared with values calculated from formulae (2.18) and (2.20). The value underlying the calculations is $\alpha = 1.6 \times 10^{-6}$.*

GROUP	n_∞	q	$\alpha \times 10^6$ OBS.	$\beta \times 10^3$ OBS.	$\alpha^* \times 10^6$ CALC. $t=0$	$\alpha^* \times 10^6$ CALC. $t=120$ SEC.	$\beta^* \times 10^3$ CALC. $t=0$	$\beta^* \times 10^3$ CALC. $t=120$ SEC.
I	1070	11.8	4.53	6.61	5.05	13.3	5.40	5.70
II	1620	21.9	3.65	8.00	4.13	11.6	6.70	7.52
III	2680	33.8	2.12	8.46	3.31	10.3	8.85	11.0

mum has been observed by Gardner with his smaller condenser ($l=3$ cm) at $P=76$ cm Hg. In all other cases it should have occurred at times t larger than those observed.

Concerning the influence of the initial density, n_0, our formula predicts a change of 3.5, 17, 272 percent for 76, 38, 10 cm Hg, respectively, if n_0 is changed from 10^6 to 10^5 at atmospheric pressure. These numbers refer to conditions in Gardner's larger vessel ($l=7$ cm) where the influence of diffusion is less marked. They agree, approximately, with the observed changes except at $P=76$ cm Hg where a discrepancy remains, the theoretical change being too small (3.5 percent as against about 20 percent).

(b) Establishment of the steady state

It was first pointed out by von Schweidler[10] that the establishment of the steady state is, in cases of weak ionization, described more accurately by a linear law than by the usual quadratic law. This fact has been confirmed by Power[11] and suggests strongly that diffusion is active.[12]

As Power's values show considerable fluctuations we have formed three groups out of the data contained in his Table VII. The first group with 6 observations where n_∞ (as corrected by Power for diffusion) ranges from 1480 to 1780, the second includes 6 values from 2130 to 2720 and the last group 5 values from 3490 to 4560. The calculations are based on the exact formulae (2.18) and (2.20), respectively, and on the normal values $D=0.035$, $\alpha=1.6\times10^{-6}$. The geometrical conditions required $l=12.6$ cm, $a=0$; α^* and β^* were calculated for $t=0$ and $t=120$ sec.[13]

It will be seen from Table II that the calculated values of β^* are much more nearly constant than those of α^* and that they agree within reasonable limits with the observed values though no constant has been chosen so as to obtain agreement. A better agreement might be attained by making α different from 1.6×10^{-6} but there can scarcely be a doubt that the apparent high values of α in Power's experiments are largely due to diffusion, in spite of the relatively large distance between the plates.

However, it must be pointed out that von Schweidler and Power report measurements with very much larger condensers in which the value of α appears to be as high as 1×10^{-4}. Under these conditions the observed values cannot be explained by diffusion to the walls alone. These discrepancies at large volumes, as well as the discrepancy mentioned above, indicate that some other influence is active. It seems reasonable to assume that besides diffusion in molecular dimensions (initial recombination) and diffusion in macroscopic dimensions (the factor studied here) some intermediate inhomogeneity in the initial distribution may play a part. It is, however, premature to assert such an influence before further measurements in this direction have been carried out.

[10] E. von Schweidler, Akad. Wiss. Wien **127**, (2a), 953–967 (1918); **128**, (2a), 947–955 (1919).

[11] A. D. Power, J. Frank. Inst. **196**, 327 (1923).

[12] The author is indebted to Professor J. W. Broxon for making accessible to him, at the University of Colorado, a Doctor's thesis by G. T. Merideth on recombination at high pressures. In the measurements of Dr. Merideth the same fact was observed.

[13] For $t=120$ sec. asymptotic values and the legitimate approximation (2.21) were introduced.

On the Energy Loss of Heavy Ions

JULIAN KNIPP, *Purdue University, Lafayette, Indiana*

AND

EDWARD TELLER, *George Washington University, Washington, D. C.*

(Received February 28, 1941)

The energy loss of heavy ions is due to collisions with electrons and with nuclei. The first process is essentially determined by the ionic charge, which in turn depends on the ratio of the velocities of the most loosely bound electron within the ion, and of the ion. The former velocity is calculated from the Thomas-Fermi model while the ratio of the two velocities is adjusted to empirical data. The nuclear contribution to the stopping cross section is calculated by the known classical method. Though approximations could not be avoided, the procedure lends itself to the systematization of experimental data on intermediate and heavy ions.

I. INTRODUCTION

THE energy loss of a heavy ion in its passage through air or other materials differs from the energy loss of protons and alpha-particles in two respects. First, the effective charge of a proton or alpha-particle remains constant during most of its path, while the energetic heavy ion has initially a high positive charge, which diminishes as the ion is slowed down. Second, the energy loss of a heavy ion of low charge proceeds to a considerable extent through its interaction with the nuclei rather than with the electrons of the atoms.

One of the best sources of heavy ions of high energy is the uranium fission process. The slowing down of particles produced by fission has been considered by Bohr[1] and by Lamb.[2] Both authors recognize that it is practically impossible to give a detailed discussion of the capture and loss of electrons by the heavy ion during its passage through the decelerating medium. Bohr assumes, instead, that at each point of the path the ion retains all electrons the orbital velocities of which are greater than the velocity of the ion. The electrons with smaller velocities are torn off by collisions. Indeed, the removal of electrons of high velocity is very improbable since for such electrons the collision is adiabatic. On the other hand, if the velocity of the ion is much larger than the velocity of the electron within the ion, the probability for capture is much smaller than the probability for loss. The capture cross section decreases with a very high inverse power of the velocity of the ion, while the cross section for loss falls off roughly with the inverse first to second power of the velocity, having much the same velocity dependence as the stopping cross section of a charged particle.[3] It may be expected that capture and loss probabilities become equal when the ratio of electronic to ionic velocities is not far from unity. Bohr actually assumes this ratio to be unity.

Lamb's calculation of the average charge is based on an assumption about the energy rather than the velocity of the outermost electrons in the ion. He considers the electrons within the decelerating medium as practically free and assumes that the kinetic energy of these electrons relative to the ion is, under equilibrium conditions, equal to the ionization energy of the outermost electron within the ion. This procedure has the advantage that in making the calculations empirical ionization potentials can be used. In doing so, Lamb obtains for the fission particles ranges which agree satisfactorily with the available rough observations. Of course, Lamb's assumption is not meant to hold rigorously. Only those electrons of the decelerating medium can be considered as approximately free the orbital velocities of which are small compared to the velocity of the ion. Actually, over a considerable fraction of the range the ionic velocity is smaller than the orbital velocities of most of the electrons

[1] N. Bohr, Phys. Rev. **58**, 654 (1940); **59**, 270 (1941).
[2] W. E. Lamb, Jr., Phys. Rev. **58**, 696 (1940).
[3] E. Rutherford, Phil. Mag. **47**, 277 (1924); L. H. Thomas, Proc. Roy. Soc. **114**, 561 (1927); J. R. Oppenheimer, Phys. Rev. **31**, 349 (1928); H. C. Brinkman and H. A. Kramers, Proc. K. Akad. Amst. **33**, 973 (1930).

of the medium. Collisions with electrons that can be considered as free will not lead to ionization unless Lamb's condition is fulfilled; but ionization may still be very improbable even though enough energy is available. The qualitative justification of Lamb's assumption lies in its relation to Bohr's criterion. If each electron of the ion were moving in a central Coulomb field, then, according to the virial theorem, the two methods of treatment would be identical. However, the average field in the ion deviates from a Coulomb field sufficiently to cause noticeable differences in the results of the two procedures.

In this paper we shall assume, in agreement with Bohr, that the average charge of the ion depends primarily on the ratio of electronic to ionic velocities. We shall, however, not postulate that the velocity of the outermost electron in the ion be exactly equal to the velocity of the ion. Rather we shall try to find from available experimental data just what the ratio of the velocities is. In doing so, we shall make use of measurements on protons, alpha-particles, and medium weight ions produced in alpha-recoils, and also of the observed properties of fission particles. The electronic velocities within the ions will be obtained from the Thomas-Fermi model. In the numerical calculations we shall restrict ourselves to air as the stopping substance.

II. Electronic Velocities within the Ion

As a measure of the velocity of the most loosely bound electron within the ion, we take the root mean square value, V_e, of this velocity. We use the Thomas-Fermi model to estimate V_e as a function of the ionic charge. Let Z be the atomic number of the ion and i the number of electrons necessary to neutralize the ion. Let $X(r)$ be the electrostatic potential at a distance r from the center of the ion. At a distance r_0 from the center, the electronic density is assumed to vanish; this distance is called the radius of the ion and the value of the potential at this distance is denoted by X_0. The number of electrons the energies of which lie in the infinitesimal range between $e(X_0-\Delta X_0)$ and eX_0 is

$$(4me\Delta X_0/\pi\hbar^3)\int_0^{r_0} dr r^2[2me(X(r)-X_0)]^{\frac{1}{2}}. \quad (1)$$

The mean square velocity of the electrons in this range is obtained by multiplying the integrand by $(1/m^2)[2me(X-X_0)]$, integrating, and dividing by (1). This procedure gives

$$\frac{\int_0^{r_0} dr r^2[2me(X(r)-X_0)]^{\frac{1}{2}}}{m^2\int_0^{r_0} dr r^2[2me(X(r)-X_0)]^{\frac{1}{2}}}. \quad (2)$$

We set this equal to V_e^2 and introduce the dimensionless quantity $v_e=V_e\hbar/e^2$. Introducing in addition the standard quantities

$$\varphi=r(X(r)-X_0)/Ze,$$
$$x=Z^{\frac{1}{3}}(128/9\pi^2)^{\frac{1}{2}}rme^2/\hbar^2, \quad (3)$$

one obtains

$$\frac{v_e^2}{Z^{4/3}}=\left(\frac{1024}{9\pi^2}\right)^{\frac{1}{2}}\int_0^{x_0} dx x^{\frac{1}{2}}\varphi^{\frac{1}{2}}\Big/\int_0^{x_0} dx x^{\frac{1}{2}}\varphi^{\frac{3}{2}}. \quad (4)$$

where the limit of integration is the value of x for $r=r_0$. Integrating the electron density over the whole ion, one finds

$$\int_0^{x_0} dx x^{\frac{1}{2}}\varphi^{\frac{3}{2}}=(Z-i)/Z. \quad (5)$$

We have evaluated

$$I=\int_0^{x_0} dx x^{\frac{1}{2}}\varphi^{\frac{1}{2}} \quad (6)$$

for a number of values of i/Z by numerical integration. The functional dependence of φ on x has been taken from tables calculated by Fermi and by Miranda.[4] The results are given in Table I. Figure 1 shows i/Z as a function of $v_e/Z^{\frac{1}{2}}$.

Table I. *Numerical values of I, $v_e^2/z^{4/3}$, and $v_e/z^{2/3}$ calculated for the Thomas-Fermi ion for various values of i/z, the ratio of ionic to nuclear charge.*

i/z	I	$v_e^2/z^{4/3}$	$v_e/z^{2/3}$
0.01	180	0.012	0.11
0.02	96	0.023	0.15
0.05	52	0.041	0.21
0.10	26	0.078	0.28
0.121	22.8	0.087	0.295
0.223	10.4	0.169	0.411
0.522	1.90	0.57	0.75
0.761	0.379	1.42	1.19
0.949	0.0221	5.21	2.29

[4] E. Fermi, Mem. d. R. Accad. d'Italia **1**, 3 (1930); C. Miranda, Mem. d. R. Accad. d'Italia **5**, 286 (1934).

Because of the finite size of the electronic charge, the velocity of the most loosely bound electron cannot be obtained from the point corresponding to the charge i in Fig. 1, but is rather an average value of the velocities calculated from a section of Fig. 1 which corresponds to charges between i and $i+1$. If capture and loss probabilities are equal for the most loosely bound electron of an ion with charge i, then the charge averaged over a sufficiently short section of the path of the ion will lie between i and $i+1$. We shall, therefore, assume that the average velocity of the outermost electron and the average charge of the ion (resulting from capture and loss) correspond to the same intermediate point on the curve. Thus, instead of considering finite sections of the curve, we shall read the average ionic charge $\bar{i}$ corresponding to a desired electronic velocity directly from the curve.

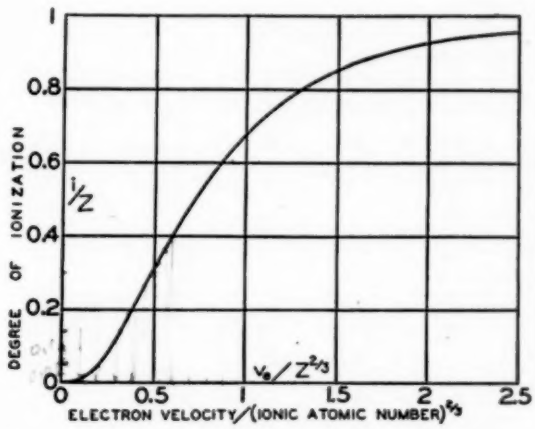

FIG. 1. The ratio of the ionic to nuclear charge i/z plotted as a function of the velocity of the most loosely bound electron (in units $Z^{2/3}e^2/\hbar$).

III. The Methods of the Energy Loss

The energy loss of the particle or ion per centimeter of path is

$$-dE/dx=N\sigma, \tag{7}$$

where N is the number of atoms per cubic centimeter (5.1×10^{19} atoms/cm^3 for air at 15°C and 76 cm pressure) and σ is the stopping cross section per atom. σ is the sum of three terms; one, σ_e, is the stopping cross section due to the electrons of the atom; another, σ_n, is the stopping cross section arising from the interaction with the atomic nucleus; and the third, σ_h, is the stopping cross section due to collisions with the atom as a whole (hard collisions). We shall see that these terms become successively most important in the order given as the ion is slowed down. More particularly, σ_e, is most important for $v\gg1$, σ_n for $v\backsimeq1$, and σ_h for $v\ll1$, ($v=V\hbar/e^2$).

For a given velocity of the ion, σ_e is given by

$$\sigma_e=\langle\bar{i}^2\rangle_{Av}\sigma_e', \tag{8}$$

where $\langle\bar{i}^2\rangle_{Av}$ is the mean square charge of the ion and σ_e' is the *specific* electronic stopping cross section, that is the cross section which would be obtained for a unit charge in the absence of capture and loss. $\langle\bar{i}^2\rangle_{Av}$ and σ_e' are to be taken for the velocity in question.

According to the perturbation calculation carried out by Bethe,[5] (8) is valid as long as the radius of the ion is sufficiently small and the fluctuations of $\langle\bar{i}^2\rangle_{Av}$ can be neglected. The original discussion given by Bohr[6] leads to a slightly different dependence of the cross section on the ionic charge. Lamb has shown that in the present case some deviation from (8) is to be expected. According to Bloch,[7] Bethe's and Bohr's treatments apply respectively for $i/v\ll1$ and $i/v\gg1$. In the following discussion i/v does not differ greatly from unity. However, deviations from (8) become considerable only when the logarithmic factor in the stopping cross section is small. This happens around $v=1$. At these velocities, however, collisions with nuclei become important and have the effect of reducing the uncertainty in the range which would otherwise be present.

The specific stopping cross section, σ_e', has been calculated by the authors referred to above.[5-7] These calculations necessarily involve more or less rough assumptions about the electronic structure of the stopping material.[8] In our present discussion, we shall rely on an experimental determination of σ_e'.

The stopping cross section for air is known very accurately for protons and alpha-particles. At high energies both particles are completely

[5] H. A. Bethe, Ann. d. Physik **5**, 325 (1930).
[6] N. Bohr, Phil. Mag. **25**, 10 (1913); **30**, 581 (1915).
[7] F. Bloch, Ann. d. Physik **16**, 285 (1933).
[8] The Thomas-Fermi distribution has been used by F. Bloch, Zeits. f. Physik **81**, 363 (1933).

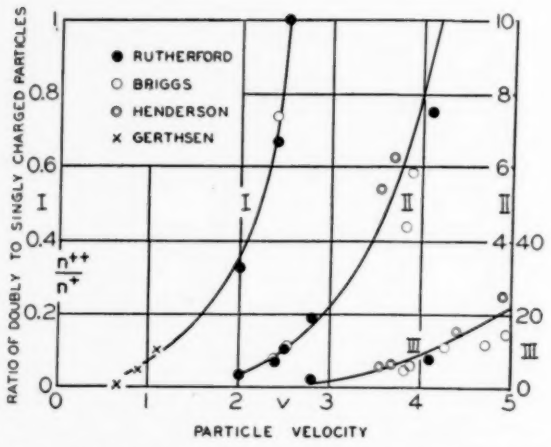

FIG. 2. Ratio of the number of doubly to singly charged alpha-particles plotted against the particle velocity, in units $e^2/\hbar$. All curves have the same abscissa. Curve I has its ordinate scale to the left and curves II and III have their ordinate scales to the right.

ionized and the stopping cross section of alpha-particles is exactly four times the stopping cross section of protons of the same *velocity*. Deviations from this rule set in due to the capture and loss of electrons with alpha-particles of about 2.5 Mev ($v \leqq 5$). The specific stopping cross section is obtainable directly from these data for high velocities. For low velocities it becomes necessary to know the mean square charge of one or the other of these particles as a function of velocity.

Now Rutherford has measured the ratio of singly to doubly charged alphas by deflecting a beam emerging from a mica foil in a magnetic field.[9] On the other hand, Kapitza used very strong magnetic fields to obtain the average curvature of alpha-particles in an air-filled Wilson chamber, and by this expedient he was able to find the ratio of mean charge to velocity at different points along the track.[10] By using these data it is possible to calculate the specific stopping cross section, σ_e', from the stopping cross section of alpha-particles in air.

Let n, n^+ and n^{++} be the number of neutral, singly charged, and doubly charged particles in a beam of alpha-particles passing through a medium. Then the mean charge, $\bar{\imath}$, is given by

$$\bar{\imath} = \frac{n^+ + 2n^{++}}{n + n^+ + n^{++}}; \tag{9}$$

also the mean square charge is given by

$$\langle i^2 \rangle_{Av} = \frac{n^+ + 4n^{++}}{n + n^+ + n^{++}}. \tag{10}$$

Therefore

$$\langle \bar{\imath}^2 \rangle_{Av} = \bar{\imath} \frac{1 + 4(n^{++}/n^+)}{1 + 2(n^{++}/n^+)}. \tag{11}$$

The ratio n^{++}/n^+ has been found by Henderson[11] to be quite independent of the nature of the material through which the particles are passing. No detectable difference was noted for such different substances as aluminum, mica, copper, silver and gold. Since the average atomic weight of mica is not much greater than that of air, it is assumed that the ratio for air is the same as for mica. In Fig. 2 are plotted the experimental values found for mica by Rutherford,[9] Henderson[11] and Briggs,[12] and in addition a few values found for air by Gerthsen.[13]

Kapitza's observations on alphas in air extend down only to a residual range of 0.4 cm ($v = 2.54$). However, his data for alphas in hydrogen gas extend down to a residual range of 0.2 cm (in hydrogen, $v = 0.57$). We shall use both sets of data since they give rise to curves for $\bar{\imath}$ against v which overlap slightly and connect very smoothly. (See Table II.) Points for the mean charge $\bar{\imath}$ are plotted in Fig. 3.

The mean square charge, $\langle \bar{\imath}^2 \rangle_{Av}$ is calculated from (11) taking $\bar{\imath}$ from the solid curve in Fig. 3 and n^{++}/n^+ from the curves of Fig. 2. Thus we have assumed that the average charge in air for a given velocity differs but little from the average

TABLE II. *Analysis of data by Kapitza on the ratio of mean charge to velocity of alpha-particles in air and hydrogen.*

Range cm	v		$\bar{\imath}/v$		$\bar{\imath}$	
	Air	H_2	Air	H_2	Air	H_2
0.2		0.57		0.327		0.18
0.4	2.54	1.023	0.586	0.469	1.49	0.48
0.6	3.30	1.41	0.532	0.555	1.76	0.78
0.8	3.89	1.74	0.487	0.591	1.89	1.03
1.0	4.38	2.11	0.444	0.618	1.95	1.30
1.2	4.77	2.34	0.413	0.620	1.97	1.45
1.4	5.09	2.54	0.388	0.604	1.98	1.53
1.6	5.37	2.75	0.370	0.577	1.99	1.59

[9] E. Rutherford, Phil. Mag. **47**, 277 (1924).
[10] P. L. Kapitza, Proc. Roy. Soc. **106**, 602 (1924).
[11] G. H. Henderson, Proc. Roy. Soc. **109**, 157 (1925).
[12] G. H. Briggs, Proc. Roy. Soc. **114**, 241 (1927).
[13] C. Gerthsen, Physik. Zeits. **31**, 948 (1930).

charge in hydrogen for the same velocity.[14] The calculation is given in Table III and the results also plotted in Fig. 3 (dashed curve).

We have taken σ_e from curves by Livingston and Bethe.[15] To get σ_e', σ_e is divided by $\langle i^2\rangle_{Av}$ from Table III. Values are listed in Table IV. The specific cross section obtained in this way is plotted in Fig. 4.

The existing data for capture and loss by protons in air are in disagreement with similar measurements for protons in nitrogen and in oxygen.[16] Therefore we have not attempted to calculate σ_c' from the stopping cross section for protons.

For high values of the mean charge of the heavy ion, we shall simply substitute $\bar{i}^2$ for $\langle i^2\rangle_{Av}$ in the formula $\sigma_c=\langle i^2\rangle_{Av}\sigma_e'$. The difference between $\bar{i}^2$ and $\langle i^2\rangle_{Av}$ becomes important for low values of the mean charge. Moreover, the Thomas-Fermi model becomes rather unreliable for low degrees of ionization. However we shall continue to use the values derived in the previous section for $\bar{i}$ as a function of v down through the range where $\bar{i}$ is comparable to or smaller than unity. However to obtain $\langle i^2\rangle_{Av}$ in the range $0\leq\bar{i}\leq 2$, we shall again use experimental data on alpha-particles. In Fig. 5 is shown the dependence of the root mean square charge as a function of the mean charge as observed for alpha-particles. For low values of

TABLE III. *Calculation of the mean square charge from the mean charge taken from Fig. 3 and n^{++}/n^{+} obtained from Fig. 2.*

v	$\bar{i}$	n^{++}/n^{+}	$\langle i^2\rangle_{Av}$
0.5	0.15		0.15
1.0	0.46	0.06	0.51
1.5	0.85	0.17	1.07
2.0	1.22	0.36	1.73
2.5	1.49	0.95	2.47
3.0	1.68	2.2	3.05
3.5	1.82	4.2	3.44
4.0	1.90	9.0	3.70
4.5	1.95	15	3.84
5.0	1.98	22	3.92

[14] See in this connection P. M. S. Blackett, Proc. Roy. Soc. **135**, 132 (1932). Blackett suggests that the same mean charge in hydrogen and air may be due to the presence of water vapor in the Wilson chamber.

[15] M. S. Livingston and H. A. Bethe, Rev. Mod. Phys. **9**, 270 (1937). The values for $v<1$ have been calculated directly from the data of P. M. S. Blackett and D. S. Lees, Proc. Roy. Soc. **134**, 658 (1932), which data extend down to 0.7×10^8 cm/sec.

[16] E. Rüchardt, Ann. d. Physik **71**, 377 (1923); H. Bartels, Ann. d. Physik **6**, 957 (1930).

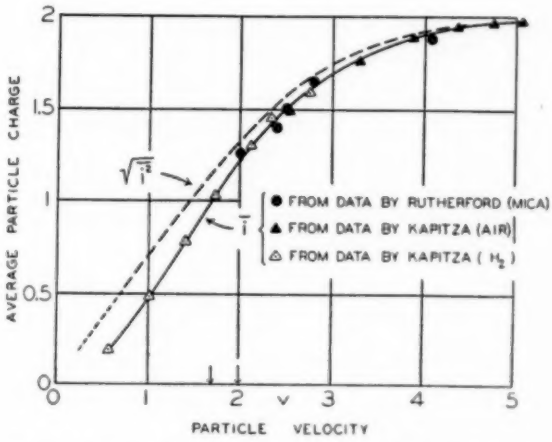

FIG. 3. Mean charge of alpha-particles plotted against velocity, in units $e^2/\hbar$ (all indicated points and the solid curve). In addition to the experimental points from the data by Kapitza (solid triangles for alpha-particles in air; open triangles for alpha-particles in hydrogen) are some points calculated from Rutherford's data for n^{++}/n^{+} from the simplified formula $(1+2n^{++}/n^{+})/(1+n^{++}/n^{+})$, valid if $n\ll1$. These points fit in with the others very well. The data indicate that $\bar{i}$ for alpha-particles in air is not greatly different from $\bar{i}$ for alphas in hydrogen. The dashed curve is the root mean square charge plotted against the velocity. This curve is calculated from the solid curve and (11) with n^{++}/n^{+} from Fig. 2.

$\bar{i}$ this dependence, of course, must be parabolic. In the neighborhood of $\bar{i}=2$ the slope $d\langle i^2\rangle_{Av}^{\frac{1}{2}}/d\bar{i}$ has the value $\frac{3}{4}$, as one sees readily from (9) and (10). When, for heavy ions, $\bar{i}$ as calculated in the previous section is greater than 2, we arbitrarily set $\langle i^2\rangle_{Av}=\bar{i}^2$; when $\bar{i}$ is less than 2, we take the value of $\langle i^2\rangle_{Av}^{\frac{1}{2}}$ from Fig. 5. We thus introduce a change in slope at $\bar{i}=2$.

The stopping cross section for energy loss to atomic nuclei is given by the expression due to Bohr[6, 1]

$$\sigma_n=2\pi\int_{p_{\min}}^{p_{\max}}dpp\frac{1}{2\mu}\left[\frac{2ZZ_ae^2}{pV}\right]^2, \qquad (12)$$

where $\mu=MMa/(M+Ma)$ is the reduced mass of the two particles (M and Ma are the masses of the ion and atom, respectively, and Z and Z_a are their nuclear charges), and p is the collision parameter. The reduced mass is used rather than the atomic mass since we count as energy lost not only the kinetic energy transferred to the atom but also the kinetic energy transferred to motion of the ion in a direction perpendicular to its original path. Thus we suppose the range to be measured not along the path but rather in the direction of the original ionic motion. The above

expression then holds as long as the angular deflections are not too great. The lower limit of the integration is the Coulomb limit, $p_{\min}=2ZZ_a e^2/\mu V^2$. The upper limit is determined by the shielding of the electrons.

The upper limit is roughly the smaller of the two distances, R and R_a, where R is the distance from the nucleus of the ion at which the effective charge of the nucleus is $Z^2/2$ and R_a is similarly defined. The effective charge in the Thomas-Fermi model is $Z(\varphi-x\varphi')$. The quantity $(\varphi-x\varphi')^2$ is $\frac{1}{2}$ at $x=0.97$. Thus if $Z>Z_a$, $p_{\max}\backsimeq 0.97(0.88)\hbar^2/Z^{\frac{1}{3}}me^2$. Substituting in (12) gives

$$\sigma_n=\frac{4\pi Z_a{}^2Z^2e^4}{\mu V^2}\log\frac{0.85\hbar^2/Z^{\frac{1}{3}}me^2}{2ZZ_ae^2/\mu V^2}. \qquad (13)$$

For air, using $Z_a=7.22$, this expression becomes

$$\sigma_n=\frac{mZ^2 990}{\mu v^2}\log\frac{v}{4.1(mZ^{4/3}/\mu)^{\frac{1}{2}}}10^{-21}\text{ Mev cm}^2. \qquad (14)$$

This formula differs in its logarithmic term from the expression given by Bohr. It is of the greatest relative importance if Z is great and ionic charge is low.

TABLE IV. *The stopping cross section, mean square charge of alpha-particles, specific stopping cross section for air, and the specific stopping cross section for air calculated from Livingston and Bethe's interpolation formula for different velocities of the particle (in units $e^2/\hbar$). The interpolation formula, rewritten in our units, is $(137/v^2)\log(v/1.22)$ 10^{-21} Mev cm². Here the factor 137 follows from the usual expression for the theoretical stopping cross section with $z_a=7.22$. The denominator 1.22 has been calculated with Livingston and Bethe's experimentally determined value of 80.5 volts for the average ionization potential for air.*

v	$10^{-21}\frac{\sigma_a}{\text{Mev cm}^2/\text{Atom}}$	$\langle i^2\rangle_{Av}$	$10^{-21}\frac{\sigma_a'}{\text{Mev cm}^2/\text{Atom}}$	$\frac{137}{v^2}\log\frac{v}{1.22}$
0.25	11.5	0.05	~230	
0.5	17.1	0.15	114	
0.75	21.5	0.31	69	
1.0	26.0	0.51	51	
1.5	34.5	1.07	32.2	12.6
2	40.8	1.73	23.6	16.9
2.5	45.0	2.47	18.2	15.7
3.0	47.3	3.05	15.5	13.7
3.5	45.5	3.44	13.2	11.8
4	39.2	3.70	10.6	10.2
4.5	34.5	3.84	9.0	8.8
5	30.0	3.92	7.7	7.7
6	23.6	3.96	5.96	6.1
7	19.2	3.98	4.82	4.9
8	15.7	4.0	3.92	4.03
9	13.2	4.0	3.40	3.38
10	11.4	4.0	2.85	2.88
14	6.8	4.0	1.70	1.71
18	4.4	4.0	1.10	1.14
22	3.2	4.0	0.80	0.79

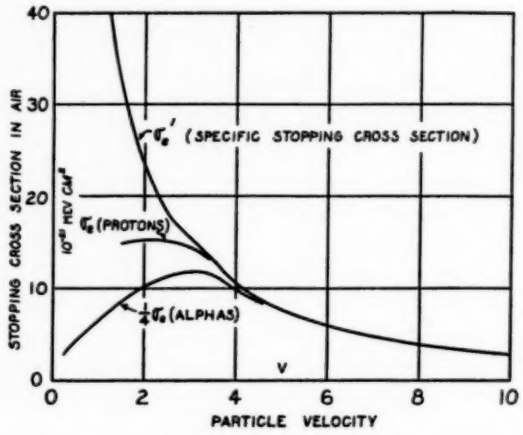

FIG. 4. Stopping cross sections in air plotted against the particle velocity, in units $e^2/\hbar$. The three curves show the specific stopping cross section of air σ_e', the stopping cross section of protons in air, and one-quarter the stopping cross section of alpha-particles in air.

It is interesting to note that in nuclear collisions the whole electronic cloud is deformed but that this deformation does not influence the result very greatly. The change in the electronic configuration is approximately adiabatic. In fact for $v<1$ it is almost completely adiabatic. The forces resulting from the electronic deformations are considerable but they are small compared to the direct interaction of the nuclei. This condition holds up to the region near $p_{\max}$. In this region the influence of the electrons is due not only to the shielding but also to the changes in the electronic distribution. It, therefore, becomes difficult to obtain an expression more accurate than (13).

When the collision parameter is less than the Coulomb limit, a considerable amount of energy is transferred to the atom struck and this energy loss has not been included in the stopping cross section. σ_n vanishes when the limits of integration become equal, that is at a velocity

$$v=1.53(mZ_aZ^{4/3}/\mu)^{\frac{1}{2}}. \qquad (15)$$

Below this velocity the energy loss is chiefly due to hard collisions. In this velocity region the cross-sectional radius is smaller than the Coulomb limit because of the electronic shielding. However, the radius continues to rise with decreasing velocities and reaches for very low velocities the

sum of the atomic radii. The total range for velocities smaller than those given by (15) is never much greater than 0.1 cm. The detailed measurements on the range of slow argon particles in argon[17] show a residual range of about 10^{-2} cm for $v=0.25$. A quantitative treatment of these experimental results would probably require a more detailed discussion of the hard collisions.

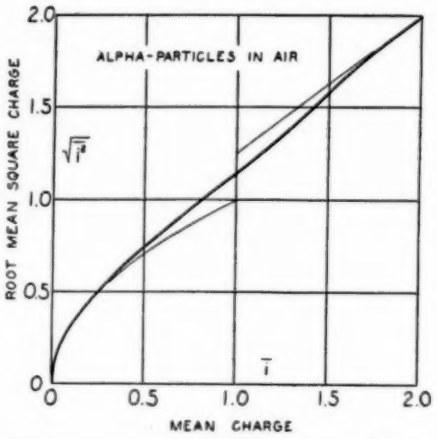

FIG. 5. The root mean square charge of alpha-particles in air, as determined from experiment, plotted as a function of the mean charge.

IV. THE RANGE-VELOCITY RELATION IN AIR

As has been stated in the introduction, the velocity of the least strongly bound electron within the ion is approximately equal to the ionic velocity. For quantitative calculations, we shall introduce the ratio $\gamma=V_e/V$, where V_e is the electronic velocity and V is that velocity of the ion at which capture and loss probabilities are equal. In calculating the mean charge from Fig. 1 or Table I, we set $v_e=\gamma v$.

From observations by Rüchardt,[16] Bartels,[18] and Rutherford[3] we find $\gamma=0.8\pm0.1$ if there is only one electron, that is if the electron is hydrogen-like. Thus $H\rightleftarrows H^+$ in H_2 gives $\gamma=0.7$; $H\rightleftarrows H^+$ in N_2, O_2, and air gives $\gamma=0.9$; and $He^+\rightleftarrows He^{++}$ in mica gives $\gamma=0.8$. On the other hand, the experiments of Rutherford and Kapitza lead to $\gamma=1.6$ for $He\rightleftarrows He^+$.

This striking difference in the values of γ for the first and second electrons of He is probably due for the most part to statistical factors. In the $H\rightarrow H^+$ and $He^+\rightarrow He^{++}$ processes only one electron can be lost while in the $He\rightarrow He^+$ process two electrons of equal average velocity are available and either can be lost. At the same time the "*a priori* probability" of the $He^+\rightarrow He$ process is approximately four times smaller than that of the $He^{++}\rightarrow He^+$ process. Indeed, according to Brinkman and Kramers[3] the electron capture is in most cases a direct capture into the S state. In $He^{++}\rightarrow He^+$ any approaching electron has a chance to be captured while for $He^+\rightarrow He$ only those electrons can be attached which form a singlet state with the electron already present. If the electron forms a triplet state with the electron in He^+, it is ineffective. Thus only one-fourth of the encounters are effective. This argument continues to be qualitatively correct even if the possibility of electron capture into higher He^+ and He states is taken into account. Capture into a triplet He state will be followed in most cases by a loss of one of the electrons in a subsequent collision rather than by the improbable triplet-singlet transition. The comparatively high value of the $He\rightarrow He^+$ probability and the low value of $He^+\rightarrow He$ probability help to make understandable the fact that these two proba-

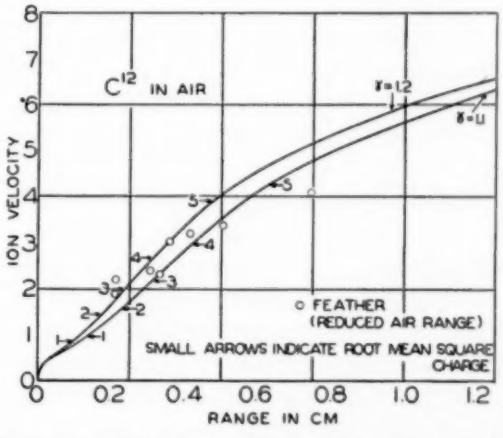

FIG. 6. Range in air of C^{12} ions plotted against the velocity (in units $e^2/\hbar$). The parameter γ, which is the ratio of electronic to particle velocity, is assumed to be a constant throughout the range. The two curves are for two values of this parameter. The numbers along the curves give the root mean square charge, in electronic units, at the points indicated by the small arrows. The circles are experimental observations on individual recoil tracks made by Feather in a helium-carbon tetrafluoride mixture and reduced by comparison with alpha-particle behavior to air ranges.

[17] P. M. S. Blackett and D. S. Lees, Proc. Roy. Soc. **134**, 658 (1932).

[18] H. Bartels, Ann. d. Physik **6**, 957 (1930); **13**, 373 (1932).

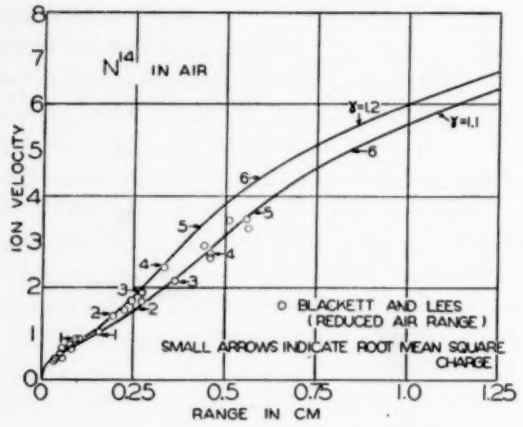

FIG. 7. Range in air of N^{14} ions plotted against the velocity (in units $e^2/\hbar$). The experimental points are from observations by Blackett and Lees on recoils in a nitrogen-oxygen-hydrogen mixture, reduced to air ranges.

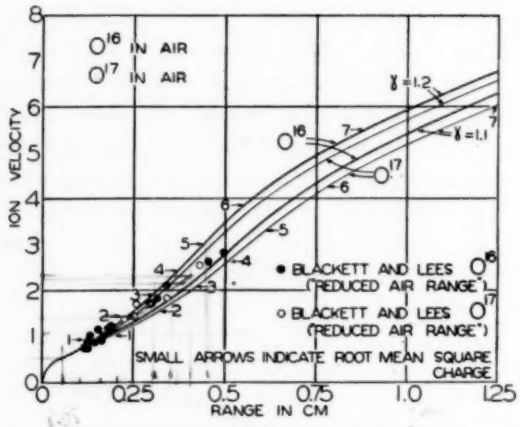
O^{16} IN AIR
O^{17} IN AIR
ION VELOCITY
RANGE IN CM
γ=1.2
γ=1.1
● BLACKETT AND LEES O^{16} (REDUCED AIR RANGE)
○ BLACKETT AND LEES O^{17} (REDUCED AIR RANGE*)
SMALL ARROWS INDICATE ROOT MEAN SQUARE CHARGE

FIG. 8. Ranges in air of O^{16} and O^{17} ions plotted against the velocity (in units $e^2/\hbar$). The experimental points for O^{16} are from observations by Blackett and Lees on recoils in an argon-oxygen-hydrogen mixture and those for O^{17} are from data by Blackett and Lees (based on observations by Blackett) on disintegration products of alpha-bombardment of nitrogen in a nitrogen-oxygen mixture, all reduced to air ranges.

bilities become equal at a rather low velocity ($v \leqq 1.1$).

Extensive observations have been made on the velocity-range relation for intermediate ions by Blackett,[19] Blackett and Lees,[17] and Feather.[20] The measurements are on carbon, nitrogen, oxygen and fluorine tracks formed in recoil from incident alpha-particles or as disintegration products. Unfortunately, the actual measurements were always made with tracks formed in gas mixtures other than air and the results given as "air equivalent" or "reduced ranges." The process of reduction is one based on the known behavior of alpha-particles in the gas mixture as compared to their behavior in air. The electronic stopping alone is important for alpha-particles. However, except at high velocities, such is not the case for intermediate and heavy ions. Such a "reduction" may lead to a velocity-range curve which is distorted at low velocities compared to the true curve for air. Fortunately, however, the presence of hydrogen and helium in the proportions used does not lead to distortions outside the experimental accuracy because the stopping powers of these gases are small and the proportions such that the contributions to the stopping cross sections are not large. The observations on O^{16}, on the other hand, were in a gas mixture of 50 percent argon, 10 percent oxygen and 40 percent hydrogen. The presence

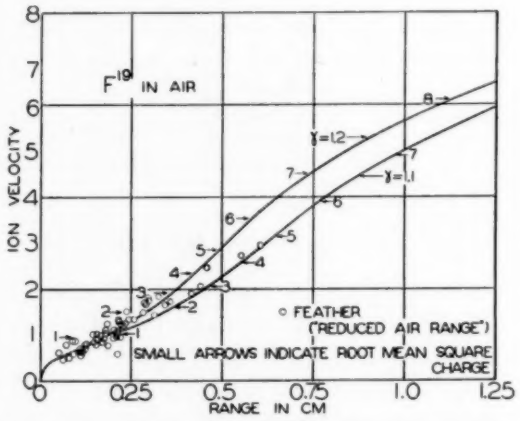

FIG. 9. Range in air of F^{19} ions plotted against the velocity (in units $e^2/\hbar$). The experimental points are from observations by Feather on recoils in a helium-carbon tetrafluoride mixture, reduced to air ranges.

of the argon will surely distort the curve at very low velocities. However, the shortest tracks measured were for $v=0.75$. At this velocity the nuclear stopping is already less than one-half the electronic stopping. The observations on A^{40} noted in an earlier section were made in this same gas mixture. These observations extend from $v=0.22$ to $v=1.3$. This is just the region in which distortion is to be expected.

Theoretical velocity-range curves for intermediate ions are compared with the observed points in Figs. 6, 7, 8 and 9. It has been assumed in calculating these curves that the parameter γ

[19] P. M. S. Blackett, Proc. Roy. Soc. **107**, 349 (1925).
[20] N. Feather, Proc. Roy. Soc. **141**, 194 (1933).

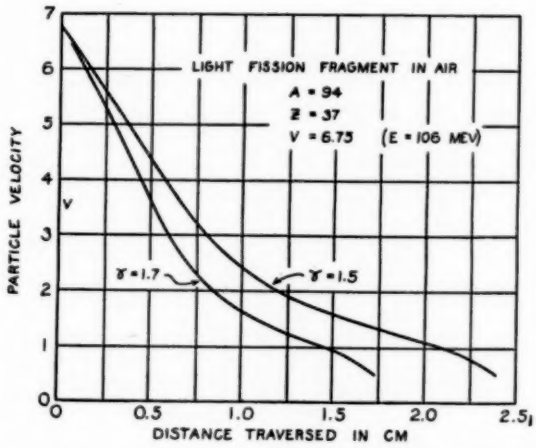

FIG. 10. Velocity (in units $e^2/\hbar$) of the light fission particle plotted against distance in air, measured from the point where fission took place, for two values of the parameter γ. The range of the light fission particle is observed to be about 2.5 cm. For this range $\gamma \backsimeq 1.5$.

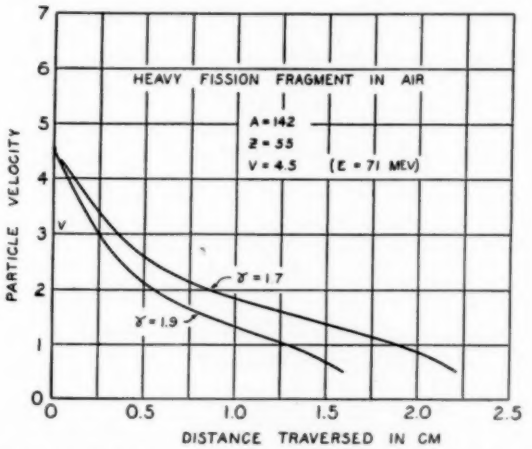

FIG. 11. Velocity of the heavy fission particle plotted against the distance in air, measured from the point where the fission took place, for two values of the parameter γ. The range of the heavy fission particles is observed to be about 2 cm. For this range $\gamma \backsimeq 1.8$.

retains the same value throughout the whole path of the ion. This assumption is certainly not rigorously correct. The small arrows with numbers attached indicate the root mean square charge at the corresponding velocity. The values $\gamma = 1.1$ and $\gamma = 1.2$ give curves in reasonable agreement with the experimental data.[21]

[21] The experimental conditions were as follows: C^{12} (Feather), recoils from alphas in a mixture of 80 percent helium and 20 percent carbon tetrafluoride; N^{14} (Blackett and Lees), recoils from alphas in a mixture of 50 percent nitrogen, 10 percent oxygen and 40 percent hydrogen mixture; O^{16} (Blackett and Lees), recoils from alphas in a mixture of 50 percent argon, 10 percent oxygen and 40 percent hydrogen mixture; O^{17} (Blackett, Blackett and Lees), disintegration products of alpha-bombardment of N^{14} with proton ejection in nitrogen gas with 5 to 20 percent oxygen; F^{19} (Feather), recoils from alphas in a mixture of 80 percent helium and 20 percent carbon tetrafluoride.

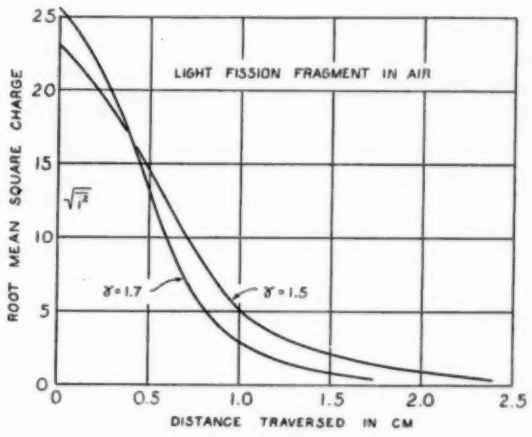

FIG. 12. Root mean square charge of the light fission particle plotted against the distance traversed in air for the two values of the parameter γ used in Fig. 10.

The three parts of the velocity-range curve of an ion are well illustrated in these diagrams. Below unit charge the energy loss is primarily due to collisions with nuclei. In this range the energy loss decreases rapidly with increasing velocity and the range is roughly proportional to the fourth power of the velocity. Following this portion of the curve comes a part in which the particle is partially ionized. The slope, dv/dx, in this region is fairly independent of the velocity. This follows since the square of the particle charge is roughly proportional to v^2, the specific stopping cross section to $1/v^2$ times the number of "active" electrons in the dissipating medium ($\sim v$), and these together compensate the factor v appearing in the relation $dE \sim v dv$.[22] In the third part of the curve the ionization is practically complete and the range starts again to increase more rapidly with velocity. The highest experimental points correspond to about fivefold ionization. It is possible that experimental points at higher v values would deviate from the curves given due to the fact that the influence of the K shell is not well accounted for in these calculations.

Velocity-range curves for fission particles are shown in Figs. 10 and 11. For the lighter fission fragment we take the mass 94, the nuclear charge 37, and the initial energy 106 Mev ($v = 6.75$). For the heavier fission fragment we

[22] See reference 1.

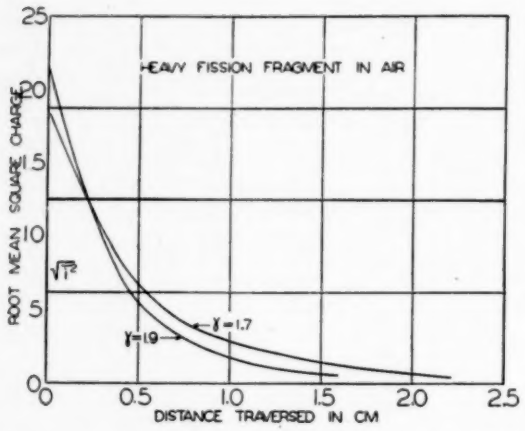

FIG. 13. Root mean square charge of the heavy fission particle plotted against the distance traversed in air for the two values of the parameter γ used in Fig. 11.

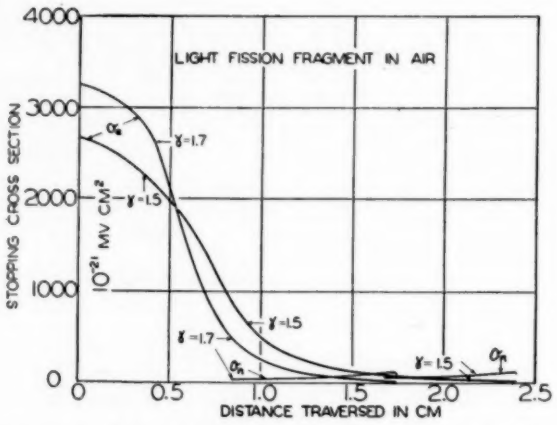

FIG. 14. Electronic stopping cross section σ_e and nuclear stopping cross section σ_n of the light fission particle plotted against the distance traversed in air for the two values of the parameter γ used in Fig. 10.

take the mass 142, the nuclear charge 55, and the energy 71 Mev ($v=4.5$). The curves have been drawn for two γ values leading to ranges in air between 1.5 and 2.5 cm. Velocities are plotted against distances measured from the point where fission took place, since the initial velocity is fixed and variations with velocity are to be studied only by investigating different parts of the path. The curves are not extended below $v=0.5$ because of the growing influence of the hard collisions which have not been included in the calculations. The residual ranges at these velocities will hardly exceed a millimeter and are probably much less than that amount.

The root mean square charge of the fission particles is shown in Figs. 12 and 13 as a function of the distance traversed.

The electronic and nuclear stopping cross sections are plotted in Figs. 14 and 15 as functions of the distance traversed. The ionization produced in the stopping material is for the most part connected with the electronic stopping cross section and is roughly proportional to it. For very small particle velocities, electronic excitation may become relatively more important than ionization. Close nuclear collisions may produce recoils of high velocity which can give rise to secondary ionization. However a large fraction of the energy loss due to nuclear stopping does not contribute to the ionization of the medium.

The density of ions along the path may be expected to be quite different for the two fission

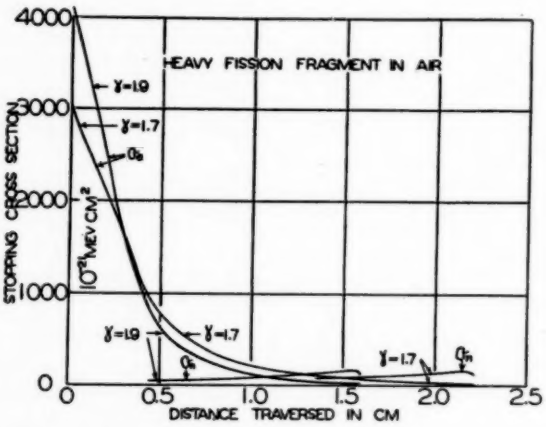

FIG. 15. Electronic stopping cross section σ_e and nuclear stopping cross section σ_n of the heavy fission particle plotted against the distance traversed in air for the values of the parameter γ used in Fig. 11.

fragments. The electronic stopping cross section has a maximum which is reached when a good fraction of the electrons are lost. This maximum has just been reached at the beginning of its path for the light fission particle, but is far from being reached for the heavy particle. The differences are clearly shown in Figs. 14 and 15.

V. LIMITS OF ACCURACY

If the mean charge is great compared to unity, the most serious approximation made is probably the assumed constancy of γ. At low ionic charges the calculation of the electronic stopping power is unsatisfactory. The Thomas-Fermi approximation becomes inapplicable and the averaging

process as well as the formula $\sigma_e = \langle i^2 \rangle_{Av} \sigma_e'$ becomes doubtful. Relatively good results are to be expected for high nuclear charges since, for these, collisions with nuclei are unimportant. The calculation of the nuclear stopping becomes unreliable when the energy drops to such a value that even the hardest collisions are strongly influenced by electronic shielding.

This paper grew out of a discussion, last summer, with Professor K. Lark-Horovitz about the difference between the appearance of tracks due to alpha-particles and fission particles. We are greatly indebted to him for his continued interest. Discussions in the early stages of our work with Professor H. A. Bethe have proved most helpful.

APRIL 15, 1941 PHYSICAL REVIEW VOLUME 59

The Intrinsic Inelasticity of Large Plates

CLARENCE ZENER
Washington State College, Pullman, Washington
(Received February 21, 1941)

A theory is developed for the reaction of plates to forces of such short duration that the waves reflected from the boundary may be neglected. It is found that the velocity of the point of application of the force is proportional to the force, and hence the total displacement is proportional to the impulse of the force. The theory is applied to the impact of spheres with large plates. The coefficient of restitution is obtained as a function of the parameters of the impact. Complete agreement is obtained with previous experiments.

LARGE plates react in a curious manner to normal impulsive forces. A radial disturbance is, of course, propagated outwards. However, the center of the disturbance, the point where the impulse acted, remains stationary until the return of the disturbance reflected from the boundary of the plate. During the interim, the center behaves as if the plate were perfectly inelastic. The disturbance is shown diagrammatically in Fig. 1(a). An analogous phenomenon may be readily demonstrated with a loaded taut string. The disturbance initiated by an impulsive force is shown in Fig. 1(b) for this case. In each case the displacement U of the point of application is proportional to the impulse P,

$$U = \alpha P. \tag{1}$$

The theory of this effect is developed in §1. The proportionality constant α is given by Eqs. (9) and (10) for the plate and taut string, respectively.

This property of plates enables us to solve the problem of the bouncing of elastic spheres off large thin plates. The motion of the plate, and hence the energy it absorbs, could be calculated by standard methods if the force with which the sphere acts upon it were known. But this force, in turn, depends upon the motion of the plate. This dilemma is overcome by using the information contained in Eq. (1). The analysis is given in §2. The coefficient of restitution e of the sphere depends upon the various parameters of the collision, radius, mass, and initial velocity of sphere, etc., only through a single dimensionless parameter λ. We shall call this the inelasticity parameter. It is defined by Eq. (17a). The dependence of e upon λ is given by the graph of Fig. 2.

Raman published, in 1920, extensive experiments on the coefficients of restitution of hard elastic spheres rebounding off large thin glass

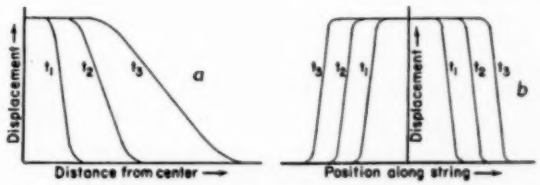

FIG. 1. (a) Propagation over a thin plate of a disturbance caused by an impulsive force. (b) Propagation along a string of a disturbance caused by an impulsive force.

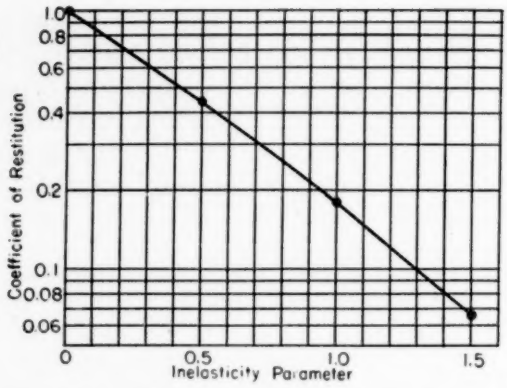

FIG. 2. Theoretical variation of coefficient of restitution with inelasticity parameter. The nearly straight line has been drawn through the four calculated points at $\lambda=0$, 0.5, 1.0, 1.5.

plates.[1] He gave a semi-empirical formula which fitted his data for values of e greater than 0.5, but which diverged rapidly as e became smaller. Recently this formula has been derived theoretically by an approximate method.[2] Raman's data are compared in §3 with the theory here developed. The coefficient of restitution obtained by this theory agrees completely with these data, as is shown in Fig. 4.

§1. ANALYSIS

In this analysis of the reaction of large plates to localized impulsive forces, we shall use the usual approximate theory of thin plates.[3] In this theory it is assumed that the radius of curvature of the plate is everywhere large compared with its thickness, and that the angle between the plate and the original plane is everywhere small. This approximate theory yields the following differential equation for the transverse displacement $U(x, y, t)$ of the plate:

$$(D\nabla^4+2\rho h\partial^2/\partial t^2)U=Z. \tag{2}$$

In this equation, ρ is the density, $2h$ the thickness of the plate. The rigidity modulus D is defined by

$$D=(\tfrac{2}{3})h^3E', \quad E'=E/(1-\sigma^2), \tag{3}$$

where E is Young's modulus, σ Poisson's ratio. The operator ∇^2 represents $\partial^2/\partial x^2+\partial^2/\partial y^2$. Finally, $Z(x, y, t)$ is the surface density of the normal force.

The formal solution of Eq. (2) will be obtained in terms of the eigenfunctions of the auxiliary equation

$$\{(D/2\rho h)^{\frac{1}{2}}\nabla^2+\omega\}W(x, y)=0, \tag{2a}$$

and of the boundary conditions at the edge of the plate. The eigenvalues and normalized eigenfunctions of these equations will be denoted by ω_n and U_n, respectively. In order to obtain the coefficients in the expansion

$$U(x, y, t)=\textstyle\sum_n C_n(t)U_n(x, y), \tag{4}$$

we substitute this expansion into Eq. (2), multiply by U_k, and integrate over the surface of the plate. Using the orthogonality property of the eigenfunctions, we obtain

$$(d^2/dt^2+\omega_k^2)C_k=(2\rho h)^{-1}\textstyle\int U_kZdS. \tag{5}$$

In the cases in which we are interested, the force is localized about a point, so that we may set

$$\textstyle\int U_kZdS=U_k(0)F(t).$$

Here $U_k(0)$ is the value of U_k at the point of application of the force, which is denoted by $F(t)$. The force will be taken as first applied at $t=0$. Then the solution of Eq. (5), corresponding to the plate being initially stationary, is

$$C_k(t)=(2\rho h\omega_k)^{-1}U_k(0)\int_0^t F(t')\sin\omega_k(t-t')dt'.$$

The formal solution of our problem is now obtained by substituting this coefficient into the expansion (4). This substitution gives for the displacement at the point of application

$$U(0, t)=(2\rho h)^{-1}\textstyle\sum_n \omega_n^{-1}U_n^2(0)\times\int_0^t F(t')\sin\omega_n(t-t')dt'. \tag{6}$$

This solution will now be simplified by performing the sum

$$\textstyle\sum \omega_n^{-1}U_n^2(0)\sin\omega_n(t-t') \tag{7}$$

before integrating with respect to t'. This sum will obviously not depend upon the shape of the plate, or upon the nature of the boundary conditions, as long as t is so small that the disturbance

[1] C. V. Raman, Phys. Rev. **15**, 277 (1920).
[2] C. Zener and H. Feshbach, J. App. Mech. **6**, A–67 (1939).
[3] See A. E. H. Love, *Mathematical Theory of Elasticity* (Cambridge, 1927), Fourth Edition, p. 487.

has not been reflected by the boundaries. By choosing a square plate, and by imposing the condition that the plate is free to pivot about fixed lines on its edges, we obtain the eigenfunctions

$$(2/L)\sin(\pi lx/L)\sin(\pi my/L), \quad 0<x, y<L \qquad l, m=1, 2, \cdots.$$

We first sum over all states for which l^2+m^2 lies within a narrow range. The effect of this summation is to replace $U_n^2(0)$ by its average value $1/L^2$. The expression (7) may thus be replaced by

$$L^{-2}\sum_n \omega_n^{-1}\sin\omega_n(t-t').$$

This summation is now converted into an integration by making the plate indefinitely large. From the relation

$$(D/2\rho h)^{\frac{1}{2}}(2\pi/\lambda)^2=\omega$$

between wave-length λ and ω, which may be obtained from Eq. (2a), we find that the number of states associated with a range $d\omega$ is

$$\{L^2(2\rho h/D)^{\frac{1}{2}}/4\pi\}d\omega.$$

The combination of a two-dimensional medium with the dispersion associated with flexural vibrations has rendered the coefficient of $d\omega$ independent of ω, as in a taut string. This is why plates and taut strings react similarly to normal impulsive forces. Noting that

$$\int_0^\infty \omega^{-1}\sin\omega(t-t')d\omega=\pi/2,$$

we obtain for the summation of (7)

$$(2\rho h/D)^{\frac{1}{2}}/8.$$

Substituting back into Eq. (6), we obtain finally

$$U(0, t)=\alpha\int_0^t F(t')dt' \tag{8}$$

with

$$\alpha=(3\rho/E')^{\frac{1}{2}}/16\rho h^2. \tag{9}$$

In the case of a taut string, it may readily be shown that

$$\alpha=(2mc)^{-1}, \tag{10}$$

where m is the mass per unit length, and c is the velocity of transverse waves.

§2. Application to Impacts of Spheres with Plates

One application of the preceding theory is to the elastic normal impact of spheres with plates so large that the impact is over before the return of waves reflected from the boundaries.

In this application we must solve simultaneously the equations of motion of the sphere and of the plate. The first equation is

$$d^2z/dt^2=-m^{-1}F, \tag{11}$$

where z will be taken as the displacement of the center of the sphere from its position at contact, m is the mass of the sphere, and F is the reaction of plate on the sphere. The motion of the plate in the contact region is given by Eq. (1), which we shall write in the form

$$U=\alpha\int^t F dt. \tag{12}$$

The displacement U refers strictly to the displacement of the mid-plane of plate.

The force F is a function only of the relative displacement of sphere and plate, namely of

$$s=z-U.$$

We may thus obtain a single equation in only the one dependent variable s by differentiating Eq. (12) twice with respect to time, and then subtracting this equation from Eq. (11).

$$d^2s/dt^2+m^{-1}F(s)+\alpha dF(s)/dt=0. \tag{13}$$

In order to obtain the appropriate boundary condition for this equation, we observe that U is constant when F is zero, that is, at the beginning and end of the collision. The appropriate boundary conditions are thus

$$\left.\begin{aligned} s&=0\\ ds/dt&=v_0\end{aligned}\right\} \quad \text{at} \quad t=0, \tag{14}$$

where v_0 is the incident velocity of the sphere. The velocity of rebound, ev_0, is then given by ds/dt where s has again returned to zero.

The reaction of the plate on the sphere is given explicitly as[4]

$$F(s)=ks^{\frac{1}{2}},$$

where

$$k=(4/3)r^{\frac{1}{2}}\{E_1'E_2'/(E_1'+E_2')\}.$$

[4] Reference 3, p. 198.

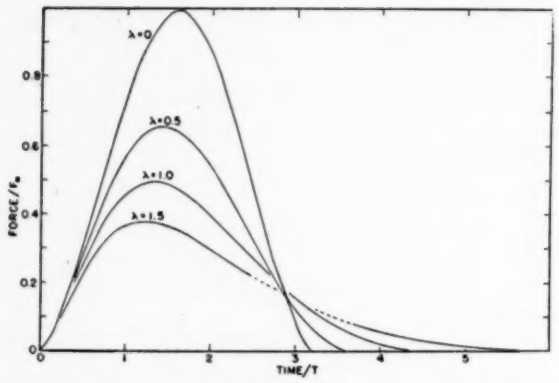

FIG. 3. Force exerted by a sphere upon a large plate during impact. F_M denotes the maximum force in the case of a plate of infinite thickness.

Here r is the radius of the sphere, E_1' and E_2' refer to the elastic moduli of Eq. (3) for the sphere and plate, respectively.

In order to introduce dimensionless variables, we make the transformation

$$s=Tv_0\sigma; \quad t=T\tau,$$

where T is a constant with dimensions of time. The boundary conditions then become

$$\left.\begin{matrix}\sigma=0\\ d\sigma/d\tau=1\end{matrix}\right\} \quad \text{at} \quad \tau=0.$$

The coefficient of restitution will be the value of $d\sigma/d\tau$ where σ returns to zero. The constant T will be so chosen that the first two coefficients in Eq. (13) are unity, that is, so that Eq. (13) becomes

$$d^2\sigma/d\tau^2+(1+\lambda d/d\tau)\sigma^{\frac{1}{2}}=0. \tag{15}$$

We find

$$T=(m/kv_0^{1/2})^{2/5}, \tag{16}$$

which is $0.311T_H$, where T_H is the duration, calculated by Hertz, of the impact in the case of a plate of infinite thickness.[4] The inelasticity parameter λ is given by

$$\lambda=\alpha m/T. \tag{17}$$

The dependence of λ upon the parameters of the impact is best seen from the following product of dimensionless factors:

$$\lambda=\frac{\pi^{3/5}}{3^{1/2}}\left(\frac{r}{2h}\right)^2\left(\frac{V_0}{V'}\right)^{1/5}\left(\frac{\rho_1}{\rho_2}\right)^{3/5}\left(\frac{E_1'}{E_1'+E_2'}\right)^{2/5}. \tag{17a}$$

Here ρ_1 and ρ_2 are the densities of the sphere and plate, respectively, while the velocity v' is defined by

$$v'=(E_2'/\rho_2)^{\frac{1}{2}}.$$

Equation (15) has been integrated numerically for several values of the inelasticity parameter. The coefficients of restitution, e, thus found are given in Table I. Intermediate values may be

TABLE I. *Coefficient of restitution.*

λ	0	0.5	1.0	1.5
e	1	0.44	0.18	0.067

quite accurately found by interpolation on semi-log paper, as demonstrated in Fig. 2. In Fig. 3 the force F is shown as a function of time for these same values of λ. As λ increases, the force is seen to decrease with time in a nearly exponential manner. This behavior may be seen as a direct consequence of the equations of motion (11) and (12). For when the coefficient of restitution is small, the sphere and plate move almost with the same velocity during the latter part of the impact, or

$$d^2U/dt^2 \backsimeq d^2z/dt^2.$$

From this it follows directly that

$$dF/dt \backsimeq -(1/m\alpha)F.$$

§3. COMPARISON WITH EXPERIMENT

Raman's experiments with hard steel balls rebounding off glass plates are compared in Fig. 4 with his semi-empirical formula, and with

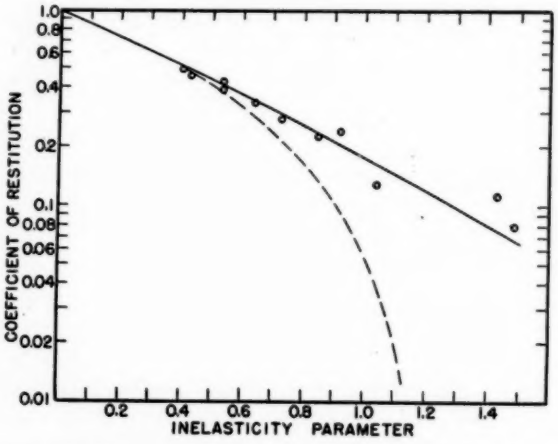

FIG. 4. Comparison of Raman's data with theory. The dashed line is given by Raman's formula, the full line by the present theory. Only those data are shown for which $e<0.5$. For $e>0.5$, the observations are in agreement with both theories.

the present theory. His formula agreed with experiment for values of e above 0.5. The present theory agrees with experiment over the entire investigated range. The present theory shows that e approaches zero only asymptotically as λ increases. The several cases of zero e recorded by Raman must be attributed to experimental difficulties in measuring small rebound velocities.

In our notation, Raman's formula is

$$e=(1-0.88\lambda)/(1+0.88\lambda).$$

In view of the success of this formula for small values of λ, it is of interest to see the relation between this formula and the present theory. This relation is given below.

According to the definition of e, the change in velocity of the sphere during impact is $(1+e)v_0$. It is also equal to $\int m^{-1}Fdt$. Hence

$$(1+e)v_0=\int m^{-1}Fdt. \tag{18}$$

Likewise, according to the definition of e, the energy lost by the sphere during impact is $(1-e^2)mv_0^2/2$. But this is equal to the energy absorbed by the plate, namely, $\int F(dU/dt)dt$, or by Eq. (1), $\alpha\int F^2dt$. Hence

$$(1-e^2)mv_0^2/2=\alpha\int F^2dt. \tag{19}$$

Upon dividing Eq. (19) by the square of Eq. (18), we obtain

$$(1-e)/(1+e)=R,$$

and hence

$$e=(1-R)/(1+R)$$

where

$$R=2m\alpha\int F^2dt/(\int Fdt)^2,$$

or, by Eq. (17),

$$R=2\lambda\{\int\sigma^3d\tau/(\int\sigma^{\frac{1}{2}}d\tau)^2\}.$$

When the inelasticity parameter λ is small, the bracketed ratio will be only slightly different from its value for $\lambda=0$. The value of this ratio has been calculated numerically for the case $\lambda=0$, and found to be 0.42. Hence in the limit of small λ,

$$R=0.84\lambda,$$

which is nearly the value used by Raman.

APRIL 15, 1941 PHYSICAL REVIEW VOLUME 59

On the Polar Vibrations of Alkali Halides

R. H. LYDDANE, *University of North Carolina, Chapel Hill, North Carolina*

AND

R. G. SACHS* AND E. TELLER, *George Washington University, Washington, D. C.*

(Received February 10, 1941)

The long wave-length, polar lattice vibrations of alkali halide crystals are discussed without making any specific assumptions about the detailed interactions between the ions. This is made possible by the introduction of the effective charge, e^*, of an ion defined as follows: All of the positive ions in a crystal slab are displaced by an equal amount in a direction perpendicular to the faces of the slab and all of the negative ions in the opposite direction. Then e^* is the ratio of the dipole moment per ion pair induced in the slab by this displacement to the relative displacement of the positive and the negative ions. Expressions are obtained for the frequency, ω_l, of the longitudinal vibration and the frequency, ω_t, of the transverse vibration in terms of the dielectric constant, k, of the crystal, the dielectric constant, k_0, obtained by extrapolating the square of the index of refraction of the crystal from high frequencies to zero frequency, and e^*. The ratio of the two frequencies is found to be independent of e^* and given by $\omega_l/\omega_t=(k/k_0)^{\frac{1}{2}}$.

THE calculation of a property of an ionic crystal which involves the lattice vibrations usually requires that detailed assumptions be made about the microscopic behavior of the crystal. However, statements that are independent of such a full knowledge can be made when the vibrations in question are of wave-length long compared to the lattice distance but short compared to the size of the crystal. Under

* Now at Purdue University, Lafayette Indiana.

these conditions there exist two sharply defined types of vibration, the longitudinal and the transverse. It has already been demonstrated by Lyddane and Herzfeld[1] and by Fröhlich and Mott[2] that in the case of the vibrations for which oppositely charged ions move in opposite directions (polar vibrations) the frequency of the longitudinal vibration is higher than that of the transverse because of the accumulation of charge near the nodes for the former. However, in these calculations, the polarizability of the ions has been neglected entirely or considered only in part.

The purpose of the present paper is to find the ratio of the frequencies of the longitudinal and transverse polar vibrations. It will be shown that this ratio can be derived without making any specific hypothesis about the detailed structure of the crystal.

I

First we consider the force on an ion when a crystal slab is placed in a uniform external field E_0 perpendicular to the faces of the slab. This force is defined as follows: If, in the presence of the field E_0, all the positive ions are displaced in one direction and all the negative ions in the opposite direction so that their relative displacement is the infinitesimal quantity dx, then the force on an ion is the total change in energy per ion pair caused by this displacement divided by the relative displacement dx.

When the ions are displaced as described above, there is a dipole field at great distances from the crystal corresponding to a dipole moment p of the crystal. The interaction energy of the polarized crystal with the field E_0 is the same as the interaction energy of the charges giving rise to E_0 with the field of the crystal. Assuming, then, that these charges are at a great distance from the crystal, the interaction energy is pE_0. This result is independent of the position of the charges giving rise to E_0 since it must be the same for any uniform field of magnitude E_0.

Since all displacements x which are to be considered are small, the dipole moment may be expanded in powers of x and only the first term need be retained. Therefore the dipole moment per ion pair, that is, p divided by the number of ion pairs in the slab, is also proportional to x and may be written e^*x. The constant of proportionality, e^*, will be called the "effective charge" of an ion since for a crystal made up of nonpolarizable, infinitely small ions, e^* is just equal to the charge on an ion. The energy per ion pair is pE_0 divided by the number of ion pairs; thus it is equal to e^*xE_0 and the change in energy per ion pair due to the displacement dx is e^*dxE_0. Dividing by dx, we find that the force on an ion due to the external field is e^*E_0.

In addition to this force caused by the external field, there is a restoring force acting on the ions due to the presence of the other ions in the slab. If the latter force is assumed to be harmonic with force constant q, its contribution to the total force is $-qx$. When the slab is allowed to come to equilibrium in the presence of the field E_0, the total force on an ion vanishes, or

$$e^*E_0=qx. \tag{1}$$

The field E_0 may be expressed in terms of the density of polarization, P, in the slab and the dielectric constant, k, of the crystal. For the electric displacement in the slab is numerically equal to E_0 so that E_0 satisfies the relation

$$4\pi P=(1-1/k)E_0. \tag{2}$$

The polarization P is the sum of two terms. The first is the contribution of the dipole moments e^*x and is equal to $e^*x/2a^3$ where a is the lattice distance and $2a^3$ is the volume per ion pair. The other is the contribution of the polarization induced on the ions by the external field. This may be measured in terms of the dielectric constant k_0 obtained by extrapolating the square of the index of refraction from high (visible) frequencies to zero frequency. k_0 is the dielectric constant that the crystal would have if the atomic nuclei were held fixed in the positions they had before the field was turned on. The density of polarization under this condition is equal to $P-e^*x/2a^3$ and this polarization satisfies the equation

$$4\pi(P-e^*x/2a^3)=(1-1/k_0)E_0. \tag{2'}$$

[1] R. H. Lyddane and K. F. Herzfeld, Phys. Rev. **54**, 846 (1938).

[2] H. Fröhlich and N. F. Mott, Proc. Roy. Soc. **A171**, 496 (1939).

Subtracting Eq. (2′) from Eq. (2), we obtain

$$(1/k_0-1/k)E_0=4\pi e^*x/2a^3,$$

and substituting for E_0, Eq. (1) becomes

$$q=\beta kk_0/(k-k_0), \qquad (3)$$

if $\beta=2\pi e^{*2}/a^3$.

II

We now consider a large crystal slab[3] and assume that there is no external field present. The ions are displaced perpendicularly to the faces of the crystal into positions corresponding to the amplitudes in a longitudinal vibration with nodal planes parallel to these faces. Then there is a restoring force on each ion of magnitude $-\mu\omega_l^2x$ where x is the relative displacement of the positive and the negative ions, μ the reduced mass of an ion pair, and ω_l the frequency of the longitudinal vibration. We wish to show that the force constant q defined above is just equal to $\mu\omega_l^2$ if the wave-length of the vibration is long compared to the lattice distance.

Consider the crystal to be divided into slabs parallel to the nodal planes and of thickness small compared to the wave-length of the vibration under consideration but large compared to the lattice distance. Then if the ions of the crystal are displaced as described above, each one of the slabs will be uniformly polarized. Such a uniformly polarized slab is equivalent to a parallel plate condenser so, disregarding end effects,[4] it gives rise to no external field. Thus the force on an ion pair in one slab is due only to the displaced ions in that slab. Therefore this force will be the same as that found in Section I for a uniformly polarized slab, that is, $-qx$. From this it follows that $q=\mu\omega_l^2$, and Eq. (3) becomes

$$\mu\omega_l^2=\beta kk_0/(k-k_0). \qquad (3')$$

III

Those transverse modes of vibration of the large crystal slab that have their nodal planes parallel to the surface of the crystal will now be considered. In this case, the displacements of the ions are parallel to the crystal faces. It is assumed that the crystal wave-length is long compared to the lattice distance, but short compared to the thickness of the crystal.

A small slab with its faces perpendicular to the planes bounding the crystal is cut from within the crystal when its ions are in their equilibrium positions. All dimensions of the slab are chosen to be small compared to the wave-length of the vibration under consideration but large compared to the lattice distance. The ions in the crystal are now displaced according to the amplitudes in the transverse vibration and the displacements are chosen to be perpendicular to the face of the cavity. Then there will be a field in the cavity.

We now put the small slab back into the cavity and displace its ions in such a way as to complete the transverse displacement of the crystal. The force on an ion is then the sum of two forces, the first of which is the force due to the other ions within the slab. Since the ions in the slab are uniformly displaced, this force is the same as that discussed in the previous section, which is $-\mu\omega_l^2x$. The second force is caused by the field that was present in the cavity so the difference between the longitudinal and the transverse frequencies is due to this field.

To calculate the field in the cavity, we observe that charges appear on the edges of the large crystal slab and the faces of the cavity. Since the former charges are alternatingly positive and negative, their field does not extend deeply into the crystal and their contribution to the field in the cavity may be neglected. The charge distribution on the face of the cavity is practically uniform, since the dimensions of the cavity are small compared to the wave-length. The corresponding charge density, σ, produces a field $4\pi\sigma$ in the cavity. Since σ is numerically equal to the density of polarization, P, in the neighborhood of the cavity, the field in the cavity is $4\pi P$.[5] The value of P is not affected by the removal or the replacement of the small slab because this slab acts like a condenser and produces no external fields.

[3] It can be shown that the results to be obtained are independent of the shape of the crystal as long as the crystal is large compared to the wave-length of the vibration. The crystal slab will be considered throughout since the treatment in this case is particularly simple.

[4] At great distances from the slab the end effects become important and give rise to the dipole field discussed in Section I.

[5] Cf. R. H. Lyddane, K. F. Herzfeld and R. G. Sachs, Phys. Rev. **58**, 1008 (1940).

All of the considerations of Section I may be applied to the uniform field $4\pi P$, so, if the slab is replaced in this field, the force on an ion in the slab due to the field is $4\pi e^* P$. Therefore, when the ions have a relative displacement x, the difference in force for the longitudinal and the transverse displacements is

$$\mu(\omega_l^2-\omega_t^2)x=4\pi e^* P. \tag{4}$$

The density of polarization of the crystal around the cavity is the same as that of the slab. This polarization is made up of two parts. The first is that which would be obtained if the ions in the slab were held fixed. Its magnitude is $(1-1/k_0)/4\pi$ times the external field. The second part is due to the displacement of the ions, and its magnitude is $e^* x/2a^3$. Since in the present case the external field acting on the replaced slab is $4\pi P$ we obtain the equation

$$P=(1-1/k_0)P+e^* x/2a^3,$$

so that

$$4\pi e^* P=\beta k_0 x.$$

Thus Eq. (4) yields

$$\mu(\omega_l^2-\omega_t^2)=\beta k_0. \tag{4'}$$

A relation that corresponds to the well-known Born[6] formula may be obtained by subtracting Eq. (4) from Eq. (3'). The result is

$$\mu\omega_t^2=\beta k_0^2/(k-k_0), \tag{5}$$

which differs from the usual formula by the factor $e^{*2}k_0^2/e^2$ where e is the electronic charge.

Dividing Eq. (3') by Eq. (5) the quantity β and with it the unknown charge e^* drops out and we get for the relation between ω_l and ω_t

$$\omega_l^2/\omega_t^2=k/k_0. \tag{6}$$

[6] M. Born, Preuss. Akad. Wiss. (Berlin) **29**, 604 (1918); Physik. Zeits. **19**, 539 (1918). M. Born and M. Goeppert-Mayer, *Handbuch der Physik* **24/2**, p. 646.

IV

In the previous considerations, it has been found convenient to define the effective charge, e^*, of an ion in terms of a polarized slab. It is apparent that an effective charge can be defined in the same way for a crystal of any other geometrical shape. In general, the effective charge will depend on the shape of the crystal considered. There are two configurations other than the slab that are of particular interest in any discussion of the dielectric behavior of a solid, the needle and the sphere. If we define the effective charges of the needle and the sphere to be e_n and e_s, respectively, and β_n, β_s to be $2\pi e_n^2/a^3$ and $2\pi e_s^2/a^3$, respectively, then all of the calculations can be carried out in a manner similar to the foregoing. The results of these calculations are the following: Eq. (5) is replaced by

$$\mu\omega_t^2=\beta_n/(k-k_0) \tag{5'}$$

in the case of the needle and by

$$\mu\omega_t^2=\beta_s(k_0+2)^2/9(k-k_0) \tag{5''}$$

in the case of the sphere. In all cases Eq. (6) remains, of course, the same.

It is of interest to note that Eq. (5') is of the same form as the Born formula and Eq. (5'') is the same as the corresponding equation given by Wolf and Herzfeld[7] if the quantity that they call p_4 is set equal to e_s^2/e^2. In order that Eqs. (5), (5') and (5'') be consistent, it is necessary that the effective charges satisfy

$$e_n=k_0 e^*=e_s(k_0+2)/3.$$

There is, of course, no generally valid reason why e^*, e_n, or e_s should be equal to the elementary charge.

[7] K. L. Wolf and K. F. Herzfeld, *Handbuch der Physik* Vol. **20**, p. 517.

Letters to the Editor

PROMPT publication of brief reports of important discoveries in physics may be secured by addressing them to this department. Closing dates for this department are, for the first issue of the month, the eighteenth of the preceding month, for the second issue, the third of the month. Because of the late closing dates for the section no proof can be shown to authors. The Board of Editors does not hold itself responsible or the opinions expressed by the correspondents.

Communications should not in general exceed 600 words in length.

Fission Products of Uranium by Fast Neutrons

Y. NISHINA AND T. YASAKI
Nuclear Research Laboratory, Institute of Physical and Chemical Research, Tokyo, Japan

AND

K. KIMURA AND M. IKAWA
Chemical Institute, Faculty of Science, Imperial University of Tokyo, Tokyo, Japan

March 3, 1941

IN our previous note[1] on the above problem, we reported having obtained a rhodium isotope of a half-life 34 hours and ruthenium isotopes of half-lives 4 hours and 60 hours, respectively. Since then we succeeded in obtaining a stronger ruthenium fraction and closer studies revealed that the decay curve of the 60-hour ruthenium was in reality the superposition of the growth and decay curve of the 34-hour rhodium produced from the 4-hour ruthenium and the decay curve of a ruthenium isotope of a few months period.

The experimental procedure was as follows. From the sample which was purified and irradiated exactly as before, ruthenium was separated as tetroxide, RuO_4, which was freed from all known fission products. The tetroxide was then reduced to metal and its activity measured. The decay curve showed at first a period of 4 hours.

To see if there is any daughter product of the ruthenium, rhodium was separated from this sample after 12 hours from the time of the first separation of ruthenium and tested for its activity. The decay curve showed a single period of 34 hours. We thus conclude that the 4-hour ruthenium is the mother substance of the 34-hour rhodium.

The ruthenium metal obtained from the same sample gave again a complicated decay curve, which is the superposition of the growth and decay curve of rhodium and ruthenium as mentioned above.

Recently Segrè and Seaborg[2] also reported in this column having obtained the 4-hour ruthenium as a fission product of uranium and thorium. These authors established the genetic relationship between Pd^{111} (26 mo.) and Ag^{111} (7.5 days), which we could not find owing to the lack of intensities in our case.

The above investigations were carried out as a part of the work of the Atomic Nucleus Sub-Committee of the Japan Society for the Promotion of Scientific Research. We acknowledge the assistance given by our laboratory colleagues in connection with the irradiation of samples.

[1] Y. Nishina, T. Yasaki, K. Kimura and M. Ikawa, Phys. Rev. **59**, 323 (1941).
[2] E. Segrè and G. T. Seaborg, Phys. Rev. **59**, 212 (1941).

On the Einstein Condensation Phenomenon*

W. E. LAMB, JR. AND A. NORDSIECK
Columbia University, New York, New York

March 29, 1941

IN a recent paper, L. Goldstein[1] has discussed the behavior of an ideal Bose-Einstein gas in the presence of an external force field. He did not apply his general results to the case of a gas in a gravitational field, but in view of the long debate[2-5] on the subject of the condensation of a Bose-Einstein gas in coordinate and momentum spaces, it seems worth while to examine this particular case in more detail. Goldstein found that for temperatures below the critical temperature T_f, a condensation occurs in which a finite fraction N_0/N of the atoms are found in the regions of phase space of lowest momentum and least potential energy. His distribution function is essentially a delta function in both momentum and coordinate spaces, i.e., the condensed phase is all to be found on the bottom of the vessel with zero velocity. As it stands, of course, this result is inconsistent with the uncertainty principle, because for convenience, the preceding calculations were carried out in the partly classical limit in which an integral over the vertical coordinates was used in the sum of states. If instead, one considers the discrete character of the energy spectrum for the lowest states in the potential field present, one finds that the condensed phase is all to be found in the lowest quantum state for the vertical motion, and that the thickness of the layer on the floor is of the order

$$t=1.8(\hbar^2/m^2g)^{\frac{1}{3}}$$

(as may be estimated with sufficient accuracy by the WKB method) where g is the acceleration due to gravity, m is the mass of the atom. It is assumed here that the height of the box is large compared with t. For helium in the earth's gravitational field, one finds $t=5.5\times10^{-3}$ cm, a small but not microscopic distance. At a height $z>t_0$, the density falls off proportionally to $\exp-4.8[(z-t)/t]^{\frac{1}{2}}$.

The forces between the atoms in an actual gas and the forces due to the walls would considerably modify the above behavior, but some remnant of it might be found if the Einstein condensation plays any role in the case of liquid helium II.

* Publication assisted by the Ernest Kempton Adams Fund for Physical Research of Columbia University.
[1] L. Goldstein, J. Chem. Phys. **9**, 273 (1941).
[2] A. Einstein, Ber. d. Berl. Akad. p. 3 (1925).
[3] G. E. Uhlenbeck, "Over statistische Methoden in de Theorie der Quanta," thesis (Leiden, 1927).
[4] L. Brillouin, *Die Quantenstatistik*, p. 142.
[5] F. London, Nature **141**, 643 (1938); Phys. Rev. **54**, 947 (1939); J. Phys. Chem. **43**, 49 (1939).

Geomagnetic Character and Cosmic-Ray Intensity Pulses

JAMES W. BROXON
Department of Physics, University of Colorado, Boulder, Colorado
March 19, 1941

RECENT applications[1] of Chree's[2] method of geomagnetic analysis have shown a primary pulse of about one percent or less and secondary pulses about one-third or one-fourth as large, which occur in the cosmic-ray intensity at 27- or 28-day intervals from the primary. The period suggests that the cosmic-ray as well as the magnetic disturbances are to be associated with the rotation of the sun. Differences between the magnitude characteristics of the two types of disturbances, however, have led to the suggestion that they may result from different solar phenomena. For instance, while Chree has shown the damped magnetic pulses are associated with the transitory sunspots, the more persistent cosmic-ray pulses might be due to changes of the earth's position in the sun's magnetic field as the sun rotates.

The writer decided to investigate a possible relation between the two types of disturbances. By employing De Bilt international character figures, a Chree magnetic pulse curve was constructed. For this the zero-days were *not* taken to be the magnetically calm or disturbed days. Instead, the *identical* zero-days used in the study of cosmic-ray recurrence phenomena were employed. These were the five days during each of the 18 months (June, 1938–November, 1939) on which the cosmic-ray intensity was greatest (for the "positive" pulses) and the five per month of least intensity (for the "negative" pulses). See Figs. 1 and 2.

If there were no relation between the cosmic-ray and terrestrial magnetic disturbances, one should expect a curve with only small and irregular deviations from the mean to result from this treatment. Instead, a very striking relation was shown in the region $n=-10$ to $n=10$ for the 18 months. Associated with the cosmic-ray primary "positive" pulse with its peak necessarily at $n=0$, there was a correspondingly sharp trough in the magnetic curve just one day earlier, descending 27 percent below the average. Associated with the cosmic-ray primary "negative" pulse with its deepest depression necessarily at $n=0$, there was an even sharper peak in the magnetic curve, extending 44 percent above the average and again occurring just one day before the cosmic-ray low point.

These magnetic pulses depart only about one-third or one-fourth as far from the average as do Chree's primary pulses when referred to magnetically most "calm" or "disturbed" days. They correspond in magnitude to the first secondary pulses obtained in that manner. However, it is noteworthy that the peak of Chree's primary character-figure pulse for the 11 years, 1890–1900, *with zero-days determined by sunspot area*, was only about 9 percent from the average, although individual years exhibited considerable variations. This might be regarded as indicating a relation between cosmic-ray fluctuations and disturbances in the earth's magnetic field, quite as intimate as that between the magnetic disturbances and sunspots, a relation now generally recognized. Whether the suggested relation is direct or indirect is not established, of course.

In view of the relation found between cosmic-ray and magnetic disturbances, and Chree's success in associating the latter with sunspot areas, it will be interesting to find whether or not cosmic rays and sunspots are similarly related. It seems reasonable to suppose that if the cosmic-ray pulses and magnetic disturbances are not directly related, then they may be due largely to a common origin, at least so far as the primary pulse is concerned. The

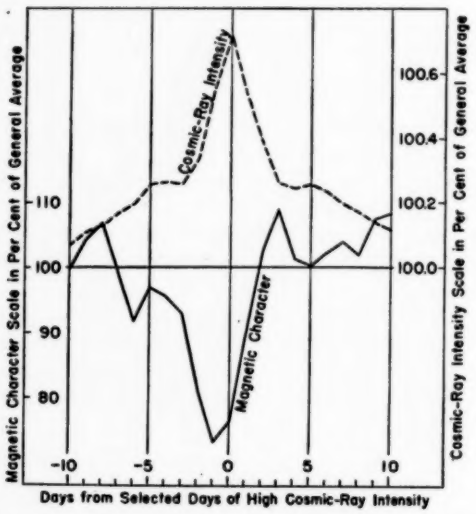

FIG. 1. Primary cosmic-ray intensity and magnetic character-figure pulses. For both these curves the selected "zero" days were the five days of *greatest* average *cosmic-ray intensity* in each of the 18 months, June, 1938 through November, 1939.

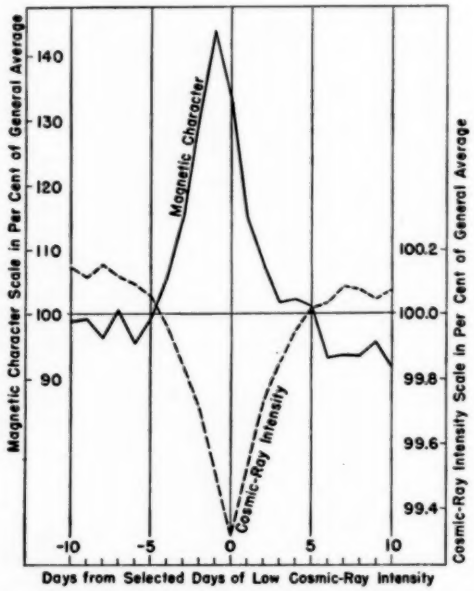

FIG. 2. Primary cosmic-ray intensity and magnetic character-figure pulses. For both these curves the selected "zero" days were the five days of *least cosmic-ray intensity* in each of the 18 months, June, 1938 through November, 1939.

secondary magnetic pulses appear not to be associated in a simple manner with the cosmic-ray secondary pulses nor with a definite time interval except at a considerable distance from the primary. Because of the time relation between the primary and secondary cosmic-ray pulses, it would seem they could not be due to different causes.

[1] James W. Broxon, Phys. Rev. **59**, 470 (1941).
[2] C. Chree, Phil. Trans. Roy. Soc. **A212**, 75 (1913); **A213**, 245 (1914); C. Chree and J. M. Stagg, *ibid.* **A227**, 21 (1928).

Cosmic-Ray Intensities and Typhoons

Y. NISHINA, Y. SEKIDO AND H. SIMAMURA
Institute of Physical and Chemical Research, Tokyo, Japan
AND
H. ARAKAWA
Central Meteorological Observatory, Tokyo, Japan
March 4, 1941

SOME time ago we reported in this column[1] the effect on cosmic-ray intensities of an individual warm or cold front. Since then we studied the similar effect caused by typhoons. Here we give the results for two typical ones.

The center of the one typhoon passed the Sea of Japan to the northwest of Tokyo at its closest distance of about 430 km at 6 P.M. on September 11, 1937 and that of the other crossed the Sea to the southeast of Tokyo at its closest distance of about 400 km at noon on September 23, 1939.

Cosmic-ray data were obtained in Tokyo with a Steinke apparatus in 1937 and with an IPCR cosmic-ray meter in 1939, both being placed inside 10 cm Pb. Hourly means of observed intensities were reduced, as before, to the values at a standard pressure 755 mm Hg by using a true absorption coefficient $\mu = 9.5 \times 10^{-3}$/cm Hg for air. In Fig. 1 we show the intensity variations during the approach and passage of the respective typhoons. While the cosmic-ray intensities in Tokyo remained nearly constant during the southeast passage of the typhoon, they decreased beyond doubt during the northwest passage, as represented in Fig. 1 (a) and (b), respectively.

Since the upper air structure in the north quadrant of a typhoon is quite the same as in the case of an ordinary extratropical cyclone, the constancy of cosmic-ray intensities observed above during the southeast passage is just in accordance with our previous results[2] in which it was statistically shown that in the northwest quadrant of the cyclone, the cosmic-ray intensities remained constant. On the other hand, the fresh tropical air advances rapidly to the north in the south quadrant of a typhoon. Consequently the decrease in cosmic-ray intensities as observed in Fig. 1 (b) is to be expected for the northwest passage of a typhoon, because of the temperature effect of cosmic rays, which is brought about by the decay of the meson.

These considerations are quite in agreement with the general trend of the aerological observations in the typhoon area.[3]

This work was carried out as a part of the program of the Cosmic-Ray Sub-Committee of the Japan Society for the Promotion of Scientific Research.

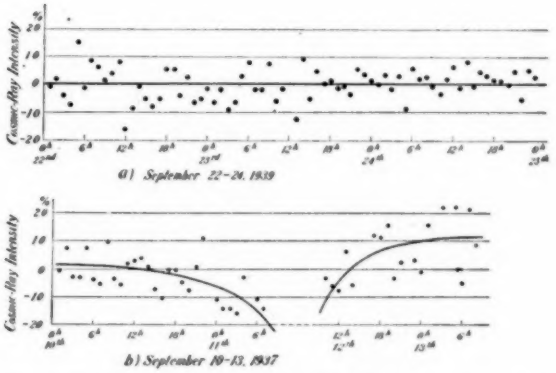

FIG. 1. Variation of cosmic-ray intensities during the approach and passage of typhoons. (a) Passage of a typhoon to the southeast of Tokyo at its closest distance of about 400 km. (b) Passage of a typhoon to the northwest of Tokyo at its closest distance of about 430 km.

[1] Y. Nishina, H. Arakawa, Y. Sekido and H. Simamura, Phys. Rev. **57**, 1050 (1940).
[2] Y. Nishina, H. Arakawa, Y. Sekido and H. Simamura, Nature **146**, 95 (1940).
[3] H. Arakawa, Beitr. z. Phys. frei. Atm. **24**, 156 (1937); Bull. Am. Meteorolog. Soc. **17**, 313 (1936).

Deuteron Bombardment of Oxygen

S. B. WELLES
Sloane Physics Laboratory, Yale University, New Haven, Connecticut
March 17, 1941

OXYGEN, enriched in the two heavy isotopes O^{17} and O^{18}, has been obtained by the method of thermal diffusion. The ordinary abundance of these rare isotopes is 0.04 percent and 0.2 percent, respectively. The apparatus consisted of six three-meter columns in series, convectively coupled. The first three were of the inner cylinder type at a temperature of 300°C, and the second three of the hot platinum wire type at 700°C.

Mass spectroscopic analysis indicates a separation factor, after 115 days of continuous running, for O^{18} of 81, i.e., 14 percent. Because of the more rapid approach to equilibrium of the concentration of O^{17}, an enrichment factor of approximately 20, i.e., 0.8 percent, is to be expected, rather than the square root of 81.

Two tungsten oxide targets, one containing ordinary oxygen and the other an equal amount of oxygen enriched in the heavy isotopes, were bombarded by 3.7-Mev deuterons. The intensity of the beam and the bombarding time was the same for each target. After the disappearance of short-life activity due to carbon contamination, the intensity of the 114-minute activity of F^{18} was measured. An increase for the enriched oxygen target was found, which amounted to a factor of 19. This is in agreement with the magnitude of the O^{17} enrichment. The sign of the charge and the energy of the positrons from F^{18} were checked.

This is definite proof of the correctness of the supposition of Davidson[1] that the reaction is of the (d, n) type due to the rare O^{17} and not of the (d, γ) type from the very abundant O^{16}, which was thought more probable by Yasaki and Watanabe.[2]

[1] W. L. Davidson, Jr., Phys. Rev. **57**, 1086 (1940).
[2] Yasaki and Watanabe, Nature **141**, 787 (1938).

Formation of the Solar System by the Rotational Fission of a Star: the Fission Being Initiated by a Passing Second Star

Ross Gunn
U. S. Naval Research Laboratory, Washington, D. C.
March 27, 1941

IT is well known that a gravitating mass revolving about a star of the same uniform density cannot be in equilibrium if it is nearer to the star than 2.4 times the star's radius (Roche's limit). Investigation shows that the actual limit of stability extends indefinitely beyond the Roche limit if the rotational velocity of the gravitating mass approaches its critical fission value. This effective limit of stability R is given by

$$R=2.3B\left[\frac{\rho_s}{\rho_e(1-(\omega_e/\omega_{ec})^2)}\right]^{\frac{1}{3}},$$

where ρ_s and ρ_e are the densities of the star and rotating mass, respectively, B is the mean radius of the combined masses, while ω_e/ω_{ec} is the ratio of the actual to critical angular velocities for the rotating mass. Stars, passing well inside this limit, will be disrupted by the superposed tidal forces even though their angular velocity is notably below the critical value. Thus, rapidly rotating stars break up by fission preferentially in the vicinity of another star.

Assuming that the rapidly rotating star and a second star approach each other with velocities slightly exceeding their parabolic value and assuming various values for the distance of closest approach and the direction and magnitude of the axial rotation, it has been found by graphical means that after the approach (a) the stars may separate without permanent change; (b) the rotating star may divide by fission forming a binary star; (c) the rotating star may divide by fission, the nearer component being captured by the second star and the outer component proceeding as a single star; (d) the rotating star may divide by fission and both components be captured. One component with the second star forms a close binary while the other describes an open eccentric orbit about the other two.

The third possibility may be of importance in describing the origin of the solar system. Consider a rapidly rotating star which approaches another star and suppose that the angular velocities of rotation and revolution have the same direction. Suppose further that it rotates with an angular velocity somewhat less than, but approximating, its critical value. Now as this rotating star approaches the second star they are both grossly deformed by tidal forces and some of the orbital energy is utilized to separate the components and to change their angular velocity. Tidal forces acting in conjunction with the centrifugal forces cause the star to break up and simultaneously produce zones of instability on the inner and outer faces of the rotating star. Condensed masses of planetary size from the outermost zones leave the surface of the component star because they possess too much momentum for stability, while masses from the inner face leave it because they are deficient in momentum. Tidal forces between the stellar companions and the second star reduce the angular velocity of rotation. The resulting slowly rotating outer component finally proceeds to infinity accompanied by two different families of satellites all marked, as a result of their birth process, by definite asymmetries. The details of planetary formation follow those suggested in earlier papers.[1] No serious inconsistency of energy or momentum has emerged as a result of the calculations and it appears that a stellar encounter of the type considered will produce a distribution of masses remarkably like the solar system.

Because close encounters are highly improbable in the present disperse universe, it seems necessary to assume that stars, ages ago, were very close together. All other leading theories, except that referenced above, are similarly embarrassed.

[1] Ross Gunn, Phys. Rev. **39**, 130, 311 (1932).

Fission of Uranium by Alpha-Particles

E. Fermi and E. Segrè
Department of Physics, Radiation Laboratory, University of California, Berkeley, California
February 24, 1941

FISSION of uranium has been produced by neutrons, deuterons and gamma-rays. The 60″ cyclotron of the Crocker Radiation Laboratory with its 32-Mev alpha-particles afforded the possibility of trying to produce fission by alpha-bombardment of uranium.

A layer of ammonium uranate, a few millimeters thick was bombarded with a beam of several milliamperes intensity of 32-Mev alpha-particles for about one minute and was afterwards tested chemically for some of the characteristic fission products of uranium. The following were found: iodine (54 minutes), iodine (3.4 hours), I^{133} (22 hours), I^{131} (8 days). In some cases we found also tellurium members of the same chains.

In order to check that the activation was not due to secondary neutrons, both faces of the thick uranium target were tested. The face not directly exposed to the beam showed practically no activity. In order to rule out also the possibility of a deuteron contamination of the beam itself, it was checked that the ratio between the activity of 93^{239} and fission products was less, by order of magnitude, than the same ratio under deuteron bombardment. The 93 activity itself was possibly due to a small residual deuteron contamination of the beam or to secondary neutrons.

We looked also for possible delayed fission by bringing the sample a few minutes after the end of the bombardment in front of an ionization chamber connected to a linear amplifier. No big kicks due to fission were observed.

The Gamow barrier for alpha-particles colliding with uranium is estimated to be almost 30 Mev. However, the transparency of the barrier for particles up to 4 or 5 Mev below the top of the barrier is still large enough to allow them to penetrate inside the nucleus with a large probability. If these estimates are correct, the formation of a compound nucleus by uranium and alpha-particles would have a large cross section even for energies somewhat below 25 Mev.

The excitation energy of the compound nucleus is less

than the kinetic energy of the alpha-particle because at the top of the periodic system the process of emitting alpha-particles from the nucleus is exothermic. On account of this fact the excitation energy of the compound nucleus is probably from 5 to 10 Mev less than the kinetic energy of the alpha-particle. This leaves an excitation which may vary according to the energy of the primary particle from 15 to 27 Mev, and is therefore amply sufficient to produce the fission of the compound nucleus. Indeed it is so large that 2 or 3 neutrons may be evaporated, still leaving a sufficient energy available for the fission.

In conclusion, we wish to thank Professor E. O. Lawrence for his interest in this work, the Research Corporation for financial support and the Hitchcock Foundation for providing the opportunity for one of us to visit the Radiation Laboratory.

Excitation of Gamma-Rays by Fast Neutrons of Different Energy

ITARU NONAKA
Research Laboratory, Matuda Division, Tokyo-Sibaura Electric Company, Kawasaki, Kanagawaken, Japan
March 3, 1941

ATOMIC cross sections of Al, Si, Fe, Co, Cu, Ag, Cd and Pb for gamma-ray excitation by fast neutrons of different energies from 2.25 to 2.90 Mev were determined. The neutron source used was a *D–D* type with 200-kv acceleration, and the neutron energy was varied by changing the angle φ between the paths of the neutrons and the deuterons. The gamma-rays emitted were measured by a thin-wall Geiger-Müller counter surrounded by a sheet of lead 1 mm in thickness.

In a *D–D* neutron source, not only the energy but also the number of neutrons emitted depends on φ. Therefore, the number was measured by an ionization chamber filled with a mixture of hydrogen and nitrogen to 14.1 atmospheres pressure, the purpose of adding nitrogen being to make the range of recoil protons short compared with the dimension of the chamber.

The results obtained for the cross sections σ_γ are shown in Fig. 1, where the neutron energy was calculated by taking $Q=3.32$ Mev[1] and assuming the deuteron beam to be 40 percent atomic and 60 percent molecular and that the heavy water ice target was thick. General features of the curves for Al, Fe, Cu and Cd agree qualitatively with the results of H. Kallmann and E. Kuhn,[2] but precise comparison cannot be made, as they have made measurements only at three different values of neutron energy. In the present experiment, anomalies were observed in most cases. The absolute magnitude of the cross section for Cu at 90° ($E_n=2.52$ Mev) was estimated to be 2×10^{-24} cm² by calculating the absolute number of neutrons incident on the measuring system from the absolute value of the ionization current in the chamber and by taking the efficiency of the counter for the gamma-rays to be one per-

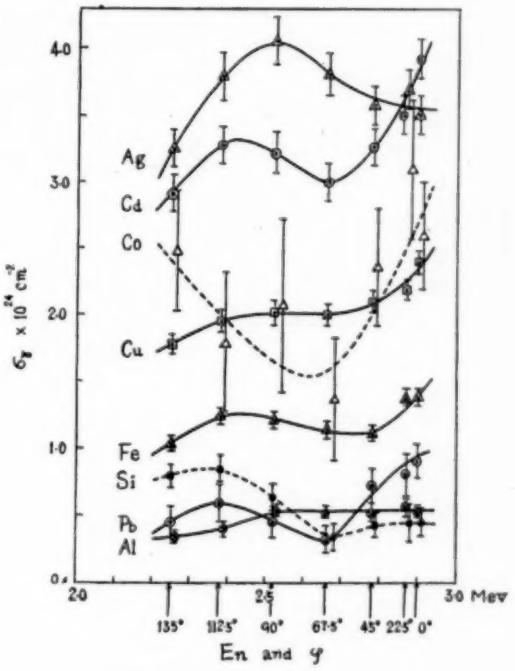

FIG. 1. Energy cross section curves.

cent.[3] This absolute value of σ_γ is about seven times greater than the value estimated by H. Aoki,[4] and is about 80 percent of the total cross section σ_t. As the mean number of gamma-ray quanta emitted per one inelastic collision of a *D–D* neutron is considered to be not so large (perhaps smaller than two, because of the comparatively low excitation of the residual nucleus), σ_γ may be only a little larger than the cross section of inelastic collision σ_{inelast}. From these considerations and the above results, it may be said that for nuclei of medium weight such as Fe, Co, Cu, Ag or Cd a considerable part of the scattering of *D–D* neutrons is inelastic.

H. Aoki[5] has observed many anomalies in the total cross sections of Si, Al, Fe, Pb, etc. The positions of anomalies observed in σ_γ lie near those of σ_t (when we recalculate E_n by taking $Q=3.32$ Mev), and the magnitudes of the variations are almost equal in both cases; especially for Pb the variations of σ_γ and of σ_t are very similar in the positions of maximum and minimum and in the magnitude. At any rate, the anomalies in σ_t observed by H. Aoki or M. R. MacPhail[6] cannot be considered to be entirely due to elastic scatterings.

A detailed report will be published in the *Proceedings of the Physico-Mathematical Society of Japan.*

[1] L. G. Bonner, Nature **143**, 681 (1939).
[2] H. Kallmann and E. Kuhn, Naturwiss. **26**, 107 (1938).
[3] F. Norling, Phys. Rev. **58**, 277 (1940).
[4] H. Aoki, Proc. Phys.-Math. Soc. Japan **19**, 369 (1937).
[5] H. Aoki, Proc. Phys.-Math. Soc. Japan **21**, 232 (1939).
[6] M. R. MacPhail, Phys. Rev. **57**, 669 (1940).

Proceedings of the American Physical Society

Minutes of the Cambridge, Massachusetts, Meeting

February 21 and 22, 1941

THE 240th regular meeting of the American Physical Society occurred at Cambridge, Massachusetts, in conjunction with the Optical Society of America on February 21 and 22, 1941. The sessions of both societies were held at the Massachusetts Institute of Technology on Friday and at Harvard University on Saturday.

A joint session of both societies took place on the morning of Friday, February 21. It was a symposium of three invited papers, pertaining to the advances of the last decade in measurement and specification of color and to problems still unsolved; they were adorned by lantern slides, motion pictures, and vivid demonstrations. The speakers and the titles were: Arthur C. Hardy, Massachusetts Institute of Technology on "Spectrophotometry, a basis for color measurement"; David L. MacAdam, Eastman Kodak Company on "Colorimetry and the standard observer"; and Deane B. Judd, National Bureau of Standards on "Color perception and its relation to color measurement." The chairman was K. S. Gibson, National Bureau of Standards. Several hundred attended.

The remainder of the scientific program of the Society consisted of the presentation of forty-four ten-minute papers at five sessions. The abstracts of these papers, and of three others (38, 46, 47) which were not presented, are printed hereinafter. An *Author Index* will be found at the end.

A joint dinner of the two societies was held at the Hotel Commander on Friday evening, February 21. It was presided over by the President of the Physical Society, Dean George B. Pegram. The after-dinner speakers were President Karl T. Compton of the Massachusetts Institute of Technology, Professor J. H. Van Vleck of Harvard University, and Professors J. C. Slater and G. R. Harrison of the Massachusetts Institute of Technology. About two hundred attended.

The Council met on Friday afternoon, February 21, 1941, and elected one fellow (Lyman Spitzer, Jr., previously a member), and forty-six new members, *viz.*, Arthur Adel, Kathryn Blevins, M. Hildred Blewett, Charles Brand, James G. Buck, John R. Clark, Curtis Clayton, Robert L. Cummerow, Mario A. da Silva, Henri-Georges Doll, Vernon Esgar, Marvin P. Feyerherm, James Fisher, Stanley V. Forgue, John G. Fox, Jerome B. Freier, William S. Gallaway, Kensuke Harada, Henry Hurwitz, Jr., Elmer L. Kelly, Hedwig Kohn, Herbert D. Landahl, Ralph E. Lapp, Willard D. Lewis, Albert J. Lovell, Henry C. Meadow, Stewart E. Miller, William R. Monroe, Charles Mueller, George R. Newton, Ernest C. Okress, Paul Olum, Glen Peterson, Joseph G. Reid, Jr., Darwin S. Renner, Hugh T. Richards, Henry E. Robinson, Clarence E. Rose, George Rudinger, W. Scholten, Leo W. Scott, John C. Southard, Francis E. Throw, Richard E. Vollrath, Henry T. Wensel and Francis T. Worrell.

Word was received by the Council of the death of two fellows (William J. A. Bliss and Arthur Haas) and one member (Daniel W. Morehouse).

The death of D. C. Miller, a former President and for many years an assiduous member of the Council of the Society, occurred on the following day.

KARL K. DARROW, *Secretary*
Columbia University, New York, New York

Abstracts of Contributed Papers

1. Note on Liouville's Theorem and the Heisenberg Uncertainty Principle. J. H. VAN VLECK, *Harvard University.*—Both the Heisenberg uncertainty $\Delta p \Delta x$ and the infinitesimal domain in Liouville's theorem can be interpreted in terms of volume elements in phase space (areas for systems with one degree of freedom), but in the usual examples the uncertainty increases with time, whereas the Liouville volume is constant. In the case, for example, of a free particle moving in one dimension this discrepancy arises because an initially rectangular Liouville area is distorted into an increasingly oblique parallelogram as time progresses, and the Heisenberg uncertainty is usually measured by the area of the rectangle inscribing the parallelogram. To have a time invariant definition of

uncertainty we must use in place of p, x the oblique coordinates $p'=p, x'=x-pm^{-1}t$ bounding the parallelogram. Classically the product $\Delta p'\Delta x'$ is obviously constant. This paper investigates whether the invariance also holds when quantum-mechanical operators are used. By transforming to momentum space it is proved that the invariance is also preserved in quantum theory. Thus, a formal definition of the Heisenberg uncertainty can be given which is independent of time, but it may not have much operational significance in terms of physical measurement. Details will appear in *Philosophy of Science*.

2. Reaction of the Absorber as the Mechanism of Radiative Damping. R. P. FEYNMAN AND JOHN ARCHIBALD WHEELER, *Princeton University*.—Radiative damping arises from retarded interactions between the various parts of an electron of finite size, according to Lorentz. At high frequencies this damping depends on the electron's structure. Non-electric stresses are required to hold the electron together. Dirac abandoned this picture and postulated a point electron. Guided by considerations of relativistic invariance he proposed essentially the first term in Lorentz's expression as a possible exact law for radiative damping. We postulate (1) that an accelerated point charge in otherwise charge free space does *not* radiate energy; (2) that, in general, the fields which act on a given particle arise only from *other* particles; (3) that these fields are represented by one-half the retarded plus one-half the advanced Lienard-Wiechert solutions of Maxwell's equations. In a universe in which all light is eventually absorbed, the absorbing material scatters back to an accelerated charge a field, part of which is found to be independent of the properties of the material. This part is equivalent to one-half the retarded field *minus* one-half the advanced field generated by the charge. It produces radiative damping (Dirac's expression) and combines with the field of the source to give retarded effects alone.

3. Statistics of the Two-Dimensional Ferromagnet. GREGORY H. WANNIER, *University of Texas*.—Rigorous statistical study of the Curie transition of ferromagnetics is possible for a two-dimensional square net of spins with coupling between neighbors. Kramers (unpublished), dealing with strips of spins infinite one way and finite the other, showed that the partition function λ is the largest eigenvalue of some finite matrix, $M(K)$, K standing for $1/kT\times$coupling energy between neighbors. (Order of matrix $=2^{n-1}$, $n=$number of spins along finite dimension.) Since ferromagnetism needs at least two infinite dimensions we want the limit of $\lambda(K)$ for large matrix order. The properties of M show that if λ possesses one singularity it lies at $K=0.4407$, where $\sinh 2K=1$. The energy there must be continuous and the specific heat can have no finite jump. For further study the specific heat is computed by matrix calculus. The numerical sequence of finite solutions increases as $\log n$. Consequently, the two-dimensional ferromagnet has an infinite specific heat at the Curie point.

4. On Position Measurements of Heavy Particles. O. HALPERN AND M. H. JOHNSON, *New York University*.—It has previously[1] been shown that a consistent application of relativistic quantum mechanics disproves the possibility of measuring exactly certain *individual* observables; e.g., the position of an electron or the component of an electric field strength. We have extended these deliberations to a discussion of the measurement of the position of heavy particles (protons). While the diversity of the possible arrangements does not allow a single sharp limit to the accuracy of observation to be given, it has been found that the minimum error involved is always close to the *electronic* rather than the protonic Compton wave-lengths.

[1] Paper submitted to *The Physical Review*.

5. Self-Consistent Field with Exchange for Si V and Si IV. MILLARD F. MANNING, *University of Pittsburgh*, AND W. HARTREE AND D. R. HARTREE, *University of Manchester, Manchester, England*.—Solutions of Fock's equations for the normal state of Si V and for a number of states of Si IV are reported. In Table I are shown the comparisons between the calculated and observed term values.

TABLE I. *Comparisons of calculated and observed term values for* Si IV.

	3s	4s	5s	3p	4p	5p
Calculated	359,400	168,800	98,000	289,600	144,100	87,000
Observed	364,100	170,100	98,700	292,500	145,700	87,500
	3d	4d	5d	4f	5g	
Calculated	201,800	113,400	72,200	109,800	70,240	
Observed	203,700	114,100	72,600	110,000	70,260	

TABLE II. *Comparison of calculated and observed doublet separations.*

	3p	4p	5p	3d	4d	4f
Calculated	430	149	70	19	9	2.3
Observed	460	162	75	small	small	1.3

The wave functions have been used to calculate spin-orbit interactions for the valence electron in different states. The results are given in Table II. It is noted that for the p states the agreement is satisfactory and hence the simple theory is a good approximation. For the d and f states the agreement is not satisfactory, indicating that the simple theory is not adequate.

6. Unexplained Irregularities in the Z Dependence of the Energy Differences Within the Configuration $3d^3$. J. E. MACK, *University of Wisconsin*, AND E. E. ANDERSON, *Milwaukee-Downer College*.—Of the 19 levels of the configuration $3d^3$, the 13 levels $^4FP\,^2GDH$ are well established experimentally from Ti II to Ni VIII, inclusive, in the scandium-like isoelectronic sequence. The graph of energy (with respect to $^4F_{3/2}$) against Z is, on the whole, so smooth that extrapolations can be made with an uncertainty of only about 100 cm^{-1}. In both Co VII and Ni VIII, however, ^2G and ^2H are almost 1000 cm^{-1} higher and ^2D almost 1000 cm^{-1} lower than would have been expected by extrapolation from Fe VI. This unexpected shift between VI and VII and the retention of the shifted value in VIII are the more puzzling in view of the large and smoothly increasing distance ($\doteq 3\cdot 10^5$ cm^{-1}) to the nearest neighboring configuration, $3d^24s$. The doublet separations behave

smoothly. The phenomenon cannot be self-consistently expressed in terms of changes in the Slater integrals F_2 and F_4. (There are also smaller irregularities in ^4P, apparently unrelated to the foregoing, at the same values of Z.)

7. Term Energies in the Configuration d^5. OTTO LAPORTE, *University of Michigan.*—Among all configurations of equivalent d electrons the configuration d^5 will, because of its central position, give rise to the largest numbers of levels. However its complexity is somewhat lessened by the fact that in first approximation the spin orbit interaction vanishes for all of its terms. For the case of Russell-Saunders coupling the term energies have been computed as functions of three radial integrals F_0, F_2 and F_4. An unexpected simplification of the resulting formulae is that the quadratic equations for the two pairs of doubly occurring terms ($^2G_\pm$ and $^2F_\pm$) possess rational roots and that the cubic equation for the three ^2D terms possesses one root rational in the parameters. The comparison of these and similar formulae with the experiment is facilitated by a plot of relative term distances as a function of the parameter ratio $F_4 : F_2$.

8. General Considerations Concerning Term Energies of Configurations d^x. JOHN R. PLATT AND OTTO LAPORTE, *University of Michigan.*—When plotting formulae for d^x with F_2/F_4 as an independent variable it is seen that for $F_2 : F_4 = 5 : 1$ high order degeneracies occur. The five terms of d^2 and the eight terms of d^3 arrange themselves in three groups, while the sixteen terms of d^4 and d^5 coincide so as to form six superterms. The separations between these groups are all low multiples of $7F_2$. The formulae for d^4 as given by Ostrofsky[1] at first did not comply with this rule; a recalculation was therefore made and two errors were found in the expressions for the pairs $^1G_\pm$ and $^1S_\pm$. Analogous coincidences for the configurations f^x will occur for the parameter ratio $F_2 : F_4 : F_6 = 11 : 6 : 1$. This behavior can be reduced to sum rules obeyed by the Condon-Shortly coefficients $c^k(lm; l'm')$.

[1] Phys. Rev. **46**, 604 (1934).

9. The Theoretical Extension of Large Air Showers. H. A. BETHE, *Cornell University.*—According to the theory of Euler and Wergeland, the scattering of electrons causes a shower to spread over approximately 30 meters in air of atmospheric pressure. The result of Auger and collaborators who found appreciable coincidences at distances of as much as 300 meters, was therefore interpreted as evidence for mesotrons forming the "wings" of large showers. This is in contradiction to experiments of Hilberry (unpublished) and Auger himself who showed that the radiation in the wings is much softer than in the core of a large shower. A more accurate calculation of the scattering of electrons was therefore made which gave 90 meters for the root-mean-square spread of a shower. The greatest contribution comes from the divergence of the "parent" γ-rays which created the observed electrons; the angular divergence of these γ-rays is due to scattering of the "grandparent" electrons. The electron density falls off more slowly than Euler's at large distances from the core of the shower; it increases more strongly (as $r^{-4/3}$) at small distances. A re-evaluation of Auger's experiments gives numerical results which by accident are very similar to his own and confirm the $E^{-1.9}$ law for the energy distribution of primary electrons.

10. An Instrument for Studying the Topographies of Fine Textured Surfaces. F. W. ADAMS, LEE DEVOL, AND H. R. LETNER, *Mellon Institute of Industrial Research.*—A profilograph, using a tracing point and optical lever system, makes profiles of fine textured surfaces, magnifying the elevations and depressions by as much as 6000×. With this instrument it is possible to detect surface variations as small as 0.04 micron. It is also possible to make a series of profiles along parallel paths from which topographic or relief maps can be prepared. Uses include the study of machined, lapped, and etched surfaces of importance in industry. The high accuracy is obtained with no more difficult machine work than the simultaneous lapping of two tapered bearings mounted on a single shaft. The use of torsion elements of special design for supporting the mirror makes the instrument relatively insensitive to vibration. These torsion elements are capable of supporting a mirror large enough to permit several reflections of the light beam, giving the instrument its high resolving power.

11. The Input Impedance of a Symmetrical Antenna. RONOLD KING, *Harvard University.*—The input resistance and reactance of a symmetrical, center-driven, cylindrical antenna have been derived from the rigorous expression for the input impedance given by Hallén.[1] Resonance conditions and conditions for maximum input resistance have been derived in terms of the length and radius of the antenna. From these it can be shown that extreme values of the input resistance occur practically at resonance. Extensive curves for the input resistance and reactance as functions of the length and radius of the antenna and the driving frequency are being computed. A few typical cases have been completed and compared with the corresponding curves calculated by Labus[2] under the assumption of a sine current distribution. The new curves are a good approximation for all lengths and a wide range of radii, whereas all those based on a sine distribution of current are entirely incorrect over ranges of lengths near those for which they become infinite, and considerably in error for all but vanishingly small radii. The radii of many self-supporting ultra-high frequency antennas are sufficiently large to contribute appreciably to the input impedance.

[1] E. Hallén, Uppsala (1938).
[2] J. Labus, Zeits. f. Hochfrequenztech. **41**, 17 (1933).

12. A Magnetic Lens Beta-Ray Spectrometer. MARTIN DEUTSCH, *Massachusetts Institute of Technology.*—A beta-ray spectrometer has been constructed, utilizing the chromatic aberration of a "short" magnetic electron lens as proposed by Klemperer.[1] The resolution and "line shape" have been computed, assuming only spherical aberration to be important. The theory has been verified by experiment. The lens consists of a coil weighing about 300 lb., contains

no iron, and uses up to 2 kw. The distance between source and counter can at present be varied from 1 to 2 meters. The greatest distance of the electron paths from the axis is 7.2 cm. "Line widths" of about 2 percent have been obtained, as well as solid angles of about 0.12. Neither value represents the limits of the instrument. The upper limit of energy is at present about 5 Mev for a length of path of about 2 meters. The large solid angle and the accessibility of the source make the instrument well suited for coincidence studies. First results on Br^{82} indicate a simple spectrum (above 0.14 Mev) as shown by coincidences, with a tentative upper limit of about 0.45 Mev and no internal conversion lines between 0.14 and 1.0 Mev.

[1] O. Klemperer, Phil. Mag. **20**, 545 (1935).

13. A Further Verification of the Montgomery Theory of Geiger Counter Discharge. W. E. RAMSEY, EMMETT HUDSPETH AND WAYNE L. LEES, *Bartol Research Foundation of the Franklin Institute.*—An investigation has been made with a specially designed counter whose cylinder consisted of nine insulated segments. With various known capacities between the counter wire and ground, families of curves were obtained in which the pulse-size was observed as a function of the number of segments whose potential was at a fixed point above the starting potential. Such families were obtained for both the so-called "non-quenching" (argon) and "self-quenching" (ether) gases. In the first case it was found that pulse-size was constant (equal to the overvoltage) for counter lengths less than a certain value. This critical length l is proportional to the total capacity of the counter wire. Beyond this length the pulse-size is proportional to l except for very small capacities. This behavior is precisely that predicted by the theory.[1] In the case of the "self-quenching" counter, pulse-size is proportional to counter length for all values of l and inversely proportional to the total counter wire capacity. These results constitute additional evidence that the quenching mechanism is exactly the same in the two types of counters,[2] and that the ether counter differs from the argon counter in that it does not break multiply.

[1] C. G. and D. D. Montgomery, Phys. Rev. **57**, 1030 (1940).
[2] W. E. Ramsey, Phys. Rev. **57**, 1022 (1940).

14. The Radiation of Light by High Current Electrical Discharges. J. W. FLOWERS, *General Electric Company.*—Currents of the order of 10^5 amperes produced by high voltage discharges in air radiate considerable light as well as sound. The apparent size of such a discharge as recorded by an ordinary photograph depends almost completely on the exposure, which may vary over a range of more than 10^4-fold. In an analysis of the light with respect to time, the resolution is in general limited by the effective size of the source which has previously been unknown. A transverse slit placed near the discharge path and acting as the light source has permitted resolution limited only by film speed. High speed rotating-film photographs of such a slit clearly show the variation of the luminous cross section of the discharge with time. Microphotometer analyses of such records show the relation of luminosity with the current as recorded by the cathode-ray oscillograph. With resolution known, departure of microphotometer records from current oscillograms in some cases can be ascribed to two factors, persistence of luminosity or deionization time and mechanism of discharge. This is supported by similar analysis of currents passing between electrodes in high vacuum which show very little persistence.

15. Rigidity and Internal Friction of a Glass in Its Softening Range. FRANCIS BIRCH AND DENNISON BANCROFT, *Harvard University.*—The rigidity of boron trioxide glass has been measured by a dynamical method to approximately 300°C. The softening or "transition" region for this glass begins at about 250°. For an interval of 50°, there now exist for the first time measurements of both rigidity and viscosity[1] for a given material, as well as rough estimates of the internal friction for torsional vibrations. Between 250 and 300°, while the viscosity decreases by a factor of about 1000, the internal friction increases by a factor of 5, and the rigidity decreases by about 25 percent. The internal friction is apparently independent of frequency between 4600 and 17,000 cycles per second. Absolute values for the elastic constants of this glass are also given. This work was inspired principally by certain geological problems, but the results should be of use in the construction of a physical theory of the vitreous state.

[1] G. S. Parks and M. E. Spaght, Physics **6**, 67 (1935).

16. Impedance of the Squid Giant Nerve Fiber During Current Flow. KENNETH S. COLE AND RICHARD F. BAKER, *Columbia University.*—The change in the transverse impedance of the squid giant nerve fiber caused by direct current flow has been measured at frequencies from 1 kilocycle to 500 kilocycles. The impedance change is equivalent to an increase of membrane conductance at the cathode to a maximum value approximately the same as that obtained during the passage of a nerve impulse and a decrease at the anode to a minimum not far from zero. There is no evidence of appreciable change of the membrane capacity in either case. The membrane is a rectifier with a rectification ratio of about 100 and is comparable with the Cu–CuO and Se rectifiers commercially available. Interpreting the membrane conductance as a measure of ion permeability, this permeability is increased at the cathode and decreased at the anode.

17. A New Method for Rapidly Desiccating Human Plasma for Transfusion Purposes. T. R. FOLSOM, *Memorial Hospital, New York City.*—The preservation of large quantities of human plasma for use for transfusions in war emergencies instead of blood has been advocated. It has been demonstrated previously that human plasma may be preserved by desiccating it from the frozen state, and that this may be reconstituted later by the addition of sterile water. The problem of supplying a sufficiently fast and economical vacuum pumping system for handling quantities of water vapor has already been solved by other workers. Because of the porous nature of dried plasma,

and the low temperature permissible, heretofore heat could not be supplied rapidly enough to cause rapid evaporation, and ten to thirty hours drying time was necessary. Investigations into the thermal problem at the Memorial Hospital led to a method which permits complete drying in one hour. Plasma is injected into a rapidly pumped vacuum system so that small frozen granules are instantaneously formed by rapid evaporation. These granules fall into a vessel, which is warmed to body temperature and may be tumble-stirred. The granules remain frozen until dry and later may be poured out easily. The process permits design of apparatus about ten times faster than present equipment and permits continuously operating desiccators to be constructed if desired.

18. Measured Admittances of a Rochelle Salt Resonator. K. S. VAN DYKE AND MAYNARD C. WALTZ, *Wesleyan University.*—Bridge measurements of admittance of an x-cut, 45° Rochelle salt bar are made. The 20–50 kc range includes the long wave longitudinal resonance in the region covered, −40 to +40°C. Adherent foil electrodes are used, and as the resonator is mounted the Q is 1200 at −30°C. The resonator current is less than 1 ma/cm². Bridge balance is determined by nullity at the frequency of the source. The vector admittance circles pass almost through the origin and are centered very close to the axis of reals. To secure circular loci for temperatures between the Curie points the admittance must be measured at constant current through the resonator. For different values of current, circles are obtained which differ in diameter and in the distribution of frequency around the circle. Analysis of the circle corresponding to each temperature yields values of the dielectric, piezoelectric, viscous and elastic constants. The latter three are functions of the current for temperatures between the Curie points. d_{14} increases, while the resonance frequency and the Q decrease, with increasing current. The clamped dielectric constant is of the order of 50 even at the Curie points.

19. The Nuclear Magnetic Moments of Ba^{135} and Ba^{137}. ROBERT H. HAY, *Columbia University.*—The "molecular beam magnetic resonance method"[1,2] has been used to measure the nuclear gyromagnetic ratios of the isotopes Ba^{135} and Ba^{137}. Only two resonance minima were seen. The ν/H ratio was constant for each and the g values obtained are 0.624 ± 0.002 for the deeper minimum and 0.558 ± 0.002 for the other, in units of $e/2$ Mc. The ratio of the depths of the minima was found from curves taken in rapid succession to be 1.9 ± 0.2; the ratio of the abundance of Ba^{137} to that of Ba^{135} is 1.89, using Aston's figures for isotope abundance.[3] Therefore, the value 0.624 has been assigned to Ba^{137} and 0.558 to Ba^{135}. Benson and Sawyer give 3/2 for the nuclear spin of both isotopes.[4] This leads to $\mu=+0.837\pm0.003$ nuclear magnetons for Ba^{135} and $\mu=+0.936\pm0.003$ nuclear magnetons for Ba^{137}. The ratio of the g values is also the ratio of the moments and is 1.1174 ± 0.1 percent.

[1] Rabi, Millman, Kusch and Zacharias, Phys. Rev. **55**, 526 (1939).
[2] Millman, Phys. Rev. **52**, 628 (1939).
[3] Aston, Proc. Roy. Soc. **134**, 571 (1932).
[4] Benson and Sawyer, Phys. Rev. **52**, 1127 (1937).

20. The Nuclear Magnetic Moment of In^{115}. T. C. HARDY, *Columbia University and College of the City of New York.*—The nuclear magnetic moment of In^{115} has been determined by the study of the radiofrequency spectrum of the ground state of the indium atom.[1] Lines characterized by transitions of the type $\Delta F=0$, $\Delta m=\pm1$, were observed. Since F has two values, each of the above transitions except those involving an m value of $\pm(i+\frac{1}{2})$ gives rise to a close doublet with frequency separation $2g_i\mu_0H/h$. The magnetic field, H, was calculated from the observed mean frequency of the doublet and the known nuclear spin and $\Delta\nu$ of the $^2P_{\frac{1}{2}}$ state of In^{115}. From observations of doublet separations in fields ranging from 400 to 4000 gauss the value of the nuclear magnetic moment is found to be 5.43 ± 0.03 nuclear magnetons. This is to be compared with the value of 6.40 nuclear magnetons found by Millman, Rabi, Zacharias,[2] using the atomic beam method of zero moments. The discrepancy is probably due to the difficulties inherent in the latter method.

[1] P. Kusch, S. Millman and I. I. Rabi, Phys. Rev. **57**, 765 (1940).
[2] S. Millman, I. I. Rabi and J. R. Zacharias, Phys. Rev. **53**, 384 (1938).

21. The Induced Radioactivity of Xenon. EDWARD P. CLANCY, *Harvard University.*—The irradiation of xenon by 12-Mev deuterons produces activities of 68 minutes, 9.6 hours, and 5.4 days. Of these, the last is unambiguously due to Xe^{133}, since Wu[1] has found a 5-day period when activating the single isotope of caesium through an (n,p) reaction. In the present work this isotope has also been produced by irradiating tellurium with 24-Mev alpha-particles, through the reaction $Te^{130}(\alpha,n)Xe^{133}$. Such a bombardment yields as well a weak unassigned activity of lifetime a few hours. The 9.6-hour period is undoubtedly the same as Wu's 9.4-hour xenon[1] obtained from an (n,α) reaction on barium, and assigned by him to Xe^{135}. Therefore, it would seem most logical to assign the 68 minute activity to Xe^{137}. It is interesting that the 9.6-hour and 5.4-day periods correspond to xenon periods observed in uranium fission.[2,3]

[1] Wu, Phys. Rev. **58**, 926 (1940).
[2] Segrè and Wu, Phys. Rev. **57**, 552 (1940).
[3] Dodson and Fowler, Phys. Rev. **57**, 966 (1940).

22. Internal Conversion in Rhenium. G. E. VALLEY,* *Harvard University.*—A complicated spectrum of internal conversion electrons is found to be emitted by tungsten specimens after irradiation by 11-Mev deuterons. Approximately fourteen lines are observed in the region extending from 50 kev to 150 kev. Six of these lines indicate the emission of gamma-radiation of 86 kev, 101 kev and 135 kev, accompanying the decay of W^{187} (24-hr. half-life[1]). Five other lines indicate that gamma-rays of 113 kev and 129 kev follow longer periods. These values are good to within 2 percent. Precision determinations, as well as a complete analysis, will be presented. The special methods used for preparing targets suitable for beta-ray spectrography will be described.

* National Research Fellow.
[1] K. Fajans and W. H. Sullivan, Phys. Rev. **58**, 276 (1940).

23. The Energy of the H^3 Beta-Ray. SANBORN C. BROWN, *Massachusetts Institute of Technology*.—The energy of the H^3 beta-ray has been measured by its absorption in helium. The detector was a screen cathode G-M counter. The source was mounted on a plunger sliding in a side arm on the counter envelope. The counter was operated with one atmosphere of helium flowing slowly through it at all times. The H^3, which was generously supplied by the Radiation Laboratory at Berkeley, was in the form of water. The source for the range determination was prepared by exposing a freshly distilled P_2O_5 surface to the H^3 water vapor in an atmosphere of helium for 24 hours. The maximum range of the H^3 beta-rays in helium was determined as 13 ± 1 mm. Using a range-energy relation of Schonland[1] and others, this corresponds to an energy of 9.5 ± 2.0 kev. The correction due to changes in solid angle with changing distance between the counter and source, and the correction due to the failure of the sensitive volume of the counter to coincide with the physical limits of the cathode screen, have been experimentally evaluated, and have been taken into account in the above value of the maximum energy.

[1] B. F. J. Schonland, Proc. Roy. Soc. **108**, 187 (1925).

24. Range of Fission Fragments. W. E. LAMB, JR., *Columbia University*.—The previous calculations[1] of the ranges in air of uranium fission fragments have been improved by the use of more accurate values for the successive ionization potentials of the fragments, and by inclusion of the energy loss due to nuclear collisions. Otherwise, the model was not changed. For an assumed initial total kinetic energy of 160 Mev, the ionization chamber ranges for the possible fragments $_{37}Kr^{36}$, $_{100}Mo^{42}$, $_{124}Sn^{50}$, $_{143}Ba^{56}$ were 2.25, 1.95, 1.94, 2.0 cm, respectively. These were assumed to terminate due to background when the energy loss per cm fell below 10 Mev/cm. (Energy of 5 Mev for Mo^{42}.) The residual ranges are then 1.40, 0.74, 0.84, 0.9 cm, respectively. The range for Kr^{36} is larger primarily because, according to the model, the degree of ionization of the fragment depends on its ionization potentials. If fluctuations in charge are not too important, the division of the ranges into two groups may be due to the shell structure rather than the light mass and consequent high energy of the Kr^{36}.

[1] W. E. Lamb, Jr., Phys. Rev. **58**, 696 (1940).

25. The Scattering of Protons in Hydrogen from 200 to 300 kev. G. L. RAGAN, W. R. KANNE* AND R. F. TASCHEK, *University of Wisconsin*.—Observations have been made using two different scattering chambers. One had fixed counters at 15° intervals; the other had a pair of monitoring counters at 15° each side of the beam and a third counter which could be rotated to any position. Simultaneous counting is carried out with two different counters connected to similar amplifier-recording circuits. From these counts the ratio of scattering at the two positions is calculated directly. The counters are of the Geiger-Klemperer proportional type; several checks have been made of their performance. A study of the variation with energy of the observed 105°/60° scattering ratio for protons in helium was among these checks. A "differential pumping" system isolates the scattering chamber from the accelerating tube; a scattering pressure of about 1 mm of purified hydrogen is used. The counters are filled with purified hydrogen to about 35 mm pressure, separated from the scattering chamber by thin collodion windows. Variation of the scattering with energy and with angle has been studied. While the results are not yet entirely complete, they agree well with Breit's calculations based on a square well proton-proton interaction potential 10.500 Mev deep and $1e^2/mc^2$ radius.

* Now at Illinois Institute of Technology.

26. A Test of the Suggested Emission of Neutrinos Due to the Impact of Electrons on Heavy Nuclei. R. J. VAN DE GRAAFF AND W. W. BUECHNER, *Massachusetts Institute of Technology*.—Various investigators report from cloud-chamber experiments that the energy lost in the single scattering of 2-Mev beta-rays by heavy nuclei is several times the loss calculated from the Bethe-Heitler theory. However, Arcimovic and Chramov[1] find experimentally that the production of x-rays in this range agrees with theory. To account for the extra energy loss, Klarmann and Bothe[2] and Champion[3] have suggested the emission of neutrinos as well as x-rays. To test this hypothesis, a 2-Mev, 10-microampere beam of electrons was directed on a target immersed in 42 kg of mercury to absorb both heat and x-rays, the assembly acting as a calorimeter. The target holder could be shifted slightly for bombarding either beryllium or gold. Thus if an appreciable amount of energy is carried away by penetrating neutrinos when heavy nuclei are bombarded, the rate of heating in the calorimeter should decrease when the target is shifted from beryllium to gold. No perceptible change in heating has been observed, indicating the absence of the suggested[2,3] neutrino emission, at least in the case of gold.

[1] Arcimovic and Chramov, Comptes rendus de l'Acad. Sci. U.S.S.R. **18**, 415 (1938).
[2] Klarmann and Bothe, Zeits. f. Physik **101**, 489 (1935).
[3] Champion, *Reports on Progress in Physics* **5**, 348 (1939).

27. Non-Uniform Particle Density in Nuclear Structure. EUGENE FEENBERG, *Washington Square College, New York University*.—The Coulomb repulsion between protons must give rise to a tendency for the proton density to vary within a nucleus from a minimum value at the center to a maximum near the boundary. A non-uniform proton density may be expected to create forces which distort the neutron distribution and tend to make the two distributions vary in the same manner. If surface effects are neglected, it is possible to calculate the energy correction associated with the non-uniform densities as well as the densities themselves in a comparatively rigorous and simple manner without making special assumptions about the nuclear forces. The neglect of surface effects permits the assumption that the variations in density are small departures from essentially constant distributions. It is found that the departure from uniform density is appreciable in heavy nuclei, but the energy correction is negligible. E. Wigner has obtained a similar result from another point of view.

28. Granulation, Phase Change, and Microstructure. MELVIN AVRAMI, *Columbia University.*—The theory of the preceding papers[1] is generalized and the notation simplified. A cluster of molecules in a stable phase surrounded by an unstable phase is itself unstable until a critical size is reached, though for statistical reasons a distribution of such clusters may exist. Beyond the critical size, the cluster tends to grow steadily. A comprehensive description of the phenomena of phase change may be summarized in phase change, grain-number, and structure formulas or diagrams, giving, respectively, the transformed volume, grain, and microstructure densities as a function of time, temperature, and other variables. To facilitate the deduction of formulas for these densities the related densities of the "extended" grain population are introduced. The extended population is that system of interpenetrating volumes that would obtain if the grains granulated and grew through each other without mutual interference. The extended densities are much more readily derivable from an analysis of the fundamental processes of granulation and growth. It is shown that, under very general circumstances, the densities of the actual grain population may be expressed simply in terms of the extended population.

[1] (a) J. Chem. Phys. **7**, 1103 (1939); (b) *ibid.* **8**, 212 (1940); Philosophy of Science, Technical Section **8** (Jan. 1941).

29. Critical Currents in Superconducting Films. W. F. BRUCKSCH, JR., W. T. ZIEGLER, E. R. BLANCHARD AND D. H. ANDREWS, *The Johns Hopkins University.*—Semi-transparent films of tin and lead, 50 to 500 mμ thick, were deposited by evaporation on glass at room temperature and the following properties studied: variation of mean temperature (T_m) of superconducting transition zone with thickness, with magnetic field, and with critical current (I_c); variation of resistance with temperature within the zone. At about 2° below normal T_m, with a current (I) of about 125 ma, a steady state was maintained with $I_c - I = \Delta I = 0.0003 I_c$. An increase of 0.03 percent in current restored sufficient resistance so that the heat generated from the current caused a sudden rise in temperature and complete restoration of resistance in a kind of "trigger" effect. In this steady state, radiation from a small tungsten filament suspended above the film also produced the trigger effect. The intensity of radiation necessary to produce the effect rose sharply with increasing ΔI. Since the film acts as an energy amplifier, this suggests that the "trigger effect" might be useful for measuring radiation.

30. X-Ray Diffraction in Random Layer Lattices. B. E. WARREN AND J. BISCOE, *Massachusetts Institute of Technology.*—Heat-treated carbon black is an example of a material built up from individual layers which are parallel and equidistant but completely random in translation parallel to the layer, and in rotation about the normal. Calling the axes in the layer a, b and normal to the layer c, there will be sharp crystalline reflections of type ($00l$), two-dimensional lattice reflections of type (hk), and no reflections of type (hkl). A general theory for the intensity distribution in a two-dimensional lattice reflection has been developed. For a powder pattern the intensity of each two-dimensional reflection rises rapidly in a small range of angle, and then falls off slowly toward larger angles. The lateral dimension of the layer is given in terms of the half-maximum intensity breadth by the relation $L = 1.84\lambda/B \cos\theta$.

31. Absorption Coefficients in Lead for X-Rays Produced in the Voltage Range from 0.7 to 2.5 Mv. A. A. PETRAUSKAS, F. E. MYERS AND L. C. VAN ATTA, *Massachusetts Institute of Technology.*—X-rays produced at high voltage were collimated into a narrow beam. The intensity was measured by means of a carbon-walled thimble chamber immersed in this beam. The geometry of the collimator and other details of the apparatus, together with tests for the proper performance of equipment, will be described. The x-ray intensity in the forward direction was found to vary approximately as the 3.0 power of the voltage reaching a value of 950 r per minute per milliampere one meter from the target at 2.5 Mv. Absorption coefficients were measured in lead for various voltages and filter thicknesses. The constant values obtained by using sufficient filtration are shown in the table. Initial values

VOLTAGE (Mv)	0.7	0.9	1.3	1.6	2.0	2.5
Linear absorption coefficient	1.50	1.07	0.82	0.70	0.63	0.58

ranging from 2.9 cm^{-1} to 1.3 cm^{-1} at the lowest and highest voltages respectively were reduced to the constant values given in the table by using filter thicknesses ranging from ½ inch to 2 inches of lead.

32. Variation with Angle of the Intensity and Hardness of X-Rays Produced at 0.9, 1.6, and 2.35 Mv. L. C. VAN ATTA, F. E. MYERS AND A. A. PETRAUSKAS, *Massachusetts Institute of Technology.*—The collimator and thimble chamber mentioned in the previous abstract were mounted to pivot about a horizontal axis through the x-ray target. The variation with angle of the intensity of unfiltered and heavily filtered radiation was measured for x-rays produced at 0.9, 1.6 and 2.35 Mv. At 2.35 Mv, x-rays filtered through one inch of lead show a ratio of intensity in the forward direction to that at right angles to the electron beam of 7.4. Definite evidence was obtained for the expected minimum in the forward direction. The variation of the absorption coefficient with angle was measured at 1.6 Mv. The absorption coefficient varies from 0.70 cm^{-1} in the forward direction to 0.85 cm^{-1} at 90°. A comparison of these results with available theory will be made.

33. The Effect of van der Waals Forces on the Thermal Diffusion Coefficient of Gaseous Isotopic Mixtures. R. CLARK JONES, *Harvard University.*—The effect of attractive intermolecular forces on the value of the thermal diffusion constant α for a mixture of two isotopes has been worked out without approximation for the Lennard-Jones 9,5 model. A few of the computed results are given in the table.

$(\epsilon/kT)^{\frac{1}{2}}$	R_T	$(\epsilon/kT)^{\frac{1}{2}}$	R_T	$(\epsilon/kT)^{\frac{1}{2}}$	R_T
0.0	0.432	0.625	0.162	2.0	−0.465
0.1	0.463	0.833	−0.153	2.5	−0.232
0.25	0.475	1.0	−0.384	5.0	−0.040
0.5	0.324	1.5	−0.629	10.0	−0.023

R_T is the ratio of the computed value of α to that predicted by theory for hard elastic spheres, and ϵ is the depth of the potential energy minimum. In view of the approximate relation $kT_c=1.2\epsilon$, where T_c is the critical temperature, the table indicates that α passes through zero at the temperature $T=1.6T_c$. The reversal of the sign of α has not yet been observed experimentally. The experimental values of R_T determined by Nier for neon can be made to fall near the theoretical curve by using the value of ϵ indicated by the critical temperature, and by increasing the scale of R_T to account for the greater hardness of neon.

34. Estimation of Interaction Potentials from Molecular Scattering Experiments. I. AMDUR AND H. PEARLMAN, *Massachusetts Institute of Technology.* (*Introduced by F. G. Keyes.*)—Beams of helium atoms with kinetic energies equivalent to 300–1000 electron volts were scattered in helium gas and the axis intensities measured with a detecting system having an angular aperture of 2.5°. Total collision cross sections accurate to about 15 percent were determined as a function of beam velocity. The values varied from 3.3A² at 300 volts to 0.9A² at 1000 volts. The scattering, in the present case, is classical and due almost entirely to the mutual repulsion of two helium atoms. Attempts were made, therefore, to find a repulsive potential which could account for the experimental results. A hard sphere model, with a collision diameter derived from viscosity measurements, and a Lennard-Jones repulsive potential, $V(r)=4.45/r^{12}\times10^{-10}$ erg (r in A), were both found to be incorrect. The hard sphere model permits of no variation of cross section with velocity while the Lennard-Jones potential predicts but a slight difference in the values at 300 and 1000 volts. Moreover, in both cases predicted values are many times greater than experimental values. The "softer" exponential type potentials, $V(r)=Ae^{-a(r)^n}$, were more satisfactory and predicted cross sections whose values were quite sensitive to changes in A, a and n. The specific repulsive potential whose predictions are verified by the present experimental results is $V(r)=11.3e^{-4.63(r)^{\frac{1}{2}}}\times10^{-10}$ erg (r in A) for distances of interaction between 0.55 and 1.05A.

35. Dielectric Constants of Aliphatic Ketones. ROBERT H. COLE, *Harvard University.*—The static dielectric constants and densities of eight aliphatic ketones have been determined over nearly the entire temperature range of the liquid phase in each case. The dielectric constants were determined by a simple method making use of a cathode-ray oscillograph for quantitative comparison of impedances. The density measurements were made by a displacement method using a simple form of torsion balance. The experimental results show that dipole-dipole coupling is the important factor in determining the dielectric constants of these liquids. The results are in qualitative, but not quantitative, agreement with values calculated by Onsager's formula using known values of the dipole moments of the ketone molecules. The differences are, however, consistent with Kirkwood's extension of the Onsager theory to include the effect of correlation between orientations of neighboring molecules. An explicit calculation of this effect is unfortunately not possible in the case of the ketones.

36. The Surface Recombination of Hydrogen Atoms and Hydroxyl Radicals at Different Surfaces. W. V. SMITH, *Harvard University.* (*Introduced by O. Oldenberg.*)—Atomic hydrogen was produced in a Wood discharge. The atoms were allowed to diffuse into a side arm coated with different substances. Among the advantages of a diffusion system was simplicity of mathematical analysis. The atomic concentration at a distance x from the discharge was measured by the heating of a small platinum probe. The ratio of atomic concentration at x to that at the discharge is $n/n_0=\exp-\beta\gamma^{\frac{1}{2}}x$. γ is the coefficient of recombination describing the catalytic power of the wall as a function of the temperature. β takes account of the probability that a hydrogen atom hits the wall. The coatings are investigated at different temperatures. Probes coated with different substances are also compared. Values of γ range from 10^{-1} to 10^{-5}. They increase with increased temperature and decreased water content of the surface. Similar work was done with a water vapor discharge, detecting the hydroxyl radical by a potassium chloride probe which catalyzes hydroxyl recombination but does not catalyze atomic hydrogen recombination. Values of γ for hydroxyl lie in the same range as for atomic hydrogen.

37. The Effect of Chemical Combination on X-Ray Emission Lines. T. M. SNYDER, *Princeton University.*—Frequently, chemical combination affects the width, shape and wave-length of an element's x-ray emission lines even when the lines do not arise from transitions involving valence electrons. It is proposed that these effects are caused by electrostatic coupling between valence and x-ray electrons which splits x-ray levels and shifts their centers of gravity. The resulting fine structure of x-ray lines is unresolved but evidenced by a broadening and asymmetry dependent on the chemical state. Lines involving only deep-lying levels of heavy elements are unaffected. Slater's integrals calculated with approximate wave functions for iron group elements give roughly the observed splittings. L levels are affected far more than K and more by $3d$ than $4s$ electrons. When several $3d$ electrons with unpaired spin are present, the exchange interaction considerably exceeds the direct, giving $K\alpha$ line widths roughly proportional to the number of these electrons. A re-examination of existing data for behavior of widths and asymmetries as a function of atomic number, valence and ionic character verifies this rule. Furthermore, the number of unpaired $3d$ electrons predicted from line widths agrees with that obtained from magnetic data and gives interesting information about substances for which these data are lacking.

38. Secondary Structure in the Absorption Limits of Gases.* C. H. SHAW AND J. A. BEARDEN, *Johns Hopkins University.*—The secondary structure in the K-absorption limit of germanium in gaseous $GeCl_4$ has been measured with the two-crystal spectrometer with a resolving power of about 10,000. The magnitude as well as the position of the structure was determined. The absorption edge of the isolated germanium atom should show no fine structure. This edge was assumed to have an arc tangent shape and a width the same as that for the isolated bromine atom.[1] The ratio of the absorption coefficient of Ge in $GeCl_4$ to that of the free atom was then calculated as a function of the separation from the limit and compared with theory.[2] Considering the number and character of the approximations involved in the theory, the comparison is satisfactory.

* This research was supported by a grant-in-aid from the Research Corporation.
[1] Shaw, Phys. Rev. **57**, 877 (1940).
[2] Hartree, Kronig, Petersen, Physica **1**, 895 (1934).

39. Saturation Magnetization of Nickel-Antimony and Nickel-Tantalum Alloys. G. T. RADO AND A. R. KAUFMANN, *Massachusetts Institute of Technology.* (*Introduced by John C. Slater.*)—The absolute saturation magnetic moment per atom (M) was measured as a function of the atomic composition (τ) for nickel-antimony and nickel-tantalum solid solutions. Five alloys of each set were prepared, up to $\tau = 7$ percent. They were cast in vacuum and carefully annealed. The specimens were small spheres, $\frac{1}{16}$ of an inch in diameter. The magnetization was measured by means of a Curie method in a solenoidal electromagnet. Field strengths up to 40,000 gauss and temperatures down to 77.2°K (boiling N_2) were used. A "superposed paramagnetism" was found in some samples at 290°K and 194.5°K, but the high field strengths permitted an accurate determination of the intrinsic magnetization. Up to about $\tau = 4$ percent, $dM/d\tau$ is strictly constant and equal to -3.60 and -5.66 Bohr magnetons (μ_B) per substituted atom for Ni-Sb and Ni-Ta, respectively. The Ni-Ta results are new. Those on Ni-Sb are in disagreement with Sadron[1] and Marian,[2] but our data appear to be more consistent. The two measured $dM/d\tau$ values are definitely different and not equal to $-5\mu_B$ per substituted atom as "predicted" by the energy band theory.[3,4] A complete tabulation of $dM/d\tau$ for nickel alloys shows our results to be additional exceptions to a surprisingly large range of applicability of the theory.

[1] C. Sadron, Ann. de physique **17**, 371 (1932).
[2] V. Marian, Ann. de physique **7**, 459 (1937).
[3] J. C. Slater, Phys. Rev. **49**, 537, 931 (1936).
[4] R. M. Bozorth, Bell Sys. Tech. J. **19**, 1 (1940).

40. Magnetization of Copper-Nickel Alloys. A. R. KAUFMANN AND C. STARR, *Massachusetts Institute of Technology.*—The magnetization in fields up to 30,000 oersted of copper-nickel alloys ranging in composition from pure copper up to 50 percent nickel has been measured at various temperatures between 14°K and 1300°K. The 50 percent alloy becomes ferromagnetic between 77°K and room temperature but an alloy with 38 percent nickel does not exhibit a real ferromagnetic behavior even at 14°K. This latter alloy as well as one with 30 percent nickel does show large saturation effects at low temperatures, but the susceptibility of the specimens with 20 percent nickel and less is independent of field strength at all temperatures. At the lowest temperatures employed the susceptibility at any composition including "pure" copper shows an increase with decreasing temperature but a Curie-Weiss law is approximated only for the alloy with 50 percent nickel. In general, the lower the temperature and the higher the composition, the more nearly a Curie-Weiss behavior is approached in the alloys which do not become ferromagnetic. At high temperatures, the susceptibility of all compositions up to 30 percent nickel begins to increase again, although the effect is generally small compared with the low temperature increase. This behavior leads to a minimum in susceptibility at a certain temperature which becomes higher as the nickel content increases.

41. An Electron Configuration Change in Metallic Zr from Magnetic and Resistance Measurements. C. F. SQUIRE AND A. R. KAUFMANN, *Massachusetts Institute of Technology.*—According to theory, the paramagnetic susceptibility of electrons in a metal should decrease slightly with raising the temperature. For pure, ductile Zr, our experiments show that the paramagnetism increases with rising temperature from 80°K up to 1000°K in a linear manner. Above this temperature the susceptibility rises in a non-linear manner until at 1120°K it shows a λ point where the crystal is known to undergo a structure change.[1] Above the λ point the paramagnetism shows normal temperature dependence. We account for these and the following data by supposing that the density of electrons at the top of the filled energy states is continuously increasing. The electrical resistance was found to rise with temperature so that dR/dT became smaller and approached zero as T approached the λ point. In accord with Zwikker[2] the resistance then drops at the structure change and then rises linearly with temperature on beyond. As much as 1.36 mols of atomic hydrogen could be dissolved in a mol of Zr, increasing the volume about 8 percent, giving the specimen some unusual magnetic properties, and lowering the transition temperature to 960°K.

[1] W. G. Burgers, Physica **1**, 561 (1934).
[2] C. Zwikker, Physica **6**, 361 (1926).

42. Paramagnetic Relaxation. C. STARR, *Massachusetts Institute of Technology.*—The dynamic magnetic susceptibility of paramagnetic salts in an alternating magnetic field can be approximately described as a function of frequency by a simple dispersion formula,[1] based upon the thermal coupling between the ionic spin-system and the lattice vibrations. This dispersion is characterized by a relaxation time which is increased by a decrease of temperature or by the application of a constant parallel magnetic field. The experimental results obtained with the iron-group alums[2] agree only qualitatively with the theoretical dispersion formula. The discrepancies may be due, in part, to uncertain experimental conditions and to errors inherent in the methods used. These will be discussed in

detail. The results at liquid helium temperatures are complicated by the fact that the specific heat of the crystal lattice is comparable to that of the spin-system. At higher temperatures, the errors associated with the high frequency beat method used in these experiments have been neglected. With suitable changes in the experimental technique to minimize the errors, measurements made at liquid hydrogen temperatures should be most valuable for the investigation of this subject.

[1] Debye, Physik. Zeits. **39**, 616 (1938).
[2] Gorter, Brons, Teunissen, de Haas, *et al.* Physica, 1936–1940.

43. Scattering, Trapping, and Release of Electrons in NaCl and in Mixed Crystals NaCl-AgCl. A. VON HIPPEL AND G. M. LEE, *Massachusetts Institute of Technology.*—The dielectric strength of ionic single crystals increases rapidly with temperature, reaches a maximum, and decreases again. In glasses the low temperature dependence is absent or reversed. That the periodic order produces a positive temperature coefficient can be explained by electron scattering, but a new mechanism must be held responsible for the steep decrease of the breakdown strength at higher temperatures. Studying mixed crystals of NaCl and AgCl containing zero to five atomic percent silver between −150°C and +150°C, we found new facts: At low temperatures the breakdown characteristic of pure NaCl and of the mixed crystals has about the same positive slope; increasing silver content displaces the curves to higher breakdown values. The higher the silver concentration, the sooner the dielectric strength reaches a maximum and the steeper is the negative slope thereafter. Consequently the curves cross; and while at room temperature the electric strength of rock salt is increased by the addition of silver, the opposite is true at 150°C. The possibility of thermal breakdown can be excluded experimentally. We believe that the trapping of electrons and their release by lattice vibrations are the additional mechanisms shaping the characteristics as observed. Spectroscopic evidence supports this hypothesis.

44. The Conductivity of Glass as a Function of Field Strength. R. J. MAURER, *Massachusetts Institute of Technology.*—The conductivity of soda-lime glass has been measured, as a function of field strength, between 0°C and 110°C. The data are compared with a recent theory of electrolytic conductivity of solids.[1] With field strengths less than 7×10^5 volts/cm, the equation

$$i=\frac{2ned}{\alpha\nu^2}\left(\frac{kT}{h}\right)^3\exp\left(-\frac{U}{kT}\right)\sinh\left(\frac{ed(\epsilon+2)E}{6kT}\right)$$

describes the dependence of the current density upon field and temperature. The three atomic parameters, the frequency ν, the activation energy U, and the jump distance d can be determined and have the expected magnitudes. It is suggested that, for crystalline materials, where d is known, the validity of the Lorentz-Lorenz correction to the inner field can be tested.

[1] F. Seitz, *The Modern Theory of Solids* (McGraw-Hill).

45. A General Nuclear Model. EUGENE FEENBERG, *Washington Square College, New York University.*—A useful nuclear model is provided by the approximation in which the Coulomb interaction is neglected and the energy is expressed in terms of volume and surface energy densities which are symmetrical functions of the mean particle densities. With this model the energy can be represented rigorously by a linear combination of functions

$$A^{n/3}f_n(|N-Z|/A)$$

with n ranging in integral steps from 3 to $-\infty$. The terms with $n=3$, 2, 1 have simple physical interpretations. The radius is expressible as a linear combination of the same kind of function met with in the representation of the energy, but, in this case, n ranges in integral steps from 1 to $-\infty$. If E is the total energy, and E_s the surface energy, the following differential equation holds:

$$E(NZ)=\left(N\frac{d}{dN}+Z\frac{d}{dZ}\right)E(NZ)+\tfrac{1}{3}E_s(NZ).$$

46. Temperature Distributions in Hollow Cylindrical Systems. MELVIN AVRAMI, *Columbia University.*—The equations for the steady-state temperature distributions in a hollow cylindrical system with a cylindrically symmetric, but otherwise non-uniform, heat source on the hollow surface, are set up and solved in Fourier integral form. Such a system may be an electric or "muffled" combustion type of furnace, in which only conduction and radiation need be taken into account. The boundary value problem is novel in that it involves radiation at a non-uniform temperature. The solution gives the relation between density of heat source and resulting temperature distribution. It may be used to solve such practical problems as that of designing an *isothermal furnace*, i.e., determining the distribution of source density which will give a uniform temperature over a finite length.

47. Time Lag Studies in Geiger Counters. M. E. ROSE AND W. E. RAMSEY, *Bartol Research Foundation of the Franklin Institute.*—As an explanation of the inefficiency of air and oxygen counters, it has been proposed that the electrons are captured before the discharge is initiated and time lags are introduced due to the low mobility of the negative ions. To test this hypothesis we have measured the efficiency of an oxygen counter (diameter 2.7 cm) as a function of amplifier resolving time with a triple coincidence circuit using small parallel counters as explorers. For a fixed distance of the explorers from the wire of the central oxygen counter, the efficiency is constant and small (25 percent) at low resolving times, increases for intermediate resolving times ($\sim10^{-5}$ sec.) and approaches a constant larger value (80 percent) for long times. As the explorers are moved toward the wire of the oxygen counter the time lags are reduced in accordance with the capture hypothesis. From the results obtained with the exploring counters just overlapping the oxygen counter, we find the mean time lag is 4×10^{-5} second, the probability for capture before the electrons reach the wire is 90 percent, the capture probability per impact is $\sim10^{-4}$ and the mobility of the O^- ions is 2 cm²/sec./volt in agreement with direct measurements of these quantities.

Author Index to Abstracts of Contributed Papers Presented at the Cambridge Meeting

Adams, F. W., Lee Devol and H. R. Letner—No. 10
Amdur, I. and H. Pearlman—No. 34
Anderson, E. E.—see Mack, J. E.
Andrews, D. H.—see Brucksch, W. F., Jr.
Avrami, Melvin—Nos. 28 and 46

Baker, Richard F.—see Cole, Kenneth S.
Bancroft, Dennison—see Birch, Francis
Bearden, J. A.—see Shaw, C. H.
Bethe, H. A.—No. 9
Birch, Francis and Dennison Bancroft—No. 15
Biscoe, J.—see Warren, B. E.
Blanchard, E. R.—see Brucksch, W. F., Jr.
Brown, Sanborn C.—No. 23
Brucksch, W. F., Jr., W. T. Ziegler, E. R. Blanchard and D. H. Andrews—No. 29
Buechner, W. W.—see Van de Graaff, R. J.

Clancy, Edward P.—No. 21
Cole, Kenneth S. and Richard F. Baker—No. 16
Cole, Robert H.—No. 35

Deutsch, Martin—No. 12
Devol, Lee—see Adams, F. W.

Feenberg, Eugene—Nos. 27 and 45
Feynman, R. P. and John Archibald Wheeler—No. 2
Flowers, J. W.—No. 14
Folsom, T. R.—No. 17

Halpern, O. and M. H. Johnson—No. 4
Hardy, T. C.—No. 20
Hartree, D. R.—see Manning, Millard F.
Hartree, W.—see Manning, Millard F.
Hay, Robert H.—No. 19
Hudspeth, Emmett—see Ramsey, W. E.

Johnson, M. H.—see Halpern, O.
Jones, R. Clark—No. 33

Kanne, W. R.—see Ragan, G. L.
Kaufmann, A. R. and C. Starr—No. 40
—— see Rado, G. T.
—— see Squire, C. F.
King, Ronold—No. 11

Lamb, W. E., Jr.—No. 24
Laporte, Otto—No. 7
—— see Platt, John R.
Lee, G. M.—see von Hippel, A.
Lees, Wayne L.—see Ramsey, W. E.
Letner, H. R.—see Adams, F. W.

Mack, J. E. and E. E. Anderson—No. 6
Manning, Millard F., W. Hartree and D. R. Hartree—No. 5
Maurer, R. J.—No. 44
Myers, F. E.—see Petrauskas, A. A.
—— see Van Atta, L. C.

Pearlman, H.—see Amdur, I.
Petrauskas, A. A., F. E. Myers and L. C. Van Atta—No. 31
—— see Van Atta, L. C.
Platt, John R. and Otto Laporte—No. 8

Rado, G. T. and A. R. Kaufmann—No. 39
Ragan, G. L., W. R. Kanne and R. F. Taschek—No. 25
Ramsey, W. E., Emmett Hudspeth and Wayne L. Lees—No. 13
—— see Rose, M. E.
Rose, M. E. and W. E. Ramsey—No. 47

Shaw, C. H. and J. A. Bearden—No. 38
Smith, W. V.—No. 36
Snyder, T. M.—No. 37
Squire, C. F. and A. R. Kaufmann—No. 41
Starr, C.—No. 42
—— see A. R. Kaufmann

Taschek, R. F.—see Ragan, G. L.

Valley, G. E.—No. 22
Van Atta, L. C., F. E. Myers, and A. A. Petrauskas—No. 32
—— see Petrauskas, A. A.
Van de Graaff, R. J. and W. W. Buechner—No. 26
Van Dyke, K. S. and Maynard C. Waltz—No. 18
Van Vleck, J. H.—No. 1
von Hippel, A. and G. M. Lee—No. 43

Waltz, Maynard C.—see Van Dyke, K. S.
Wannier, Gregory H.—No. 3
Warren, B. E. and J. Biscoe—No. 30
Wheeler, John Archibald—see Feynman, R. P.

Ziegler, W. T.—see Brucksch, W. F., Jr.